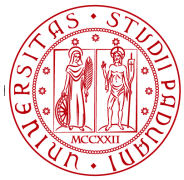

UNIVERSITÀ
DEGLI STUDI
DI PADOVA

Sede Amministrativa: Università degli Studi di Padova

Dipartimento di Scienze Biomediche Sperimentali

SCUOLA DI DOTTORATO DI RICERCA IN: BIOSCIENZE

INDIRIZZO: NEUROBIOLOGIA

CICLO XXII

EXCITATORY AND INHIBITORY SYNAPTIC TRANSMISSION AT CORTICAL SYNAPSES IN $Ca_V2.1$ KNOCK-IN MICE CARRYING FAMILIAL HEMIPLEGIC MIGRAINE MUTATIONS

Direttore della Scuola: Ch.mo Prof. Tullio Pozzan

Coordinatore d'indirizzo: Ch.mo Prof. Daniela Pietrobon

Supervisore:Ch.mo Prof. Daniela Pietrobon

Dottorando: Dania Vecchia

INDEX

RIASSUNTO

L'emicrania emiplegica familiare di tipo 1 (FHM1), un raro sottotipo di emicrania con aura, è causata da mutazioni *missense* nel gene umano *CACNA1A* che codifica per la subunità α_1 dei canali del calcio $Ca_V2.1$ (tipo P/Q) (Ophoff et al., 1996). Il mal di testa e i sintomi neurologici dell'aura che caratterizzano i tipici attacchi di FHM1 sono simili a quelli delle forme comuni di emicrania, eccetto per il sintomo dell'emiparesi (Pietrobon, 2007; Pietrobon and Striessnig, 2003). I canali $Ca_V2.1$ sono espressi nei terminali presinaptici e nelle membrane somatodendritiche di tutti i neuroni del cervello, dove svolgono un ruolo fondamentale nel controllo del rilascio di neurotrasmettitore.

Le mutazioni FHM1 determinano un guadagno di funzione della corrente Ca^{2+} dei canali ricombinanti umani $Ca_V2.1$; in particolare causano un aumento dell'influsso di Ca^{2+} a livello di singolo canale in un ampio intervallo di potenziali vicini alla soglia di attivazione del canale, dovuto a un'aumentata probabilità d'apertura del canale, causata per lo più dallo spostamento della curva di attivazione del canale verso potenziali più negativi (Hans et al., 1999; Tottene et al., 2002, 2005; Pietrobon, unpublished data). In accordo con tali risultati, i topi omozigoti *knock-in* (KI) recanti la mutazione FHM1 R192Q (RQ/RQ) presentano, in granuli di cervelletto e in cellule piramidali corticali, un aumento della densità di corrente Ca^{2+} di tipo P/Q (Tottene et al., 2009; van den Maagdenberg et al., 2004). Questi topi mostrano, inoltre, una facilitazione dell'induzione e propagazione, *in vivo,* della *cortical spreading depression* (CSD: il fenomeno neurologico che causa l'aura e il possibile *trigger* del mal di testa emicranico) (Pietrobon, 2005, 2007; van den Maagdenberg et al., 2004).

Per capire i meccanismi che determinano la facilitazione della CSD nei topi KI, in laboratorio abbiamo recentemente studiato la trasmissione sinaptica eccitatoria in neuroni corticali in microcoltura e in neuroni piramidali e interneuroni multipolari *fast-spiking* (FS) connessi tra loro sinapticamente in fettine acute talamo-corticali di topi KI RQ/RQ (Tottene et al., 2009). Lo studio della neurotrasmissione in microcolture di neuroni corticali ha rappresentato parte del mio progetto di Dottorato. I risultati hanno dimostrato un guadagno di funzione della neurotrasmissione eccitatoria dovuto a un aumentato influsso di Ca^{2+} evocato da potenziale d'azione, attraverso i canali del Ca^{2+} presinaptici di tipo P/Q, e a un'aumentata probabilità di rilascio di glutammato alle sinapsi delle cellule piramidali. Inoltre, usando un modello *in vitro* di CSD, abbiamo dimostrato una correlazione causale tra l'aumentato rilascio di glutammato alle sinapsi delle cellule piramidali e la facilitazione sperimentale della CSD nei topi KI RQ/RQ.

Abbiamo costatato che la neurotrasmissione inibitoria alle sinapsi tra gli interneuroni multipolari FS e le cellule piramidali nelle fettine talamo-corticali di topi KI RQ/RQ era invece inalterata, sebbene la trasmissione sinaptica fosse controllata dai canali del Ca^{2+} di tipo P/Q (Tottene et al., 2009). Il suddetto effetto sinapsi-specifico delle mutazioni FHM1 consolida la visione dell'emicrania come un disordine episodico dell'eccitabilità cerebrale. Infatti, la distruzione del bilancio tra eccitazione e inibizione e la conseguente iperattività dei circuiti neuronali possono costituire, in risposta a specifici *triggers*, la causa degli episodi di suscettibilità all'innesco della CSD nell'emicrania.

Mentre nei pazienti la mutazione R192Q causa tipici attacchi di FHM, la mutazione S218L causa una grave sindrome di emicrania emiplegica associata a convulsioni epilettiche, coma e grave edema cerebrale, dovuti spesso a traumi alla testa di lieve entità (Kors et al., 2001). La mutazione S218L, rispetto alla mutazione R192Q, determina un maggior spostamento verso potenziali più negativi della curva di attivazione dei canali umani ricombinanti $Ca_V2.1$ (Tottene et al., 2002, 2005). Inoltre, in accordo con il suddetto effetto, determina un maggior guadagno di funzione dell'influsso di Ca^{2+} nei neuroni a potenziali negativi e una maggiore facilitazione dell'induzione e propagazione della CSD *in vivo* nei topi omozigoti FHM1 KI S218L (SL/SL) rispetto ai topi KI RQ/RQ (van den Maagdenberg et al., 2004, 2010). L'effetto della mutazione S218L sulla corrente $Ca_V2.1$ Ca^{2+} neuronale e sulla facilitazione dell'induzione e propagazione della CSD risulta essere dipendente dal dosaggio allelico.

Al fine di investigare i meccanismi che determinano la maggior facilitazione della CSD in topi KI SL/SL rispetto ai topi KI RQ/RQ, ho studiato la trasmissione sinaptica glutamatergica in neuroni piramidali corticali di topi eterozigoti KI S218L (SL/WT) cresciuti su microisole di cellule gliali in modo da formare sinapsi su se stessi (autapsi). Ho trovato un guadagno di funzione della neurotrasmissione corticale eccitatoria dovuto a un aumentato influsso di Ca^{2+} evocato da potenziale d'azione, attraverso i canali del Ca^{2+} presinaptici di tipo P/Q e a un'aumentata probabilità di rilascio di glutammato alle sinapsi delle cellule piramidali corticali dei topi KI SL/WT. Infatti, l'ampiezza della corrente postsinaptica eccitatoria evocata (EPSC) e il contributo dei canali Ca^{2+} di tipo P/Q alla trasmissione sinaptica erano entrambi aumentati alle sinapsi dei neuroni piramidali corticali in microcoltura. Inoltre ho dimostrato che la saturazione del sensore del Ca^{2+} avveniva a minor concentrazioni esterne di Ca^{2+} e che la *paired pulse ratio* (PPR) era diminuita. I cambiamenti nell'ampiezza dell'EPSC, nella Ca^{2+} dipendenza dell'EPSC e nella PPR, trovati nei topi KI SL/WT erano quantitativamente simili a quelli rilevati nei topi KI RQ/RQ. La mutazione S218L determina quindi un aumento maggiore dell'influsso di Ca^{2+} presinaptico e del rilascio di glutammato alle sinapsi

corticali delle cellule piramidali rispetto alla mutazione R192Q che causa un fenotipo lieve di FHM1. Vista la correlazione causale tra l'aumentato rilascio di glutammato e la facilitazione sperimentale della CSD (Tottene et al., 2009), questo risultato potrebbe spiegare la maggior suscettibilità alla CSD indotta dalla mutazione S218L e il suo fenotipo grave. I dati hanno anche dimostrato che la trasmissione corticale eccitatoria in entrambi i topi FHM1 KI era meno suscettibile all'inibizione presinaptica conseguente all'attivazione dei recettori $GABA_B$ accoppiati a proteine G. Infatti, la frazione dell'EPSC inibito dal baclofen, agonista dei recettori $GABA_B$, era minore nei topi KI SL/WT e KI RQ/RQ rispetto ai topi selvatici (WT) e, conseguentemente, la neurotrasmissione eccitatoria era ulteriormente facilitata in presenza di modulazione. I topi eterozigoti KI S218L e omozigoti KI R192Q presentavano una riduzione dell'inibizione presinaptica simile. I dati suggeriscono che l'iperattività dei circuiti corticali dovuta sia all'aumentato rilascio di glutammato dipendente dai canali $Ca_V2.1$, sia alla ridotta inibizione presinaptica del rilascio di glutammato durante neuromodulazione (attraverso l'attivazione di proteine G) possono rendere la corteccia dei pazienti FHM vulnerabile all'innesco della CSD in risposta a *triggers* emicranici.

Un altro scopo del mio progetto di Dottorato consisteva nel determinare il meccanismo che causa l'effetto diverso della mutazione FHM1 R192Q sulla trasmissione sinaptica corticale eccitatoria e inibitoria, come descritto in Tottene et al. (2009). Ho studiato la neurotrasmissione inibitoria autaptica in singoli interneuroni corticali multipolari *fast-spiking* cresciuti su microisole di cellule gliali da topi WT e topi KI RQ/RQ. L'ampiezza media della corrente postsinaptica inibitoria (IPSC) evocata da potenziale d'azione era simile negli interneuroni multipolari dei topi WT e KI RQ/RQ, nonostante l'importante ruolo svolto dai canali Ca^{2+} di tipo P/Q nel controllo del rilascio di GABA a queste sinapsi. Ho trovato che il sensore del Ca^{2+} presinaptico, alle autapsi degli interneuroni multipolari nei topi WT, viene quasi saturato dall'influsso di Ca^{2+} evocato da potenziale d'azione. La mancanza del guadagno di funzione della neurotrasmissione inibitoria nei topi RQ/RQ KI non è comunque causata dalla saturazione del sensore Ca^{2+}, poiché l'ampiezza dell'IPSC in interneuroni di topi WT e KI RQ/RQ era simile anche a basse concentrazioni di Ca^{2+} esterno. Ho costatato, infatti, una simile dipendenza dell'IPSC dalle concentrazioni esterne di Ca^{2+} alle autapsi degli interneuroni multipolari WT e KI RQ/RQ. Tali risultati suggeriscono che l'inalterata neurotrasmissione corticale inibitoria nei topi KI RQ/RQ sia dovuta soprattutto ad un aumento non significativo dell'influsso di Ca^{2+}, evocato da potenziale d'azione attraverso i canali presinaptici $Ca_V2.1$ alle sinapsi degli interneuroni multipolari *fast-spiking*. Una possibile causa potrebbe essere la forma più corta del

potenziale d'azione degli interneuroni FS e/o l'espressione, in questi interneuroni, di una variante di *splicing* della subunità α_1 $Ca_V2.1$ poco influenzata dalla mutazione R192Q. L'inalterato influsso di Ca^{2+} evocato da potenziale d'azione attraverso i canali mutati presinaptici $Ca_V2.1$, alle sinapsi degli interneuroni multipolari FS, è probabilmente un effetto comune a tutte le mutazioni FHM1, poiché ho trovato inalterata anche la trasmissione sinaptica inibitoria alle autapsi degli interneuroni corticali multipolari FS nei topi eterozigoti KI S218L.

SUMMARY

Missense mutations in the human *CACNA1A* gene, which encodes the pore-forming α_1 subunit of the $Ca_V2.1$ (P/Q-type) Ca^{2+} channel, cause familial hemiplegic migraine type 1 (FHM1), a rare subtype of migraine with aura (Ophoff et al., 1996). Apart from the characteristic hemiparesis, the headache, autonomic and aura symptoms of typical attacks of FHM1 are similar to those of the common forms of migraine with aura (Pietrobon, 2007; Pietrobon and Striessnig, 2003). $Ca_V2.1$ channels are located in presynaptic terminals and somatodendritic membranes throughout the brain, where they play a dominant role in controlling neurotransmitter release.

FHM1 mutations produce gain of function of human recombinant $Ca_V2.1$ channels, mainly due to a shift of channel activation to more negative voltages and an increase of the open probability and single channel influx over a broad voltage range (Hans et al., 1999; Tottene et al., 2002, 2005; Pietrobon, unpublished data). Accordingly, homozygous knock-in (KI) mice carrying the R192Q FHM1 mutation show an increased P/Q-type Ca^{2+} current density in cerebellar granule cells and cortical pyramidal cells (Tottene et al., 2009; van den Maagdenberg et al., 2004). Interestingly, both the induction and the propagation of cortical spreading depression (CSD: the phenomenon underlying migraine aura, and a possible trigger of migraine headache) are facilitated in homozygous R192Q (RQ/RQ) FHM1 KI mice *in vivo* (Pietrobon, 2005, 2007; van den Maagdenberg et al., 2004).

To investigate the mechanisms underlying the facilitation of CSD, in my laboratory we have recently studied excitatory cortical synaptic transmission in neuronal microcultures (this was part of my PhD project) and at connected pairs of pyramidal cells and multipolar fast-spiking (FS) interneurons in acute thalamocortical slices of RQ/RQ KI mice (Tottene et al., 2009). We found gain of function of excitatory neurotransmission due to increased action potential (AP)-evoked Ca^{2+} influx through presynaptic P/Q-type Ca^{2+} channels and increased probability of glutamate release at pyramidal cell synapses. Using an *in vitro* model of CSD, we provided direct evidence of a causative link between enhanced glutamate release at pyramidal cell synapses and facilitation of experimental CSD in RQ/RQ KI mice. In striking contrast, inhibitory neurotransmission at connected pairs of multipolar FS interneurons and pyramidal cells in thalamocortical slices of RQ/RQ KI mice was unaltered, despite being initiated by P/Q-type Ca^{2+} channels (Tottene et al., 2009). The synapse-specific effect of FHM1 mutations supports the view of migraine as an episodic disorder of brain excitability, with disruption of the excitation-inhibition balance and hyperactivity of cortical circuits

in response to specific migraine triggers as the basis for episodic vulnerability to CSD ignition in migraine.

In patients, the R192Q mutation causes typical FHM attacks; in contrast, the S218L mutation causes a dramatic hemiplegic migraine syndrome that is associated with seizures, coma and severe cerebral oedema often triggered by mild head trauma (Kors et al., 2001). In comparison with R192Q, mutation S218L produces a larger shift of activation of recombinant human $Ca_V2.1$ channels towards more negative membrane potentials and, accordingly, a larger gain of function of neuronal Ca^{2+} influx at low voltages and a larger facilitation of CSD induction and propagation in homozygous S218L (SL/SL) FHM1 KI mice compared to RQ/RQ KI mice *in vivo* (Tottene et al., 2002, 2005; van den Maagdenberg et al., 2004, 2010). Moreover, the effect of the S218L mutation on the neuronal $Ca_V2.1$ Ca^{2+} current and facilitation of CSD is allele dosage-dependent.

To investigate the mechanisms underlying the greater facilitation of CSD in SL/SL KI mice compared to RQ/RQ KI mice, I studied glutamatergic synaptic transmission in cortical pyramidal cells grown on glial microislands from heterozygous S218L (SL/WT) KI mice. I found gain of function of cortical excitatory neurotransmission due to increased action potential-evoked Ca^{2+} influx through presynaptic P/Q-type Ca^{2+} channels and increased probability of glutamate release at cortical pyramidal cell synapses of SL/WT KI mice. In fact, in single cortical pyramidal cells forming autapses from mutant mice the amplitude of the evoked excitatory postsynaptic current (EPSC) and the contribution of P/Q-type Ca^{2+} channels to synaptic transmission were both increased. Moreover, saturation of the EPSC occurred at lower Ca^{2+} concentration and the paired pulse ratio (PPR) was decreased. The changes in EPSC amplitude, Ca^{2+} dependence of the EPSC and PPR in SL/WT KI mice were quantitatively similar to those measured in RQ/RQ KI mice. Therefore, the S218L mutation produces a larger increase in presynaptic Ca^{2+} influx and glutamate release at cortical pyramidal cell synapses than the mild R192Q FHM1 mutation. Given our evidence of a causative link between enhanced glutamate release and CSD facilitation (Tottene et al, 2009), this may explain the greater susceptibility to CSD induced by the S218L mutation, and possibly its dramatic clinical phenotype. I also found that cortical excitatory transmission in both FHM1 KI mice was less susceptible to presynaptic inhibition by activation of G protein-coupled $GABA_B$ receptors. In fact, the fraction of the EPSC inhibited by the $GABA_B$ receptor agonist baclofen was lower in SL/WT KI and RQ/RQ KI mice than in wild-type (WT) mice. As a consequence, excitatory neurotransmission was further facilitated in the presence of baclofen. Heterozygous S218L KI and homozygous R192Q KI mice

showed a similar reduction in presynaptic inhibition. The data suggest that hyperactivity of cortical circuits due to both enhanced $Ca_V2.1$-dependent glutamate release and reduced presynaptic inhibition of glutamate release during G protein-coupled neuromodulation may render the cortex of FHM patients vulnerable to CSD ignition in response to migraine triggers.

Another aim of my PhD project was to investigate the mechanism underlying the different effect of the R192Q FHM1 mutation on excitatory and inhibitory cortical synaptic transmission found in Tottene et al. (2009). I investigated inhibitory autaptic neurotransmission in single cortical multipolar fast-spiking interneurons grown on glial microislands from WT and RQ/RQ KI mice. The average amplitude of the AP-evoked inhibitory postsynaptic current (IPSC) was similar in multipolar interneurons of WT and RQ/RQ KI mice, despite a dominant role of P/Q Ca^{2+} channels in controlling GABA release at these synapses. I found that AP-evoked Ca^{2+} influx nearly saturates the presynaptic Ca^{2+} sensor at multipolar interneuron autapses in WT mice. However, the unaltered IPSC amplitude in RQ/RQ KI mice is not due to saturation of the Ca^{2+} sensor, because a similar IPSC at WT and RQ/RQ KI autapses was found also at low external Ca^{2+} concentrations. Indeed, I found a similar Ca^{2+} dependence of the IPSC at WT and RQ/RQ KI multipolar interneuron autapses. These findings suggest that the unaltered cortical inhibitory neurotransmission in RQ/RQ KI mice is largely due to the lack of significant increase of action potential-evoked Ca^{2+} influx through mutant presynaptic P/Q-type Ca^{2+} channels at multipolar interneuron synapse, possibly as a consequence of the short action potential and/or the expression of a splice variant of the $Ca_V2.1$ α_1 subunit little affected by the R192Q mutation in FS interneurons. The unaltered AP-evoked Ca^{2+} influx through mutant presynaptic $Ca_V2.1$ channels at multipolar FS interneuron synapses is probably a common effect of all FHM1 mutations, as I also found unaltered inhibitory synaptic transmission at multipolar FS interneuron autapses in heterozygous S218L KI mice.

1. INTRODUCTION

Calcium ion is fundamental for the cellular physiology as it is an intracellular second messenger. Important cellular processes in neurons and non excitable cells are mediated by variations in Ca^{2+} intracellular concentrations.

In the nervous system calcium controls a broad array of functions including neurotransmitter release, neurite outgrowth, synaptogenesis, neuronal excitability, as well as neuronal survival, differentiation, plasticity and gene expression. Variations in Ca^{2+} intracellular concentrations regulate contraction in muscle cells and secretion in endocrine cells. In excitable cells calcium influx is mediated by voltage-dependent calcium channels in response to membrane depolarization. The activity of these channels is essential to transduce electrical signals into chemicals signals.

1.1 Structure of voltage-dependent Ca^{2+} channels

Voltage-dependent Ca^{2+} channels are members of a gene superfamily of transmembrane ion channels proteins that includes voltage-dependent potassium and sodium channels (Catterall et al., 2005). They are multisubunit complexes composed of a pore-forming and voltage sensing α_1 subunit and several auxiliary subunits including β, $\alpha_2\delta$ and in some cases γ subunits, encoded by different genes (Figure 1.1).

The α_1 subunit of 190-250 kDa is the largest subunit, and it incorporates the conduction pore, the voltage sensors and gating apparatus, and most of the known sites of channel regulation by second messengers, drugs, and toxins (Catterall et al., 2005). The α_1 subunit is composed of about 2000 amino acid residues organized in four homologous domains (I-IV) (Catterall, 1998). Each domain of the α_1 subunit consists of six-transmembrane α helices (S1 through S6) and a membrane-associated P loop between S5 and S6 (Catterall et al., 2005). The S4 segment has been shown to play a major role in voltage sensing, whereas the P loop between S5 and S6 in each domain form the pore.

The α_1 subunits are associated with three distinct auxiliary protein subunits (Catterall and Few, 2008). The intracellular β subunit is a hydrophilic protein of 50-65 kDa. The transmembrane, disulfide-linked $\alpha_2\delta$ subunit complex (170 kDa) is encoded by a single gene, but the resulting prepolypeptide is posttranslationally cleaved and disulfide-bonded to yeld the mature α_2 and δ subunits (Catterall, 1998). Indeed, the α_2 extracellular protein is attached to the membrane through disulfide linkage to the

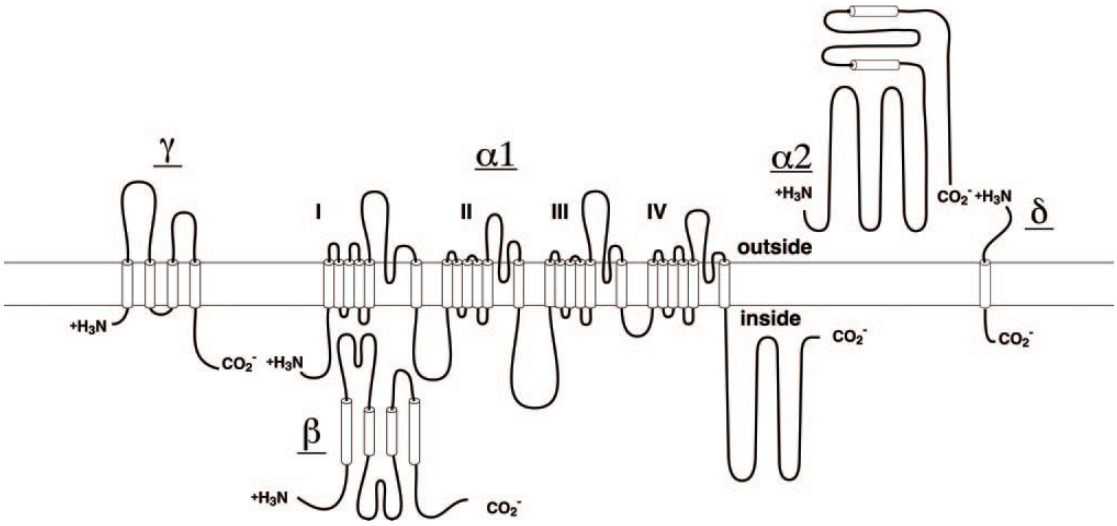

Figure 1.1. Transmembrane folding models for the Ca^{2+} channel subunits purified from skeletal muscle, adapted from Catterall (1998).

Predicted α heliches are depicted as cylinders. The lengths of lines correlate approximately to the lengths of the polypeptide segments represented.

transmembrane δ subunit. The γ subunit (33 kDa) is a glycoprotein with four transmembrane segments. It is a component of skeletal muscle Ca^{2+} channels, and related subunits are expressed in heart and brain (Catterall, 1998). Although these auxiliary subunits modulate the properties of the channel complex, the pharmacological and electrophysiological diversity of calcium channels arises primarily from the existence of multiple α_1 subunits (Catterall, 2005; description in the below paragraphs).

1.2 Classification of voltage-dependent Ca^{2+} channels

1.2.1 Biophysical and pharmacological classification of voltage-dependent Ca^{2+} channels

Calcium currents recorded in different cell types have diverse physiological and pharmacological properties, and an alphabetical nomenclature has evolved for the distinct classes of calcium currents. In base of the voltage depolarization necessarily to activate these channels they were divided in two groups: low voltage activated (LVA) and high voltage activated (HVA) channels (Hille et al., 2001). LVA channels are activated by weak depolarization and present activation and inactivation kinetics very fast, giving rise to transient currents. For this reason they are also called T-type Ca^{2+} channels.

HVA channels typically require a strong depolarization for activation and have slower kinetics than T-type Ca^{2+} channels. As HVA channels present different activation and inactivation curves, as well as, different activation and inactivation kinetics is difficult a classification bases only on their biophysical properties.

So, according to pharmacological criteria, HVA Ca^{2+} channels have been classified in four groups (Catterall et al., 2005). L-type Ca^{2+} channels are blocked by organic antagonists, including dihydropyridines (DHP), phenylalkylamines, and benzothiazepines. N-type Ca^{2+} channels are specifically and irreversibly blocked by ω-conotoxin GVIA (ω-CgTxGVIA) from the venom of the *Conus Geographus* snail. P/Q-type Ca^{2+} channels are specifically and irreversibly blocked by ω-agatoxin IVA (ω-AgaVIA) from the venom of the *Agelenopis aperta* spider and by ω-conotoxin MVIIC (ω-CTx-MVIIC) from the venom of the *Conus magus* snail that blocked reversibly also the N-type Ca^{2+} channels. R-type Ca^{2+} channels are so called because they are resistant to antagonists even if the synthetic peptide SNX-482 derived from the venom of *Hysterocrates gigas* spider is a specific blockers of some R-type Ca^{2+} channels isoforms.

In contrast with HVA channels, LVA Ca^{2+} channels are insensitive to both the DHPs, the spider and the cone snail toxins, and there are no widely useful pharmacological agents that specifically block the T-type Ca^{2+} currents (Catterall et al., 2005).

1.2.2 Molecular classification of voltage-dependent Ca^{2+} channels, localization and function

Mammalian α_1 subunit are encoded by at least ten distinct genes (CACNA1S, C, D, F, A, B, E, G, H, I). In 2000, a rational nomenclature was adopted based on the well defined potassium channel nomenclature (Ertel et al., 2000). Ca^{2+} channels were named using the chemical symbol of the principal permeating ion (Ca) with the principal physiological regulator (voltage) indicated as a subscript (Ca_V). The numerical identifier corresponds to the Ca_V channel α_1 subunit gene subfamily (1 to 3 at present) and the order of discovery of the α_1 subunit within that subfamily (1 through *n*). The complete amino acid sequences of these α_1 subunits are more than 70 % identical within a subfamily but less than 40 % identical among subfamilies (Figure 1.2). Division of Ca^{2+} channels into these three subfamilies is philogenetically ancient, as representatives of each are found in the *Caernorhabditis elegans* genome. According to this nomenclature, the Ca_V1 subfamily ($Ca_V1.1$ through $Ca_V1.4$) includes channels containing α_{1S}, α_{1C}, α_{1D},

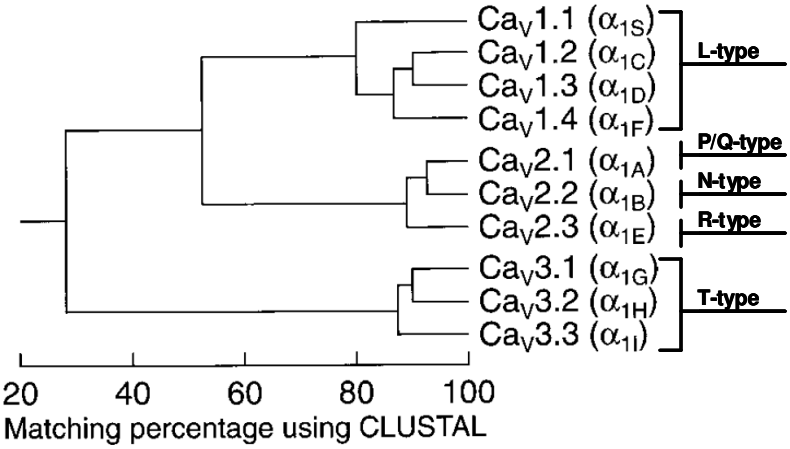

Figure 1.2. Phylogeny of voltage-dependent Ca^{2+} channel α_1 subunits, adapted from Ertel et al. (2000)

The sequence similarity of voltage-dependent calcium channel α_1 subunits were compared only for the membrane-spanning segments and pore loops (~ 350 amino acids). First, all sequence pairs were compared, which clearly defines three subfamilies with intrafamily sequence identities above 80 % (Ca_V1, Ca_V2, and Ca_V3). Then a consensus sequence was defined for each subfamily, and these three sequences were compared to one another, with intersubfamily sequence identities of ~ 52 % (Ca_V1 versus Ca_V2) and 28 % (Ca_V3 versus Ca_V1 or Ca_V2).

and $\alpha_{1F,}$ which mediate L-type Ca^{2+} currents. The Ca_V2 subfamily ($Ca_V2.1$ through $Ca_V2.3$) includes channels containing α_{1A}, α_{1B}, and $\alpha_{1E,}$ which mediate P/Q-type, N-type, and R-type Ca^{2+} currents. The Ca_V3 subfamily ($Ca_V3.1$ through $Ca_V3.3$) includes channels containing α_{1G}, α_{1H}, and $\alpha_{1I,}$ which mediate T-type Ca^{2+} currents.

Moreover, functionally different Ca^{2+} channels can be formed by different splice variant of a given α_1 subunit (Bourinet et al., 1999; Tottene et al., 2000). The different α_1 subunits are expressed in different localizations, where they mediate different physiological processes (Catterall et al., 2005). All the different Ca_V channels, except $Ca_V1.1$, are expressed in the brain, with a differential distribution in different neuronal populations and different localization with the same neuron. Different splice variants of a given subunit are also differentially distribuited and localized in the brain. In particular $Ca_V1.1$ are expressed in skeletal muscles; $Ca_V1.2$ are localized in smooth muscles, heart, endocrine cells, and in the soma and proximal dendrites in neurons; $Ca_V1.3$ are distributed in endocrine cells, in neuronal soma and dendrites, and in the cochlea; $Ca_V1.4$ are exclusively expressed in retina. Ca_V1 channels mediate different physiological processes in the different localizations: in muscles initiate contraction, in endocrine cells mediate hormone secretion, in retina control neurotransmitter release,

hearing in the cochlea, cardiac pacemaking in the heart, and in the brain these channels mediate neuronal excitability and gene expression (Catterall et al., 2005). $Ca_V2.1$ and $Ca_V2.2$ are expressed in neuroendocrine cells and in neurons in somatodendrite membranes and in the presynaptic terminals, where they initiate neurotransmission at most fast synapses and mediate Ca^{2+} entry into the neuronal bodies and dendrites (Catterall et al., 2005). $Ca_V2.3$ are predominantly localized in neuronal soma and dendrites where they mediate neuronal excitability (Catterall et al., 2005) but at some central synapses they contribute to neurotransmitter release (Gasparini et al., 2001). An accurately description of the brain localization and function of $Ca_V2.1$ channels is reported in paragraph 1.5. $Ca_V3.1$ and $Ca_V3.2$ channels are expressed in a wide variety of cell types: endocrine cells, smooth muscles but they are also expressed in heart, ovary, and placenta. Ca_V3 channels are localized in neuronal soma and dendrites where they are involved in shaping the action potential, in controlling patterns of repetitive firing (i.e in thalamic oscillations), and in neuronal integration (Catterall et al., 2005).

1.2.3 Molecular diversity and role of β, $\alpha_2\delta$ and γ subunits

The diversity of neuronal Ca^{2+} channel structure and function is substantially enhanced by multiple auxiliary subunits. Four β subunit genes have been identified, and each is subject to alternative splicing to yeld additional isoforms (Birnbaumer et al., 1994). Each of the four β subunits ($\beta_{1,2,3,4}$), all expressed in the brain, are able to associate with different Ca^{2+} channel α_1 subunits and, their localization is subunit-dependent (Mullner et al., 2004).

Four genes codifing the $\alpha_2\delta$ subunits ($\alpha_2\delta$-1, -2, -3, -4) have been discovered; each gene subjected to alternative splicing gives rise to different $\alpha_2\delta$ isoforms (Arikkath and Campbell, 2003; Klugbauer et al., 1999).

Studies conducted in heterologous expression system have demonstrated that β and $\alpha_2\delta$ subunits modulate the biophysical properties of α_1 subunit, even if the only pore-forming subunit expression is sufficient to assembly functional Ca^{2+} channels (De Waard and Campbell, 1995). In particular β subunits greatly enhance cell surface expression of the α_1 subunits and shift their kinetics and voltage dependence of activation and inactivation. However, these effects are different for individual β subunits (Catterall, 1998; De Waard and Campbell, 1995; De Waard et al., 1996).

In contrast co-expression of $\alpha_2\delta$ subunits and α_1 subunits has much smaller effects on Ca_V kinetics and voltage dependence of gating (Catterall and Few, 2008). However, the co-expression of $\alpha_2\delta$ and β subunits together with α_1 subunit has a synergic effect on

the enhance cell surface expression of α_1 subunits, in fact the increase of Ca^{2+} currents is greater when these auxiliary subunits are co-expressed than when they are expressed alone (De Waard and Campbell, 1995).

The γ subunits ($\gamma_{1,2,3,4,5,6,7,8}$) are encoded by eight different genes (Arikkath and Campbell, 2003). Even if the skeletal muscle $Ca_V1.1$ contains the γ subunit and the neuronal $Ca_V2.1$ channel contains a γ-like subunit, the functional role of the γ subunits of Ca^{2+} channels is the least well-defined (Catterall, 1998). These auxiliary subunits do not increase cell surface expression of Ca_V channels, and in some cases, reduce it substantially (Catterall and Few, 2008).

Therefore, the potential for combinatorial structural and functional heterogeneity of calcium channels is enormous, as different isoforms of the same α_1 subunit make different combinations with different isoforms of auxiliary subunits.

1.3 Voltage-dependent inhibition of Ca_V2 channels by G protein-coupled receptors

One regulatory mechanism of Ca_V2 Ca^{2+} channels that terminates Ca^{2+} influx and hence inhibits neurotransmitter release is provided by G protein-coupled receptors (GPCRs) and was discovered in 1980 by Dunlap and Fischbach (Tedford and Zamponi, 2006). GPCRs are a family of seven transmenbrane helix receptors, widely distributed in the peripheral and central nervous system, and that are activated by a variety of physiological stimuli, in most cases extracellular neurotransmitters and hormones. Autoreceptors in one nerve terminal bind neurotransmitter(s) released that terminal, whereas heteroreceptors in the same terminal may respond to neurotransmitters released by nearby nerve terminals from others neurons (Catterall and Few, 2008). Most neurotransmitters inhibits Ca^{2+} currents in this manner, including acetylcholine, glutamate, GABA, biogenic amine, and many neuropeptides (Catterall and Few, 2008; Tedford and Zamponi, 2006).

The GPCR activation determinates different voltage-dependent effects on whole-cell Ca_V2 currents: an inhibition of the current amplitude, with reduction being stronger at more hyperpolarized potentials; a depolarizing shift in the midpoint of the activation curve of the channel; a hyperpolarizing shift of the steady-state inactivation curve and, a slowing of the kinetics of current activation and inactivation (De Waard et al., 2005; Tedford and Zamponi, 2006). As depolarization (~100 mV voltage pulse applied before test pulse) relieves this form of inhibition of Ca^{2+} channels, thus rapid trains of action potentials can lead to a similar recovery from G protein inhibition, leading to the

suggestion that voltage-dependent G protein disinhibition may be important for synaptic function (Catterall and Few, 2008). This prediction has been tested in autaptic cultures of hippocampal neurons where trains of action potential-like stimuli relieve the inhibition of synaptic transmission caused by activation of $GABA_B$ or adenosine A1 receptors inducing synaptic facilitation (Brody and Yue, 2000a).

Voltage-dependent G protein inhibition of N-type Ca^{2+} channels has also been examined at the single channel level where was found an increased first latency to opening of the inhibited Ca^{2+} channel (Tedford and Zamponi, 2006).

The mechanism of inhibition of Ca_V2 follows a common mechanism of GPCR activation and action (Tedford and Zamponi, 2006). GPCRs interact, when activated by agonist, with heterotrimeric complexes of G protein αβγ subunits and stimulate exchange of Gα-bound GDP for cytoplasmatic GTP. Nucleotide exchange in turn favours dissociation of the heterotrimeric complexes into Gα-GTP and heterodimers of Gβγ, each of the latter modulate various downstream effector systems. The intrinsic GTAase activity of the Gα subunit hydrolized bound GTP back into GDP + Pi, thus terminating Gα activity and promoting the reassembly of the inactive Gα-GDPGβγ complex (De Waard et al., 2005; Tedford and Zamponi, 2006). As the GPCR-mediated inhibition of Ca_V2 seems to be sensitive to pertussis toxin, thus implicating $G\alpha_i$ and/or $G\alpha_o$ proteins. However, there is evidence that receptors coupling to others type of Gα subunit can also mediate voltage-dependent modulation (Tedford and Zamponi, 2006).

In 1996 Herlitze et al., and Ikeda established that inhibition of Ca_V2 channels is mediated by binding of Gβγ heterodimers directly to the Ca_V2 α_1 Ca^{2+} channel subunits (Tedford and Zamponi, 2006). All Ca_V2 channels contain a single Gβγ protein-binding pocket (GPBP) with multiple interactive binding sites (De Waard et al., 2005). These multiple binding sites are located as follow: one in the N-terminus, several in the loop between transmembrane domains I and II (L_{I-II}) and two in the C-terminus of the channel α subunit (Catterall and Few, 2008; De Waard et al., 2005). The sites in the N-terminus and L_{I-II} exert the most potent effects; moreover the L_{I-II} of some Ca_V2 channels is more efficient than that of others channels in controlling the Gβγ binding affinity to the channel, which probably imposes the established rank order of sensitivity to G protein mediated inhibition: $Ca_V2.2 > Ca_V2.1 >> Ca_V2.3$ (De Waard et al., 2005; Tedford and Zamponi, 2006). These structural Gβγ–Ca_V2 α_1 subunit interactions are in agreement with kinetic models. In fact, the delay in single channel opening during G protein inhibition can be explained by a stabilization of the closed state of Gβγ-bound channels, since Gβγ inhibits movement of the voltage sensor (Jones et al., 1997), suggesting that the transition from the reluctant to the willing single Ca^{2+} channel gating

mode involves the dissociation of the Gβγ complex from the channel (Tedford and Zamponi, 2006). Moreover, it was established that Gβγ binding produces only the ionic current inhibition (ON effect), whereas Gβγ unbinding, which follows channel activation, induces an apparent set of biophysical modifications that include the slowing of activation and inactivation kinetics and the depolarizing shift of the voltage dependence of channel activation (OFF effects) (Weiss et al., 2006, 2008).

Even if the more common form of Ca_V2 inhibition subsequent to GPCR activation is the voltage-dependent manner, exists also a voltage-indipendent inhibition of Ca_V2 channels that is dependent on intracellular signalling pathways and involves multiple protein kinases; this pathway of Ca^{2+} channels regulation has not yet been shown to modulate synaptic transmission (Catterall and Few, 2008; Tedford and Zamponi, 2006).

1.3.1 $GABA_B$ receptors

One of the GPCRs investigated in this thesis is $GABA_B$ receptor. $GABA_B$ is the metabotropic receptor of γ-aminobutyric acid (GABA), the major inhibitory neurotransmitter in the central nervous system, which mediates slow and prolonged synaptic inhibition (Couve et al., 2000). $GABA_B$ receptor assemble into heteromers composed of a $GABA_{B1}$ and a $GABA_{B2}$ subunit, which are both required for normal receptor functioning and mediate both presynaptic inhibition of neurotransmitter release and postsynaptic inhibition of neuronal excitability (Bettler and Tiao, 2006).

$GABA_B$ receptor belongs to the class C of GPCRs and is predominantly coupled to heterotrimeric $G_{i/o}$-type protein since most of $GABA_B$ receptor-mediated effects are inhibited by pertussis toxin (Bettler et al., 2004). Upon activation of the G protein, as described in the above paragraph, the Gβγ complex induces voltage-dependent inhibition of presynaptic N- and P/Q type Ca^{2+} channel (Bettler et al., 2004; Bowery et al., 2002). This causes a very potent negative regulation of neurotransmitter release since Ca^{2+} influx and transmitter release are correlated with a power law. A postsynaptic inhibition of Ca^{2+} channels by $GABA_B$ receptors is also present (Bettler et al., 2004; Bettler and Tiao, 2006).

Although the principal and widespread effect of stimulating presynaptic $GABA_B$ receptors is to inhibit neurotransmitter release by reducing the presynaptic Ca^{2+} current, it has been proposed, at some synapses, that $GABA_B$ receptors (but also other GPCRs) inhibit transmitter release downstream of calcium channels, but the exact mechanism is unclear (Brown and Sihra, 2008). At the calyx of Held, Sakaba and Neher (2003) reported that $GABA_B$ receptors activation leads to the direct Gβγ subunits reduction of

Ca^{2+} influx to a reduced vesicle priming exclusively mediated by a decrease in cyclic adenosine monophospate (cAMP) concentration as a consequence of the $G\alpha_{i/o}$ subunits activation that inhibits the adenylyl cyclase activity. Moreover, recent findings demonstrate that the $GABA_B$ activation decreases the fusion willingness of synaptic vesicles by directly interfering with the release machinery at hyppocampal autapses; authors did not investigate if this pathway occur through $G\beta\gamma$ complex or $G\alpha_{i/o}$ subunit activation (Rost et al., 2009). Besides the inhibition of adenylyl cyclase, it has been suggested that $G\alpha_{i/o}$ subunits mediate additional effector pathways on transcription factors and kinases (Bettler and Tiao, 2006; Bowery et al., 2002). For example, it was suggested that $GABA_B$ receptor activation leads to an increase in intracellular Ca^{2+} levels via phospholipase C and store-operated channels (Ulrich and Bettler, 2007). This pathway might also account for increased metabotropic glutamate receptor responses following $GABA_B$ receptor activation.

On the other hand postsynaptic $GABA_B$ receptors induce, by activation of $G\beta\gamma$ complex, a slow inhibitory postsynaptic current (late sIPSC) through activation of inwardly rectifying K^+ channels (GIRK or Kir3), which hyperpolarizes the membrane and shunts excitatory currents inducing an inhibition of neuronal excitability (Bettler et al., 2004; Bettler and Tiao, 2006). $GABA_B$ receptors have also recently been shown to interact with K^+ channels distinct from those that mediate the late IPSCs and to inhibit constitutively active Kir2 channels (Ulrich and Bettler, 2007). This is expected to increase rather than decrease the excitability of the neuron.

The capability of $GABA_B$ receptors to induce both presynaptic inhibition of neurotransmitter release and postsynaptic inhibition of neuronal excitability make $GABA_B$ receptors implicating in different effector pathways, in fact they are involved in the modulation of synaptic plasticity (in particular LTP), modulation of rhythmic activity in the hippocampus, population burst firing, inhibition of backpropagating action potentials, and inhibition of local spike activity (Bettler and Tiao, 2006; Couve et al., 2000; Ulrich and Bettler, 2007). In addition, the activation of glial $GABA_B$ receptors seems to be involved in the heterosynaptic depression (Bettler and Tiao, 2006).

$GABA_B$ receptors are localized on presynaptic inhibitory and excitatory terminals where they function as auto- and heteroreceptors and, more abundantly, on postsynaptic elements (Bettler and Tiao, 2006). Presynaptically, $GABA_B$ subunits were mainly detected in the extrasynaptic membrane and occasionally over the presynaptic membrane specialization of glutamatergic and, to a lesser extent, GABAergic terminals where they prevent neurotransmitter release. Indeed, $GABA_B$ receptors appear to be mostly localized near the active zone, which supports a close link with the release

machinery. Some $GABA_B$ heteroreceptors are activated by ambient GABA, others probably by GABA spillover from inhibitory terminals (Ulrich and Bettler, 2007).

Postsynaptically, $GABA_B$ subunits, not only reside in inhibitory and excitatory dendritic shafts but also in the excitatory extrasynaptic plasma membranes of head and neck spines (Bettler and Tiao, 2006; Ulrich and Bettler, 2007). In dendritic spines $GABA_B$ receptors colocalize with Kir3 channels and the $GABA_B$-mediated activation of Kir3 channels counteracts excitatory synaptic currents by hyperpolarization and shunting (Bettler and Tiao, 2006). $GABA_B$ receptors in spines and dendritic shafts are activated by spillover of GABA from neighbouring GABAergic synapses. This probably requires simultaneous activity of populations of GABAergic cells as it occurs during population oscillation or epileptic seizures (Bettler and Tiao, 2006; Scanziani, 2000) Moreover, dendritic $GABA_B$ receptors are also tonically activated by ambient GABA (Bettler and Tiao, 2006; Ulrich and Bettler, 2007).

1.4 Channelopathies of Ca_V 2.1 channels

Mutations in the human *CACNA1A* gene, located in 19p13 chromosome, that encodes the pore-forming α_1 subunit of $Ca_V2.1$ (P/Q-type) channel cause three autosomic dominant channelopathies: familial hemiplegic migraine type 1, episodic ataxia type 2 and spinocerebellar ataxia type 6 (Cannon 2006; Haan et al., 2005; Ophoff et al., 1996; Pietrobon, 2002).

Familial hemiplegic migraine type 1 (FHM1) is a rare dominantly inherited subtype of migraine with aura (MA) of childhood onset, characterized by intermittent motor weakness or paralysis (often, but not always, unilateral) lasting for hours to days (Pietrobon, 2002, 2007).

FHM1 is caused by missense mutation in the *CACNA1A* gene (Ophoff et al., 1996); all the 21 FHM1 missense mutations, reported so far, result in substitutions of conserved amino acids in important functional regions of the α_1 2.1 subunit (Figure 1.3; de Vries et al., 2009). Not all hemiplegic migraine patients are part of FHM1 families. The so-called sporadic hemiplegic migraine (SHM) patient exhibit clinical symptoms that are similar to those of FHM1 patients, but is the only one affected patient in the family (Figure 1.3 with asterisks; de Vries et al., 2009¸ Pietrobon, 2007).

Typical FHM1 attacks are characterized by unilateral and pulsating moderate-to-severe headache (lasting 4 to 72 hours), often accompanied by nausea, photophobia and photophobia preceded by the obligatory motor aura (Figure 1.3 in blue; Pietrobon, 2007). Nearly always, at least three, and often four, aura symptoms are present in

FHM1 attacks (typically in the temporal order: visual, sensory, motor, aphasic), and they last longer than in MA (in MA usually less than 60 minutes of duration). MA usually has only visual symptoms but the appearance and progression of the visual percept are similar in MA and FHM1. Also the duration of the headache is usually longer in FHM1 than MA, but all other headache characteristics are similar. In addition to typical FHM1 attacks, some FHM1 patients can have atypical severe attacks followed by fever, aphasia, prolonged hemiplegia lasting several days, impairment of consciousness or confusion, and in the more severe cases, coma and seizures (Figure 1.3 in green; Ducros et al., 2001). Moreover, about 20% of FHM1 families show permanent cerebellar symptoms of progressive cerebellar ataxia and/or nystagmus and/or dysartria (Figure 1.3 in red; Ducros et al., 2001; Pietrobon, 2007). Emotional stress and minor head trauma are among the most common triggers of FHM1 attacks (Pietrobon, 2007).

FHM1 can be consider a model for the common form of migraine because the headache and aura features, apart from the hemiparesis, are identical and FHM1 patients have, in addition to attacks of FHM, also attacks of common non-hemiplegic migraine (de Vries et al., 2009; Pietrobon, 2007). The study of FHM mechanisms may thus provide unique insights into the pathophysiology of migraine.

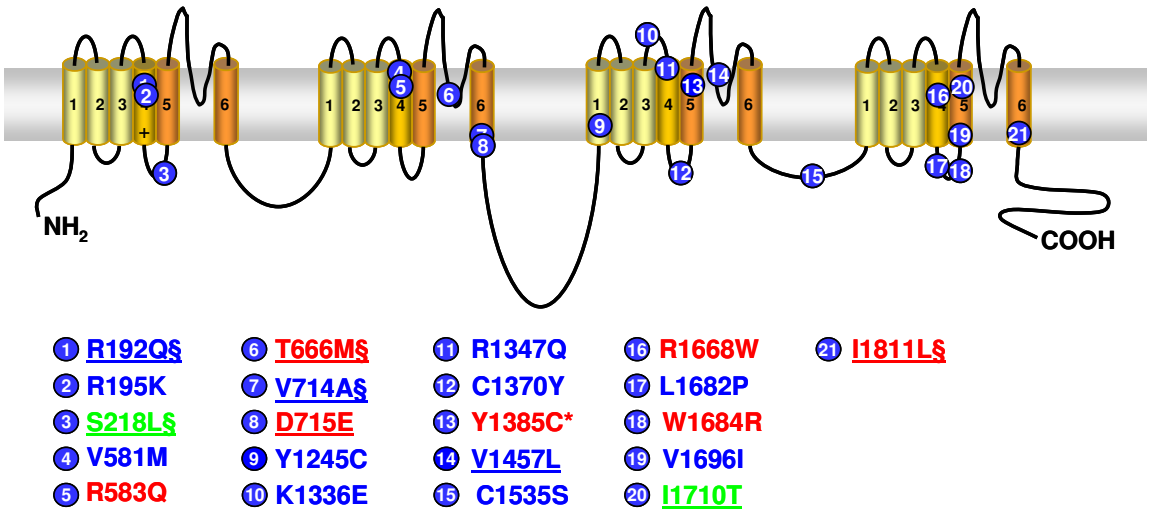

Figure 1.3. Localization of the 21 FHM1 mutations

In blue mutations that cause typical FHM1 attacks; in red mutations that cause FHM1 with cerebellar symptoms; in green mutations that cause a severe FHM1 phenotype; sporadic mutation is reported with asterisk; the eight mutations studied in the heterologous expression system are reported underline, and the five mutation expressed in neurons from $Ca_V2.1$ $\alpha_1^{-/-}$ mice are reported with §.

Episodic ataxia type 2 (EA2) is a rare dominantly inherited early-onset neurological disorder, characterized by longer episodes (lasting hours to days) of ataxia with interictal nystagmus and mildly progressive baseline ataxia (Jen et al., 2007; Pietrobon, 2002). EA-2 is caused by 50 mutations in the *CACNA1A* gene, the majority are nonsense or deletions and/or insertions mutations that disrupt the open reading frame leading to truncation of the protein (Jen, 2008; Jen et al., 2007). However, intron inclusion affecting alternative splicing and missense mutations, resulting in substitutions of conserved amino acids in important functional regions of the α_1 2.1 subunit, have been reported (Haan et al., 2005; Jen, 2008; Ophoff et al., 1996; Wan et al., 2005).

The episodic ataxia symptoms, which usually start in the first or second decade of life, consist in: truncal instability, unsteady gait, loss of limb coordination, and sometimes vertigo or dizziness, which may be precipitated by stress or fatigue (Haan et al., 2005; Pietrobon 2002). Many patients develop progressive cerebellar ataxia and cerebellar atrophy predominating on the anterior vermis, and about 50% of the patients report migraine headache during the ataxic spells (Jen, 2008; Jen et al., 2007; Pietrobon, 2002). Weakness and/or confusion, dystonia and seizures are other symptoms often associated with episodic ataxia (Pietrobon, 2002). In general, great intra- and interfamilial variability exists in the symptoms (both episodic and permanent) experienced by EA2 patients. A severe progressive ataxia in the absence of paroxysmal episodes may be part of the clinical spectrum of the disease.

Functional studies of the effects of EA2 mutations on recombinant $Ca_V2.1$ channels in heterologous expression system have revealed a loss of channel function (Pietrobon, 2007).

Spinocerebellar ataxia type 6 (SCA6) is a rare dominantly inherited disorder of late-onset progressive cerebellar dysfunction caused by abnormal expansion of a trinucleotide CAG repeat, in exon 47 of the *CACNA1A* gene, encoding an elongated tract of glutamine residues in the carboxyl terminus of the α_1 2.1 subunit (Zhuchenko et al., 1997). SCA6 patients have 19-33 glutamine repeats, whereas those without the syndrome have 4-18 (Kordasiewicz et al., 2006). SCA6 symptoms consist in limb and trunk ataxia, gait ataxia, dysarthria, and nystagmus with a slow disease progression (Cannon, 2006; Haan et al., 2005). Some patients have ataxia combined with episodic headache or nausea. Moreover, there is evidence of marked cerebellar athrophy especially in the superior vermis, with more severe loss of Purkinje cells than granule cells, and variable mild atrophy of the brainstem (Pietrobon, 2002). The median age of

onset is in the fourth decade and larger repeat burden is correlated with earlier onset of disease (Cannon, 2006).

Recently was described a child affected by permanent non-fluctuating limb and trunk ataxia with a quite early age of onset (at 14 months of age) (Tonelli et al., 2006). Interestingly, the size of the *CACNA1A* triplet repeat region in the patient was within the normal range while he carried a novel *de novo* missense mutation in this gene, a R1664Q mutation falling within the transmembrane S4 of the fourth domain of the $Ca_V2.1$ channel. The clinical picture was strange because the non episodic and progressive limb and trunk ataxia was typical of SCA6, but the early age of onset was typical of EA2. However, the phenotype of progressive ataxia associated to a point mutation in *CACNA1A* gene has already been described, but it was both associated to episodic features and FHM1 within the same family.

Functional studies of the effects of SCA6 mutations on recombinant $Ca_V2.1$ channels in heterologous expression system have revealed conflicting effects (Pietrobon, 2007). Most of the conflicting findings likely arise from the use of different splice variants of $Ca_V2.1$. Interestingly, unaltered functional properties of $Ca_V2.1$ channels with expanded polyglutamine stretches were recently confirmed in SCA6 knock-in mice carrying expanded CAG repeats in the mouse *cacna1a* locus (Watase et al., 2008).

1.4.1 Neurobiology and pathophysiology of migraine

It is generally recognized that the development of migraine headache depends on the activation of the trigeminovascular system (Dalkara et al., 2006). Indeed, within the skull pain sensitivity is primarily restricted to the meningeal blood vessels, which are densely innervated by nociceptive sensory afferent fibers of the ophthalmic division of the trigeminal nerve (Pietrobon, 2005; Pietrobon and Striessnig, 2003). In different animal models, including non human primates, activation of the meningeal trigeminovascular afferents leads to activation of second order dorsal horn neurons in the trigeminal nucleus caudalis (TNC) and the upper two divisions of the cervical spinal cord (Figure 1.4, arrows 1, 3). Impulses are then carried rostrally to brain structures involved in the perception of pain, including several thalamic nuclei and the ventrolateral area of the caudal periaqueductal gray region (PAG) (Figure 1.4, arrows 4, 5). The PAG is involved in the craniovascular pain not only through ascending projections to the thalamus but also through descending modulation (mainly inhibitory) of nociceptive afferent information via projections to serotonergic neurons in the

magnus raphae nucleus (MRN). Activation of the trigeminovascular afferents also leads to release of vasoactive neuropeptides contained in their peripheral nerve endings, including calcitonin gene-related peptide (CGRP), substance P (SP) and neurokinin A (NKA) (Figure 1.4, inset). Others vasoactive neuropeptides as vasoactive intestinal peptide (VIP), nitrix oxide (NO), and acetylcholine (ACh) are released in the meninges by parasympathetic efferents from the superior sphenopalatine ganglion (SPG) (Figure 1.4, arrow 7 and inset). These parasympathetic efferents are activated subsequently to stimulation of the superior salivatory nucleus (SSN) through the trigeminal ascending projections (Figure 1.4, arrow 6). In animal studies the released by trigeminal ganglion

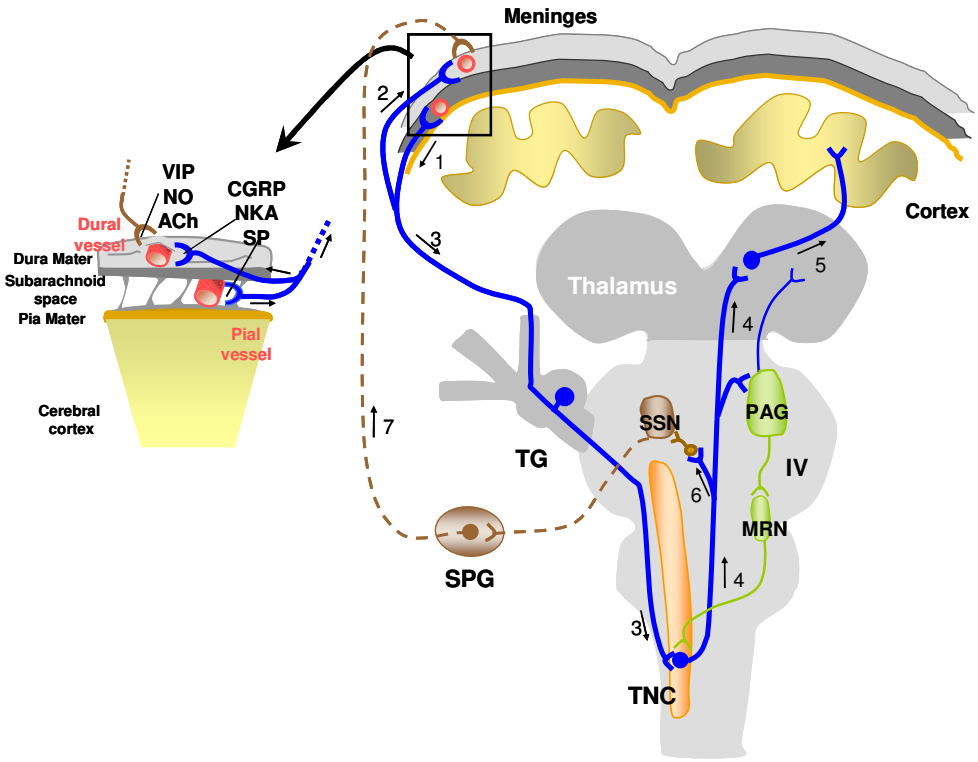

Figure 1.4. Neuronal structure and pathways involved in trigeminovascular activation and cephalic pain processing, adapted from Pietrobon (2005)

IV, fourth ventricle; ACh, acetylcholine; CGRP, calcitonin gene-related peptide; PAG, periaqueductal grey region; MRN, magnus raphe nucleus; NKA, neurokinin A; NO, nitrix oxide; SP, substance P; SPG, superior sphenopalatine ganglion; SSN, superior salivatory nucleus; TG, trigeminal ganglion; TNC, trigeminal nucleus pars caudalis; VIP, vasoactive intestinal peptide.

stimulation produce vasodilatation of the meningeal vessels (mainly due to CGRP), plasma extravasation and mast cell degranulation with secretion of other proinflammatory substances in the dura (neurogenic inflammation).

Evidence that activation of the trigeminovascular system indeed, occurs in humans during migraine is provided by the increased level of CGRP (but, interestingly, not substance P) found in both the external and internal jugular blood during migraine attacks and its return to normal levels after sumatriptan (an anti-migraine drug) treatment in parallel with headache relief (Pietrobon, 2005; Pietrobon and Striessnig, 2003).

The maintenance of the severe prolonged pain of migraine headache involves sensitization of meningeal nociceptors and self-sustained sensitization of central neurons of the trigeminovascular system, whose incompletely understood mechanisms may include alterations of descending endogenous pain modulatory pathways, including the PAG (Pietrobon, 2005; Pietrobon and Striessnig, 2003).

In the last decades, there has been further movement away from the "vascular theory of migraine" (Charles, 2009). This theory postulates that the symptoms of migraine aura are caused by transient ischemia induced by vasoconstriction, and the headache arises from rebound abnormal vasodilatation of intracranial arteries and consequent mechanical activation of perivascular sensory fibers (Pietrobon and Striessnig, 2003). Although intracranial vasodilatation is an appealingly simple explanation for migraine pain, this hypothesis has never been capable of explaining the wide range of symptoms that may precede, accompany, or follow the pain (Charles, 2009). Indeed, multiple imaging studies have confirmed that vasodilatation is not required for migraine headache, to the contrary, these studies suggest that headache begins during a cortical hypoperfusion phase and may end before the followed hyperperfusion phase resolves.

It is now generally accepted that migraine arises from a primary brain dysfunction, but the nature and mechanisms that leads to activation of the trigeminovascular system remain incompletely understood and controversial (Charles, 2009; Pietrobon and Striessnig, 2003).

Recent findings point to cortical spreading depression (CSD) as a key player in the pathogenesis of migraine (Pietrobon 2005; Pietrobon and Striessnig, 2003). CSD can be induced in animals by focal stimulation of the cerebral cortex and consists in a slowly propagating (2-6 mm/min) wave of strong depolarization of neurons and glial cells that generates a transient neuronal intense spike activity as it progresses into the tissue, followed by long-lasting neuronal suppression (Charles and Brennan, 2009; Lauritzen, 1994; Pietrobon, 2005). The depolarization phase is associated with an initial transient vasodilatation followed by an increase in regional cerebral blood flow (rCBF), whereas the phase of reduced neuronal activity is associated with a reduction in rCBF

subsequent to a sustained vasoconstriction. Neuroimaging findings indicate that migraine visual aura is due CSD (Pietrobon and Striessnig, 2003). Migraine visual aura frequently consists in a scotoma (an area of lost vision) with a scintillating border, that usually begins near the center of vision as a twinkling star and then develops into an expanding circle that slowly move across the visual field towards the periphery. Changes in blood oxygenation level-dependent (BOLD) signals observed using high-field functional magnetic resonance imaging with near-continuous recording during visual aura in three patients, demonstrated different characteristics of CSD (Hadjikani et al., 2001). A clear temporal correlation was established between the initial features of the aura percept (scintillations beginning in the paracentral left visual field) and the initial increase in the mean BOLD signal, reflecting cortical hyperemia. The subsequent decrease in mean BOLD level was temporally correlated with the scotoma following the scintillations. The BOLD signal changes developed first in the extrastriate cortex, contralateral to the visual changes. It then slowly migrated (3.5 mm/min) towards more anterior regions of the visual cortex, representing peripheral visual fields, in agreement with the progressive movement of the scintillations and scotoma from the center of vision towards the periphery. Interestingly, spreading cerebral perfusion changes have also been reported in migraine without aura, raising the possibility that CSD also occurs in patients presenting migraine without aura and causes headache without aura symptoms because it originates in a clinically silent area of the cerebral cortex (Dalkara et al., 2006; Pietrobon, 2005). Moreover, magnetoencephalography has been used to further demonstrate the presence of a CSD-like electrical activity during visual aura, as focal DC potential changes propagating across the cortex and that are produced by the neuronal depolarization in CSD, induced changes in the magnetic field outside the cranium (Bowyer et al., 2001). These observations strongly suggest an electrophysiological event such as CSD generates the aura in human visual cortex (Pietrobon, 2005, 2007).

Animal studies support the idea that CSD may also cause the migraine headache (Pietrobon, 2005, 2007). Recent experimental data clearly demonstrated that CSD is able to directly activate the meningeal nociceptors (Zhang et al., 2009), and induced a long-lasting blood-flow enhancement within the middle meningeal artery and plasma protein leakage in the dura mater (Bolay et al., 2002). Indeed, CSD induces a large increase in the extracellular concentration of K^+ and H^+ ions, NO, ATP, arachidonic acid, and prostaglandins. Many of these substances, in particular the vasoactive NO and the nociceptive messenger ATP, are able to activate the meningeal trigeminovascular afferents, either directly or by causing perivascular inflammation (Figure 1.4, inset;

Charles and Brennan, 2009; Pietrobon, 2005). Moreover, five clinically migraine prophylactic drugs, which are effective in reducing the frequency of migraine attacks with aura as well as without aura, suppress CSD susceptibility (Ayata et al., 2006). Furthermore, two knock-in mice carrying human mutations causing FHM1 show a decreased threshold for CSD initiation and an increased velocity of CSD propagation (Eikermann-Haerter et al., 2009a; van den Maagdenberg et al., 2004, 2009).

All these findings support the hypothesis that CSD may be a trigger of migraine in patients with aura, as well as, in patients that presents attacks without aura (Pietrobon, 2007). However, a direct link between CSD and headache in patients is not already demonstrated. The mechanisms that make the brain of migraineurs susceptible to episodic "spontaneous" CSDs in response to specific triggers (which might coincide with known migraine triggers such as stress or intense, repetitive long lasting sensory stimulation) are unknown. Migraineurs are hypersensitive to any kind of sensory overload and there is strong evidence for altered cortical excitability and abnormal processing of sensory information in their brain in the period between migraine attacks (Aurora and Wilkinson, 2007; Coppola et al., 2007; Pietrobon and Striessnig, 2003). The mechanisms underlying the interictal abnormalities in cortical activity are controversial and their relationship to susceptibility and/or occurrence of CSD is unclear.

1.5 Localization and function of $Ca_V2.1$ channels

$Ca_V2.1$ channels are located in presynaptic terminals and somatodendritic membranes throughout the mammalian brain (Westenbroek et al., 1995). $Ca_V2.1$ channels are expressed in all brain structures that have been implicated in the pathogenesis of migraine and/or migraine pain, including the cerebral cortex, the trigeminal ganglia, and brainstem nuclei involved in the central control of nociception, and their expression is particularly high in the cerebellum (Pietrobon and Striessnig, 2003). Most of the Ca^{2+} current of Purkinje cells, a large fraction of the Ca^{2+} current of cerebellar granule cells and 30-40% of the Ca^{2+} current in dissociated cortical pyramidal neurons, trigeminal ganglion neurons and neurons from various brainstem nuclei involved in the central control of pain are inhibited by ω-AgaIVA, the spider toxin that specifically inhibits P/Q-type Ca^{2+} channels (Pietrobon and Striessnig, 2003).

$Ca_V2.1$ channels play a prominent role in initiating action potential-evoked neurotransmitter release at central nervous system synapses (Pietrobon, 2005). At many central synapses P/Q-, N- and R-type Ca^{2+} channels cooperate in controlling

neurotransmitter release, but P/Q-type channels have a dominant role, partly because of a more efficient coupling to the exocytotic machinery (Mintz et al, 1995; Li et al, 2007 Qian and Noebels, 2000; Wu et al, 1999). Fast synchronous release is elicited by local Ca^{2+} transients produced by the opening of a few Ca^{2+} channels, that are located in close proximity to the Ca^{2+} sensors on readily releasable vesicles through specific interactions with multiple proteins of the active zones, including SNAREs, RIM and scaffolding proteins like Mint, CASK (Catterall and Few, 2008). The preferential localization of P/Q channels close to the vesicles at the release sites may account for the more efficient coupling of P/Q channel to release at the Calyx of Held and perhaps at other central synapses (Wu et al., 1999).

Of particular interest in the context of $Ca_V2.1$ channelopathies is to consider the involvement of P/Q channels in synaptic transmission at the main synapses of the neuronal microcircuits in the cerebellum and cerebral cortex, the brain areas involved in the pathogenesis of EA2, SCA6 and FHM1. In the cerebellum, $Ca_V2.1$ channels play a dominant role in initiating fast transmitter release both at the excitatory (parallel fibers (PF) and climbing fibers (CF)) and the main inhibitory synapses onto Purkinje cells (Pietrobon, 2002). Inhibitory synaptic transmission at mature synapses between PCs and deep cerebellar nuclei neurons is exclusively dependent on P/Q-type channels (after P15 in mice) (Iwasaki et al, 2000; Pietrobon, 2002).

In the cerebral cortex, excitatory synaptic transmission at pyramidal cell synapses in different cortical areas depends predominantly on P/Q-type Ca^{2+} channels (Ali and Nelson, 2006; Iwasaki et al, 2000; Koester and Sakmann, 2000; Rozov et al, 2001; Tottene et al, 2009; Zaitsev et al, 2007) with a notable exception at synapses between layer 5 pyramidal cells and burst-firing bipolar interneurons of motor cortex (Ali and Nelson, 2006). A dominant role of P/Q-type Ca^{2+} channels in excitatory transmission in the thalamocortical system is further supported by the finding that activation of the cortex following thalamic stimulation in thalamocortical slices was completely inhibited by blocking P/Q-type Ca^{2+} channels (Llinas et al, 2007). Relatively little is known on the Ca^{2+} channels initiating inhibitory neurotransmission in the cortex, since the Ca^{2+} channel pharmacology has been investigated only at the synapses between fast-spiking (FS) interneurons and pyramidal cells; neurotransmission was found to be exclusively dependent on P/Q-type Ca^{2+} channels in many cortical areas (Kruglikov and Rudy, 2008; Tottene et al, 2009; Zaitsev et al, 2007), but again with the exception of layer 5 of the motor cortex, where it was exclusively dependent on N-type Ca^{2+} channels (Ali and Nelson, 2006).

1.6 Functional consequences of FHM1 mutations

The functional consequences of eight FHM1 mutations have been investigated by expressing recombinant $Ca_V2.1$ channels in a heterologous expression system (mammalian cell line: HEK293; Figure 1.3, underlined) (Hans et al., 1999; Tottene et al., 2002, 2005; Pietrobon, unpublished data). Because $Ca_V2.1$ channels expression is almost exclusively restricted to neuronal cells, five of these mutations have also been analyzed in granule cells from $Ca_V2.1$ $\alpha_1^{-/-}$ mice expressing human $Ca_V2.1$ α_1 subunits (Figure 1.3, with §; Hans et al., 1999; Tottene et al., 2002, 2005; Pietrobon, unpublished data). The studies in the heterologous expression system showed that the FHM1 mutations alter many biophysical properties of human $Ca_V2.1$ channels, in a complex way (Pietrobon, 2007). In some cases (e.g, in the case of the channel inactivation properties), the effects are different depending on the mutation. However, a common consistent effect of FHM1 mutations is to increase Ca^{2+} influx through single human $Ca_V2.1$ channels in a broad voltage range, as given by the product of single-channel current and open probability ($i*p_o$; Figure 1.5, right) (Hans et al., 1999; Tottene et al., 2002, 2005; Pietrobon, unpublished data). The increased single channel Ca^{2+} influx is a consequence of an increased channel open probability (p_o) mainly due to a shift to lower voltages of channel activation (Figure 1.5, left). Consistent shifts to lower voltages of the current activation of human FHM1 mutants were also revealed measuring

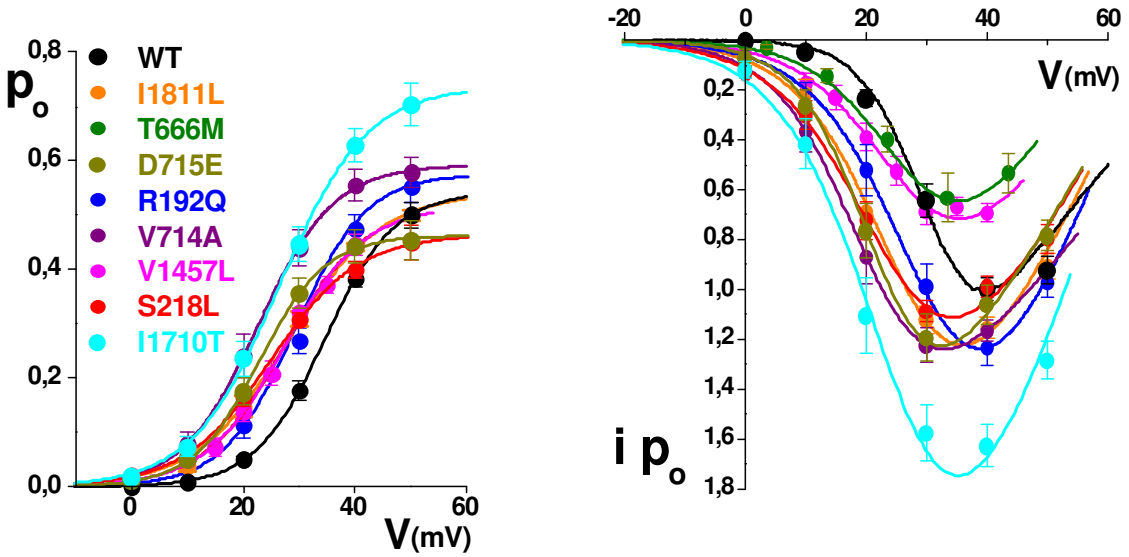

Figure 1.5. FHM1 mutations increase Ca^{2+} influx through single human $Ca_V2.1$ channels, as given by the product $i*p_o$ (right), as consequence of an increased channel open probability (p_o) mainly due to a shift to lower voltages of channel activation (left; adapted from Haan et al., 1999; Pietrobon, unpublished data; Tottene et al., 2002, 2005)

whole-cell currents in both the heterologous expression system, and in transfected neurons (Hans et al., 1999; 2004; Tottene et al., 2002, 2005). However, in transfected cells overespressing $Ca_V2.1$ channels, the shift to lower voltages of channel activation and the increased channel open probability did not result, in most cases, in an increased whole-cell current density because all the FHM1 mutations analyzed produced alterations in the density of functional channels in the membrane. The alterations of the expression of functional recombinant $Ca_V2.1$ channels produced a consistent decreased of the whole-cell current $Ca_V2.1$ density at high voltages in transfected granule cells and different effects, depending on the mutation, in the heterologous expression system (Hans et al., 1999; Tottene et al., 2002, 2005). These conflicting results lifted the necessity to create a knock-in mice carrying FHM1 mutation to study the mutant $Ca_V2.1$ channels expressed at their endogenous level.

1.6.1 The R192Q FHM1 mutation

The R192Q FHM1 mutation consisting in the substitution of a positively charged arginine with a neutral, non polar glutamine in the S4 segment of domain I, which form part of the voltage sensor, induces in patients pure attacks of hemiplegic migraine without either more severe symptoms (e.g fever, seizures, coma), neither cerebellar neurological dysfunctions (Ophoff et al., 1996).

The study of the functional consequences of the R192Q mutation in HEK293 cells revealed an increased single-channel influx through recombinant $Ca_V2.1$ channels mainly due to an increased channel open probability in all the voltage range (Hans et al., 1999; Figure 1.5). Whereas, the mutation in the heterologous expression system induced an increased whole-cell $Ca_V2.1$ current density as a consequence of an increased membrane expression of functional recombinant $Ca_V2.1$, it caused the opposite effect in transfected granule cells from $Ca_V2.1$ $\alpha_1^{-/-}$ mice (Hans et al., 1999; Tottene et al., 2002). In addition, the R192Q did not change the properties of inactivation and recovery from inactivation of the recombinant $Ca_V2.1$ channels (Hans et al., 1999).

In 2004 van den Maagdenberg et al. reported the generation of a knock-in (KI) mouse obtained introducing the human R192Q FHM1 mutation at the corresponding position in the mouse orthologous *cacna1a* gene, by homologous recombination. The homozygous R192Q KI mice were healthy and did not exhibit an overt phenotype. Moreover, no different amount of the mutant $Ca_V2.1$ α1 protein was found, as well as, no apparent brain cytoarchitectural abnormalities were observed. The whole-cell $Ca_V2.1$ current in cerebellar granule cells of the KI mouse was larger than in wild-type (WT)

neurons in a broad voltage range close to the threshold of channel activation and similar to that of WT neurons at higher voltages (Figure 1.6). In contrast, the densities of the L-, N-, and R-type Ca^{2+} current were not altered in KI neurons. The changes in whole-cell

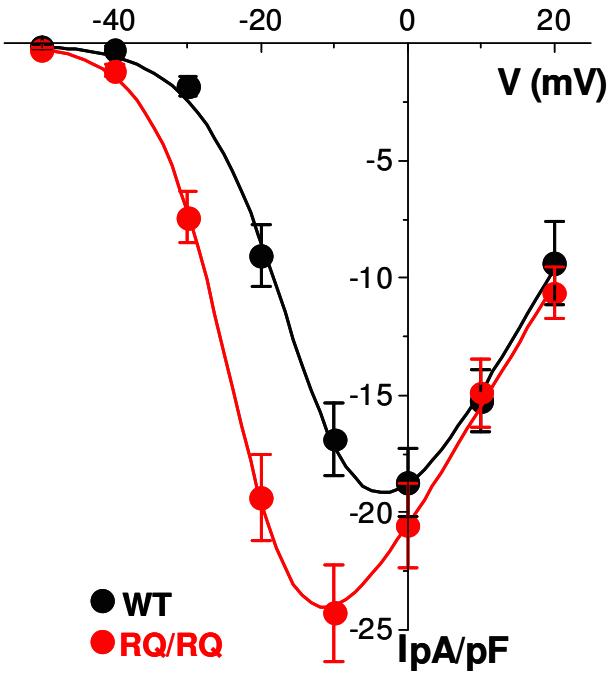

Figure 1.6. Increased $Ca_V2.1$ current density in cerebellar granule cells of homozygous R192Q KI mice, adapted from van den Maagdenberg et al. (2004)

$Ca_V2.1$ current density in neurons from KI mice were very similar to the changes in single channel Ca^{2+} influx of mutant recombinant human $Ca_V2.1$ channels, indicating that FHM1 mutations produce a similar gain-of-function of Ca^{2+} influx through mouse and human Ca^{2+} channels; mutant $Ca_V2.1$ channels open at lower voltages than WT channels and Ca^{2+} influx through mutant channels can occurs in response to small depolarizations insufficient to open WT channels (Pietrobon, 2007). Moreover, the similar $Ca_V2.1$ current densities found in both KI and WT neurons at high voltages, where open probabilities are maximal for both mutant and WT channels, revealed a similar density of functional channels (van den Maagdenberg et al., 2004). The unchanged density of functional channels when mutant $Ca_V2.1$ channels are expressed at their endogenous level in KI neurons demonstrated that the alterations in functional channel density found in transfected granule cells neurons and in the heterologous system might have been an artefact due to overexpression (Hans et al., 1999; Tottene et al., 2002; van den Maagdenberg et al., 2004).

The authors reported also an increased neurotransmission at the neuromuscular junctions (NMJ) of R192Q KI mice, in conditions where saturation of the synaptic Ca^{2+} sensors was not reached and the release probability was low (van den Maagdenberg et al., 2004). Indeed, they found that the evoked release at low Ca^{2+} and the spontaneous release, both controlled by $Ca_V2.1$ channels, were increased in KI mice. In addition, a lower threshold for CSD induction, an increased velocity of propagation, and a longer duration of the CSD depolarization were found in the R192Q KI mice *in vivo*. This result support the hypothesis of an important role of CSD in the pathogenesis of FHM1 (Pietrobon, 2005; Pietrobon, 2007). Moreover, the CSD data from the R192Q KI mice and the natural *cacna1a* mutant *leaner* and *tottering* mice support a key role of $Ca_V2.1$ channels in the initiation and propagation of CSD. Indeed, the loss of function of $Ca_V2.1$ channels in *leaner* and *tottering* mice leads to a higher threshold for CSD induction, a lower velocity of propagation, and a shorter duration of the CSD depolarization *in vivo* (Ayata et al., 2000; Pietrobon, 2005, 2007). Similar inhibitory effects on CSD initiation, propagation and duration were produced *in vivo* by NMDA-receptors antagonists in a dose-dependent manner (Pietrobon, 2005, 2007). Moreover, a decrease in intracortical glutamate was measured by *in vivo* microdialysis during high K^+ exposure in *leaner* and *tottering* mice (Ayata et al., 2000). Thus, $Ca_V2.1$-dependent release of glutamate from cortical excitatory synapses appears crucial in determining both initiation and propagation of CSD (Pietrobon, 2005, 2007). Indeed, the increased neurotransmitter release at the NMJ found in the R192Q KI mice rise the possibility, considering the prominent role of $Ca_V2.1$ channels in controlling glutamate release from cortical synapses, of an increased action potential evoked Ca^{2+} influx at the cortical active zones, as a consequence of the gain of function of the FHM1 $Ca_V2.1$ channels, and an increased glutamate release at these synapses (Pietrobon and Striessnig, 2003; van den Maagdenberg et al., 2004).

Although the mechanisms for initiation and propagation of CSD are not completely understood, is known that the interventions that can produce experimental CSD in normally metabolizing cortical tissue (such as electrical stimulation or high K^+) induce an anomalous increase in the extracellular concentration of K^+ ions and a sustained neuronal depolarization accompanied by an increase in neuronal firing (Pietrobon, 2007). With sufficiently intense stimuli, CSD ignition occurs when the regulatory mechanisms that normally keep the extracellular $[K^+]_o$ within the physiological range are overwhelmed by the build-up of $[K^+]_o$ via a positive feedback cycle that makes self-regenerating the initially gradual neuronal depolarization; this positive feedback cycle initiates when a sufficient number of V-dependent and/or $[K^+]_o$-

dependent cationic channels are activated to generate a net sustained inward current, with consequent further depolarization and further increase of the local $[K^+]_o$, leading to further activation of the cationic channels (Pietrobon, 2007; Somjen, 2001). The nature of these cationic channels remains unclear and controversial (Somjen, 2001), although there is strong pharmacological support for a key role of NMDA receptors, as above described (Pietrobon, 2005, 2007), and clear evidence that CSD initiates and propagates at the level of the dendrites of pyramidal cells (Pietrobon, 2007; Somjen, 2001) and involves an increased conductance in specific dendritic subregions (Canals et al., 2005). The proposed model for described CSD induction and propagation is based on the pivotal role played by both NMDA receptors and $Ca_V2.1$ channels (Pietrobon, 2005, 2007). Indeed, this model proposes a positive-feedback mechanism in which excessive $Ca_V2.1$-dependent release of glutamate from synaptic terminals depolarized by high K^+ and consequent activation of NMDA receptors lead to further depolarization of the postsynaptic membrane, further increase of K^+ in the extracellular space (that has narrowed, mainly as a consequence of swelling of astrocytes due to KCl uptake), further release of glutamate, further activation of the NMDA receptor and so on. The CSD threshold is reached when the regulatory mechanisms that keep the local K^+ ions concentration in the physiological range are overwhelmed by the build-up of K^+ via this positive feedback loops. In FHM1 this might occur as a consequence of cortical hyperexcitability due to excessive release of glutamate secondary to increased Ca^{2+} influx through $Ca_V2.1$ channels, inducing an unbalance between excitation and inhibition in the cortical circuits (Pietrobon, 2005, 2007). Enhanced susceptibility to CSD in FHM1 can be explained considering that, given the lowered voltage threshold for activation of mutant $Ca_V2.1$ channels, an electrical stimulation of the cortex with lower stimuli and/or a lower increase of $[K^+]_o$ are necessary to open a sufficient number of $Ca_V2.1$ channels and release enough glutamate and open enough NMDA receptors to initiate the positive feedback cycle that ignites CSD and propagates it to adjacent tissue. Moreover, the predicted enhanced release of glutamate, as a consequence of the gain of function of $Ca_V2.1$ channels, could amplify the positive feedback.

To demonstrated this model, our laboratory recently measured the whole-cell $Ca_V2.1$ current density in cortical pyramidal cells freshly dissociated from homozygous R192Q FHM1 KI mice, and investigated the cortical excitatory neurotransmission in these mice by measuring evoked excitatory postsynaptic currents in microcultures of cortical pyramidal cells and evoked excitatory postsynaptic potentials in connected pairs of layer 2/3 pyramidal cells and fast-spiking interneurons in acute thalamocortical slices of the somatosensory cortex (Tottene et al., 2009). Moreover, inhibitory

neurotransmission at connected pairs of layer 2/3 fast-spiking interneurons and pyramidal cells was also investigated. In addition, was developed an *in vitro* model of CSD to investigate a possible causative link between enhanced glutamate release and CSD facilitation in KI mice.

As the study of excitatory neurotransmission in autaptic cultures from homozygous R192Q KI and WT mice was part of my PhD project, I reported the findings from Tottene et al. (2009) in the Result section.

1.6.2 The S218L FHM1 mutation

The S218L mutation, consisting in the substitution of a serine with a leucine in the loop between the S4 and S5 segments in the I domain of the $Ca_V2.1$ α_1 subunit, produces a sever clinical phenotype in which typical attacks of FHM triggered by minor head trauma are frequently followed, after a lucid interval, by deep (even fatal) coma or profound stupor, high fever, and long lasting severe cerebral oedema (Fitzsimons and Wolfenden, 1985; Kors et al., 2001). Among the 13 S218L mutation carriers, reported at present, 12 present also ataxia and cerebellar symptoms (cerebral and/or cerebellar atrophy) (Fitzsimons et al., 1985; Kors et al., 2001; Stam et al., 2009). Recently was reported the cases of patients from 2 different families that presented FHM attacks also not triggered by head trauma but, however, accompanied by fever, impaired consciousness, cerebellar atrophy, and long-lasting hemiparesis (Chan et al., 2008; Debiais et al., 2009). The electroencephalography revealed depressed activity controlateral to the hemiparesis during acute hemiplegic migraine attacks. Interestingly, patients during childhood experienced seizures, triggered or not by minor head trauma, without hemiplegic migraine attacks. This is the first report of experienced isolated seizures by FHM1 patients; instead, is known that FHM1 patients with two different mutations can present epileptic seizures during severe hemiplegic migraine attacks (Debiais et al., 2009; Ducros et al., 2001).

The functional consequences of mutation S218L on human $Ca_V2.1$ channels expressed in HEK293 cells and in cerebellar granule cells from $Ca_V2.1$ $\alpha_1^{-/-}$ mice have been studied (Tottene et al., 2005). The authors found that mutation S218L produces a shift to lower voltages of the single-channel activation curve and a consequent increase of single-channel ion influx through human $Ca_V2.1$ channels, as described for other FHM1 mutations (Hans et al., 1999; Tottene et al., 2002) (Figure 1.5). Interestingly, compared with the R192Q mutation and other FHM1 mutations, S218L is one of the mutations that produce the largest shift to lower voltages of channel activation and the

largest gain of function especially for small depolarizations, which are insufficient to open the WT channel (Tottene et al., 2005). As a consequence of the largest shift to lower voltages of human S218L channel activation, the $Ca_V2.1$ whole-cell current density in neurons expressing the S218L mutant was larger than in neurons expressing the WT channel in a broad voltage range; this was not found for the R192Q mutation and other FHM1 mutations expressed in cerebellar granule cells from $Ca_V2.1$ $\alpha_1^{-/-}$ mice (Tottene et al., 2002, 2005). Interestingly, mutant S218L channels open and carry significant current at voltages (-60 to -50 mV) close to the resting potential of many neurons (Tottene et al., 2005). In contrast, the smaller $Ca_V2.1$ whole-cell current density found at more positive voltages in neurons expressing the S218L mutant compared with that in neurons expressing the WT channel must be the result of a reduced density of functional channels in the membrane. This is consequent to an artefact due to overexpression as described below and reported above for the R192Q mutation (van den Maagdenberg et al., 2004, 2010).

Moreover, Tottene et al. (2005) reported that mutation S218L strongly affects the kinetics of inactivation of human $Ca_V2.1$ channels. On one hand it makes fast inactivation more rapid, and on the other hand it increases the contribution of slow inactivation, introducing a large component of current that inactivates very slowly. During long depolarizations, at voltages that are attained during CSD (-10, 0 mV), the extent of inactivation was considerably smaller than that of the WT channel. Moreover, the rate of recovery from inactivation of the S218L mutant was considerably faster.

Compared with the R192Q mutation and other FHM1 mutations, the combination of a particularly low threshold of activation, a smaller and slow inactivation during long depolarizations, and a particularly fast rate of recovery from inactivation are unique to the S218L mutant (Tottene et al., 2005). Authors proposed that because these unique properties, the S218L mutation carriers may have CSD with a longer duration, and whereas in other FHM1 patients minor head trauma does not have effects, it may induce CSD in the S218L mutation carriers.

The recent generation of a knock-in (KI) mouse obtained introducing the human S218L FHM1 mutation at the corresponding position in the mouse orthologous *cacna1a* gene, by homologous recombination, have permitted to test this hypothesis (van den Maagdenberg et al., 2010).

Authors reported that homozygous S218L (SL/SL) KI mice showed a complex neurological phenotype that is remarkably similar to that of what is seen in S218L mutation carriers (van den Maagdenberg et al., 2010). Most of the time, the mice appeared phenotypically normal, except for mild cerebellar ataxia, accompanied by

reduced dendritic arborisation of cerebellar Purkinje neurons. Moreover, two types of spontaneous attacks in SL/SL KI mice were observed: periodical attacks of transient unilateral weakness resulting in episodes of slow circular locomotion, which are consistent with the attacks of hemiparesis of FHM1, and attacks of generalized seizures that were in some cases fatal. In line with the latter observation, the life expectancy of mice was significantly decreased. The spontaneous episodes of hemiparesis, the fatal seizures, and the reduced life expectancy, all appeared to be unique to the SL/SL KI mice; none were observed in heterozygous S218L KI, nor in homozygous R192Q KI mice; the latter mutation causes pure attacks of FHM in patients. Consistent with observations in S218L patients, only SL/SL KI mice, exhibited significant brain oedema 24 hours after mild head impact, and 20 % of mice died after these mild impact experiments.

Moreover, accordingly with the gain of function of human recombinant S218L $Ca_V2.1$ channels, authors found that the whole-cell $Ca_V2.1$ current in cerebellar granule cells of SL/SL KI mice was larger than in WT mice in a broad voltage range close to the threshold of channel activation (van den Maagdenberg et al., 2010). On the other hand, the whole-cell $Ca_V2.1$ current density of the SL/SL KI mice, at positive voltages, was similar to that of WT mice, indicating a similar number of functional $Ca_V2.1$ channels in the membrane of KI and WT mice, as previously reported for homozygous R192Q (RQ/RQ) KI mice (van den Maagdenberg et al., 2004, 2010; Figure 1.7). The reported shift to lower voltages of $Ca_V2.1$ channel activation and the gain-of-function of the neuronal $Ca_V2.1$ current are about twice as large in homozygous compared to heterozygous S218L KI mice, revealing an allele-dosage effect consistent with dominance of the mutation in FHM1 patients (van den Maagdenberg et al., 2010). In addition, authors controlled that the enhanced P/Q- type Ca^{2+} influx was not accompanied by significant changes in the density current of other high voltage activated Ca_V channels, except for a slight decrease in L-type currents. The effects in SL/SL KI neurons were reminiscent of the changes seen in neurons of the clinically milder R192Q KI mice, but were stronger (van den Maagdenberg et al., 2004, 2010). As a consequence of the even lower activation threshold of S218L $Ca_V2.1$ channels, the gain of function of the $Ca_V2.1$ current at low voltages was more dramatic in SL/SL KI neurons than the gain of function previously observed in RQ/RQ KI neurons, leading to Ca^{2+} influx close to the resting potential (Figure 1.6 versus 1.7). Consistent with the latter observation, the S218L mutation produced a much larger increase in the frequency of spontaneous transmitter release events (MEPPs) at the NMJ when compared with the

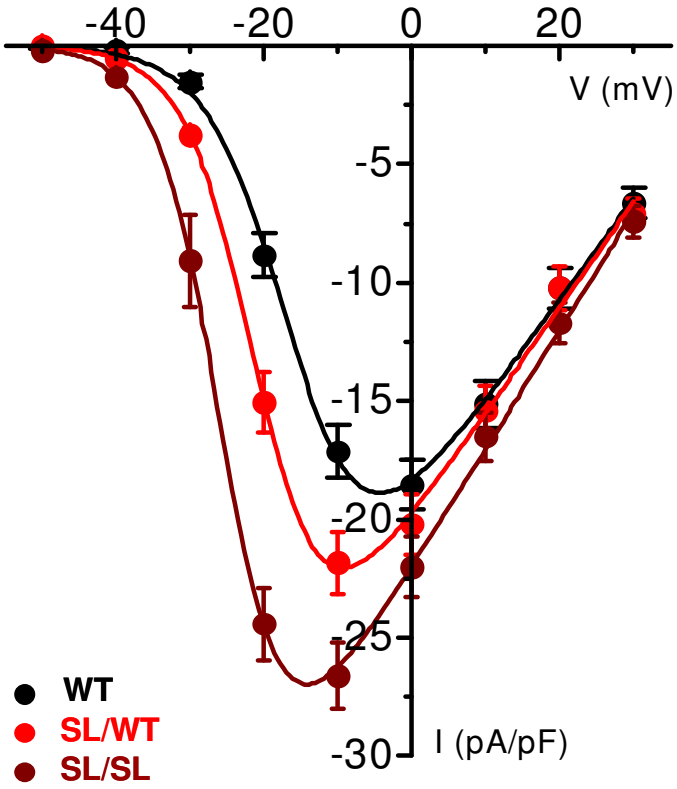

Figure 1.7. Increased $Ca_V2.1$ current density in cerebellar granule cells of homozygous and heterozygous S218L KI mice, adapted from van den Maagdenberg et al. (2010)

R192Q mutation; also for the enhanced neurotransmitter released was found an allele dosage effect for both heterozygous and homozygous S218L and R192Q KI mice (van den Maagdenberg et al., 2004, 2010). As a consequence of the increased gain of function of $Ca_V2.1$ channels in SL/SL neurons, and in correlation with the more severe phenotype of the S218L mutation, SL/SL mice showed both a lower threshold for CSD induction and a faster propagation of CSD waves compared to RQ/RQ KI mice *in vivo* (Figure 1.8) (van den Maagdenberg et al., 2004, 2010). Moreover, an allele dosage effect consistent with dominance of the mutation in FHM1 patients was found for the facilitation of induction and propagation of CSD in homozygous and heterozygous S218L and R192Q KI mice (Figure 1.8) (Eikermann-Haerter et al., 2009a; van den Maagdenberg et al., 2010). In addition, S218L mice had also an allele dosage-dependent increased probability of experiencing successive CSD events upon a single stimulus. Even if, authors reported a similar gain of function effects in $Ca_V2.1$ current density and CSD threshold and velocity in SL/WT and RQ/RQ KI mice, multiple CSD events were

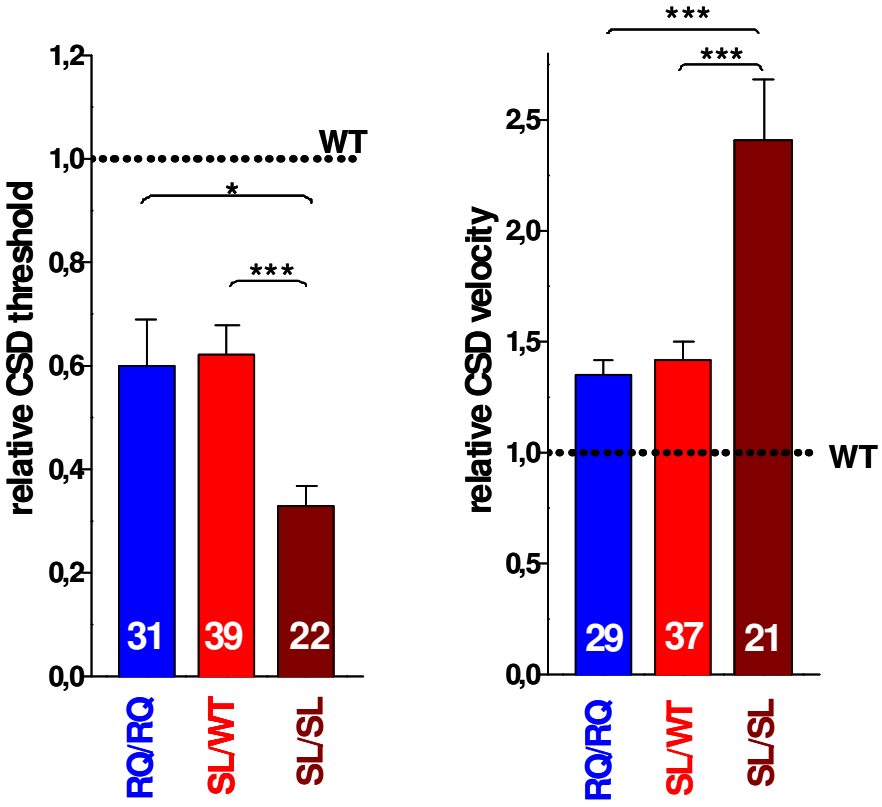

Figure 1.8. Relative CSD threshold and CSD velocity, compared to WT for SL/SL, SL/WT, and RQ/RQ KI mice, respectively (data reported are adapted from van den Maagdenberg et al., 2010)

seen only rarely in RQ/RQ KI mice and spontaneous neurotransmitter release at the NMJ was much larger in SL/WT compared to RQ/RQ KI mice, suggesting a larger Ca^{2+} influx at rest in SL/WT KI nerve terminals (van den Maagdenberg et al., 2010). Even if, the exact mechanism for recurrent CSD events following a single stimulus and the exact consequences remain to be determined, authors proposed that the unique combination of a particularly low threshold of activation and slow inactivation, and a particularly fast rate of recovery from inactivation of mutant S218L $Ca_V2.1$ channels, probably underlie the high incidence of repetitive CSDs through a mechanism sensitive at Ca^{2+} influx at rest and channel inactivation. Moreover, recurrent CSDs may open the blood-brain barrier and explain the delayed cerebral oedema and sever clinical phenotype of the S218L mutation (Pietrobon et al., 2007; van den Maagdenberg et al., 2010).

The major gain of function of S218L $Ca_V2.1$ channels compared to R192Q ones and the consequent larger susceptibility of both induction and propagation of CSD, further underline the pivotal role of P/Q-type Ca^{2+} channels and glutamate release in the proposed model of CSD induction, as described in the previous paragraph.

In line with the proposed model, one would predict also for the S218L FHM1 mutation an increased action potential evoked Ca^{2+} influx through cortical presynaptic $Ca_V2.1$ channels and an increased glutamate release at cortical synapses (Pietrobon, 2007). Because the larger facilitation of CSD in SL/SL than in RQ/RQ KI mice, and in correlation with the more severe phenotype, the S218L should cause a larger gain of function of the cortical excitatory neurotransmission. To answer this question, I investigated cortical excitatory neurotransmission in heterozygous S218L KI mice by measuring evoked excitatory postsynaptic currents in microcultures of cortical pyramidal cells. We have decided to study heterozygous S218L KI mice for different reasons: heterozygous mice are more healthy compared to homozygous mice; FHM1 is a dominant disease so in human it is expressed in heterozygouses, and we predict an allele dosage effect also for neurotransmission as it was found for P/Q current density, as well as, for facilitation of CSD (van den Maagdenberg et al., 2010).

1.6.3 FHM1 mutations alter G protein inhibition of $Ca_V2.1$ channels

A major modulation of voltage-dependent P/Q Ca^{2+} channels, with high relevance in the control of synaptic transmission, occurs via the receptor-triggered release of Gβγ subunits (Tedford and Zamponi, 2006), as previously described in the paragraph 1.3. Gβγ dimmers bind to multiple regions on the α_{1A} subunit to produce membrane-delimited voltage-dependent inhibition of the Ca^{2+} channel (De Waard et al., 2005). Inhibited channels activate at more depolarized voltage and with slower kinetics, due to a restricted movement of the voltage sensor that makes the channel more reluctant to open (Jones et al., 1997). As already described, the Gβγ binding produces only the silencing of channel activity, whereas Gβγ unbinding, which follows channel activation, induces the slowing of activation and inactivation kinetics and the depolarizing shift of the voltage dependence of channel activation, as well as, the current recovery from inhibition (Weiss et al., 2006, 2008). It was demonstrated that the speed of Gβγ unbinding is determined by the voltage dependence of channel activation, and the kinetics of channel inactivation during membrane depolarization. In particular the time costant of G protein dissociation follows the voltage dependence of channel opening (Weiss et al., 2006), and channels inactivation kinetics accelerates the recovery from inhibition but reduces the temporal window in which the process can take place, thereby reducing the maximal extent of current recovery (Weiss et al., 2007). Because FHM1 mutations affect activation and inactivation properties of $Ca_V2.1$ channels, different authors have studied if the direct G protein inhibition of mutated $Ca_V2.1$ channels is altered with interestingly consequences for the excitability of the cortex and the CSD

induction (Melliti et al., 2003; Serra et al., 2009; Weiss et al., 2008). A decrease in the direct inhibitory pathway carried by Gβγ following G protein-coupled D2 dopamine receptor or μ-opioid receptor stimulation has been reported for the R192Q and S218L FHM1 mutations expressed in HEK293 cells (Melliti et al, 2003; Weiss et al., 2008). However, an apparent controversy concerning the mechanism by which those FHM1 mutations reduce G protein inhibition of P/Q channels arise from these reports. Indeed, Melliti et al. (2003) proposed that R192Q mutation might modify the molecular mechanisms by which Gβγ dimmers association to α_{1A} alter voltage sensor movement in response to membrane potential changes, leading to a reduced extent of G protein inhibition but without affecting binding or unbinding rates. Authors postulated that the mutation R192Q, by neutralizing a positive charge in the IS4 segment, might modify electrostatic interactions and reduce the effectiveness of G protein-induced charge trapping, resulting in attenuated inhibition and prepulse facilitation of Ca^{2+} current. A more detailed study by Weiss et al. (2008) showed that the S218L and, to a lesser extent, the R192Q FHM1 mutation promote accelerated Gβγ dissociation from the activated channel without affecting the maximal G protein inhibition of P/Q channels measured at the start of the depolarization. Moreover, authors found that only the S218L mutation decreases the maximal extent of current recovery, measured 200 ms after the start of depolarization where the process of recovery is maximal and the S218L mutation causes faster inactivation kinetics, as also reported in Tottene et al. (2005). These results are consistent with the data showing that faster inactivation kinetics accelerate the recovery from inhibition but reduce the temporal window in which the process can take place (Weiss et al., 2007, 2008). The controversy results are explained by the fact that in the first study, G protein inhibition levels were measured at the peak of the current, time point where significant relief from G protein inhibition may already have occurred giving the impression of reduced G protein inhibition for the mutant channel due to a faster Gβγ dissociation (Melliti et al., 2003; Weiss et al., 2008).

Hence, by promoting a faster relief from G protein inhibition, the S218L, and less the R192Q mutation, diminish the strength of this negative feedback and are therefore likely to contribute to the gain of function of $Ca_V2.1$ channels. As a consequence, the combined diminution of channel activation threshold and decrease of the G protein mediated inhibitory pathway may contribute together to the enhanced susceptibility to CSD found in FHM1 KI mice (Melliti et al., 2003; Weiss et al., 2008).

Recently Serra et al. (2009) demonstrated that the enhanced relief of G protein inhibition on FHM1 $Ca_V2.1$ channels is probably a common consequence of different FHM1 mutations. Authors found that the Y1245C mutation, localized in the S1 segment

in the III domain of the $Ca_V2.1$ α_1 subunit, causes a hyperpolarized shift of current activation and steady-state inactivation curves, a faster activation kinetic but does not change the kinetics of inactivation and recovery from inactivation. Interestingly, also this mutation accelerates Gβγ dissociation from the channel, and reduces Gβγ inhibition of $Ca_V2.1$ channels calculated at the peak of current.

Hence, to investigate if the effect of FHM1 mutations on G protein inhibition of recombinant $Ca_V2.1$ channels is present also in FHM1 KI neurons and may contribute to a cortical hypereccitability and to the CSD facilitation, I measured cortical excitatory postsynaptic currents during G protein modulation, through $GABA_B$ receptors activation, in microcoltures of cortical pyramidal neurons from neonatal WT, heterozygous S218L KI, and homozygous R192Q KI mice.

2. RESULTS, DISCUSSION AND SUPPLEMENTAL DATA (I)

Neuron
Article

Enhanced Excitatory Transmission at Cortical Synapses as the Basis for Facilitated Spreading Depression in $Ca_V2.1$ Knockin Migraine Mice

Angelita Tottene,[1,4] Rossella Conti,[1,4] Alessandra Fabbro,[1] Dania Vecchia,[1] Maryna Shapovalova,[1] Mirko Santello,[1] Arn M.J.M. van den Maagdenberg,[2,3] Michel D. Ferrari,[2] and Daniela Pietrobon[1,*]
[1]Department of Biomedical Sciences, University of Padova and CNR Institute of Neuroscience, Viale G. Colombo 3, 35121 Padova, Italy
[2]Department of Neurology
[3]Department of Human Genetics
Leiden University Medical Centre, PO Box 9600, 2300 RC, 2333 AL Leiden, The Netherlands
[4]These authors contributed equally to this work
*Correspondence: daniela.pietrobon@unipd.it
DOI 10.1016/j.neuron.2009.01.027

SUMMARY

Migraine is a common disabling brain disorder. A subtype of migraine with aura (familial hemiplegic migraine type 1: FHM1) is caused by mutations in $Ca_V2.1$ (P/Q-type) Ca^{2+} channels. Knockin mice carrying a FHM1 mutation show increased neuronal P/Q-type current and facilitation of induction and propagation of cortical spreading depression (CSD), the phenomenon that underlies migraine aura and may activate migraine headache mechanisms. We studied cortical neurotransmission in neuronal microcultures and brain slices of FHM1 mice. We show gain of function of excitatory neurotransmission due to increased action-potential-evoked Ca^{2+} influx and increased probability of glutamate release at pyramidal cell synapses but unaltered inhibitory neurotransmission at fast-spiking interneuron synapses. Using an in vitro model of CSD, we show a causative link between enhanced glutamate release and CSD facilitation. The synapse-specific effect of FHM1 mutations points to disruption of excitation-inhibition balance and neuronal hyperactivity as the basis for episodic vulnerability to CSD ignition in migraine.

INTRODUCTION

Migraine is a common episodic brain disorder affecting more than 10% of the population; it is typically characterized by recurrent attacks of disabling headaches and associated autonomic symptoms. In one-third of patients, the headache is preceded by transient neurological symptoms (migraine with aura). Migraine arises from a primary brain dysfunction that leads to activation and sensitization of the trigeminovascular system, including trigeminal nociceptive afferents innervating the meninges, and as a consequence to headache (Goadsby et al., 2002; Pietrobon, 2005b; Pietrobon and Striessnig, 2003). A major incompletely understood issue in the neurobiology of migraine concerns the nature and mechanisms of the primary brain dysfunction that causes migraine. Neuroimaging findings indicate that migraine aura is due to cortical spreading depression (CSD), a wave of strong neuronal depolarization that slowly progresses across the cerebral cortex, generating a transient intense spike activity followed by long-lasting neural suppression (Bowyer et al., 2001; Hadjikhani et al., 2001; Lauritzen, 1994). Recent animal studies support the idea that CSD may also trigger the mechanisms for migraine headache. In the rat cortex, a single CSD can activate the trigeminovascular system (Bolay et al., 2002), and established migraine prophylactic agents from five different pharmacological classes elevate the stimulation threshold for CSD initiation (Ayata et al., 2006). Furthermore, knockin (KI) mice carrying a human mutation causing familial hemiplegic migraine type 1 (FHM1) show a decreased threshold for CSD initiation and an increased velocity of CSD propagation (van den Maagdenberg et al., 2004).

FHM1 is a rare autosomal dominant subtype of migraine with aura, which is caused by missense mutations in the *CACNA1A* gene encoding the pore-forming subunit of voltage-gated $Ca_V2.1$ (P/Q-type) Ca^{2+} channels (Ophoff et al., 1996). $Ca_V2.1$ channels are located in somatodendritic membranes and presynaptic terminals throughout the brain (Westenbroek et al., 1995), where they play a dominant role in controlling neurotransmitter release (Pietrobon, 2005a). Apart from the hemiparesis during aura, the headache, autonomic, and aura symptoms of typical attacks of FHM1 are similar to those of the common forms of migraine with aura, and most FHM1 patients also have normal migraine attacks (Thomsen et al., 2002, 2003). Investigation of the cortical mechanisms that produce facilitation of CSD in the FHM1 KI mouse models may thus provide unique insights into the unknown mechanisms that lead to CSD susceptibility and initiate migraine attacks in patients.

Most studies of the functional consequences of FHM1 mutations support the conclusion that they produce gain of function of $Ca_V2.1$ channels (Pietrobon, 2005a, 2007). In particular, the analysis of the single-channel properties of human $Ca_V2.1$ channels carrying eight different mutations revealed a consistent

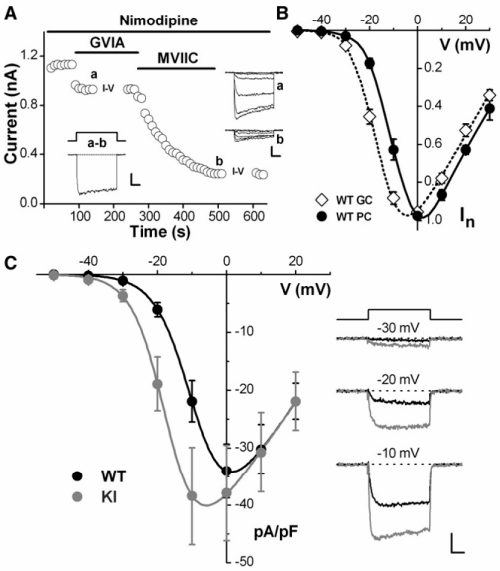

Figure 1. The P/Q-Type Ca^{2+} Current Density Is Increased in Acutely Dissociated Cortical Pyramidal Cells of R192Q KI Mice

(A) Peak whole-cell Ba^{2+} current versus time recorded from a KI cortical pyramidal cell during depolarizations at −10 mV every 10 s from −70 mV, before and after application of the indicated drugs. Inset: P/Q current trace obtained as the difference between traces at times a and b; on the right: representative traces at increasing voltage from −50 to 0 mV, taken during current-voltage (I-V) measurement at times a and b. Scale bars: 10 ms, 200 pA.

(B) Average normalized P/Q-type current as a function of voltage in dissociated cortical pyramidal cells (PC, ●, n = 10) and in cerebellar granule cells in primary culture (GC, ◇, n = 9) from WT mice. Lines are fits of equation: $I = G(V - E_{rev})\{1+\exp[(V_{1/2} - V)/k]\}^{-1}$.

(C) P/Q-type current density as a function of voltage in WT and KI cortical pyramidal cells. Average normalized I-V curves (WT, n = 10; KI, n = 9) were multiplied by the average maximal current density (n = 14 for both WT and KI). Fitting the I-V curves gave $V_{1/2} = -8 \pm 1$ mV for WT (n = 10) and $V_{1/2} = -16 \pm 1$ mV for KI (n = 9). Inset: pooled WT (black) and KI (gray) P/Q current traces at −30, −20, and −10 mV. Scale bars: 10 ms, 10 pA/pF.

Error bars: SEM.

increase in channel open probability and single-channel Ca^{2+} influx in a broad voltage range, mainly due to a shift to lower voltages of channel activation (Tottene et al., 2002, 2005). A similar increase in P/Q-type Ca^{2+} current density was measured in cerebellar neurons of FHM1 KI mice (Pietrobon, 2007; van den Maagdenberg et al., 2004). At the neuromuscular junction of these mice, evoked synaptic transmission was unaltered at physiological Ca^{2+} ion concentrations but increased at 0.2 mM Ca^{2+} (Kaja et al., 2005; van den Maagdenberg et al., 2004). So far, cortical synaptic transmission in FHM1 KI mice has not been studied.

Here, we investigated cortical excitatory neurotransmission in KI mice carrying the human R192Q FHM1 mutation (van den Maagdenberg et al., 2004) by measuring evoked excitatory postsynaptic currents in microcultures of cortical pyramidal cells and evoked excitatory postsynaptic potentials in connected pairs of pyramidal cells and fast-spiking interneurons in acute cortical slices. Our data show increased strength of cortical excitatory synaptic transmission due to increased action-potential-evoked Ca^{2+} influx through presynaptic $Ca_V2.1$ channels and increased probability of glutamate release in FHM1 KI mice. In striking contrast with excitatory neurotransmission, inhibitory neurotransmission at connected pairs of fast-spiking interneurons and pyramidal cells was unaltered in FHM1 mice, despite being also initiated by $Ca_V2.1$ channels. By using an in vitro model of CSD, we provide direct evidence that the gain of function of glutamate release at pyramidal cell synapses may explain the facilitation of experimental CSD in FHM1 KI mice.

RESULTS

We first measured whole-cell P/Q-type Ca^{2+} current density as a function of voltage in cortical pyramidal cells freshly dissociated from P13–15 wild-type (WT) and FHM1 KI mice carrying the R192Q mutation. The P/Q-type current component was obtained as the amount of whole-cell current inhibited by ω-CTxMVIIC (MVIIC, 3 μM) applied after the specific N-type channel blocker ω-CgTxGVIA (GVIA, 1 μM), in the presence of nimodipine (5 μM) to inhibit L-type channels (Figure 1A). Previous investigation of neuronal $Ca_V2.1$ channels in R192Q KI mice was performed in cerebellar granule cells, where they were found to activate at about 9 mV more negative voltages than the corresponding WT channels (van den Maagdenberg et al., 2004). The $Ca_V2.1$ channels expressed in cortical pyramidal cells are functionally different from those in cerebellar granule cells, as shown by the different P/Q-type current-voltage (I-V) relationships recorded under identical conditions in the two types of neurons from WT mice (Figure 1B). Fitting of the normalized I-V relationships gave half voltage of activation values ($V_{1/2}$) of −8 ± 1 (n = 10) and of −15 ± 2 mV (n = 9) for $Ca_V2.1$ channels in cortical and cerebellar neurons, respectively. While the molecular mechanism(s) underlying the different activation properties of cortical and cerebellar $Ca_V2.1$ channels remains unknown, possible mechanisms include the expression of different splicing variants of the $Ca_V2.1\alpha_1$ subunit and/or the expression of different auxiliary subunits and/or other modulatory proteins. Nonetheless, the gain-of-function effect of the FHM1 mutation was similar for the functionally different cortical and cerebellar $Ca_V2.1$ channels, as shown by the (8 mV) shift to lower voltages of channel activation and the increase in P/Q current density in a wide voltage range in cortical pyramidal cells of KI compared to WT mice (Figure 1C). At higher voltages, eliciting maximal $Ca_V2.1$ channel open probability (Hans et al., 1999), P/Q current densities were similar in KI and WT cortical pyramidal cells, indicating similar densities of functional $Ca_V2.1$ channels (van den Maagdenberg et al., 2004). Also similar were the maximal N- and R-type Ca^{2+} current densities (N-type: 13 ± 2 pA/pF, n = 19, versus 17 ± 2 pA/pF, n = 16; R-type: 17 ± 2 pA/pF, n = 13, versus 20 ± 5 pA/pF, n = 14, in WT versus KI), thus confirming the absence of compensatory changes in the other Ca^{2+} channels previously shown in cerebellar neurons (van den Maagdenberg et al., 2004).

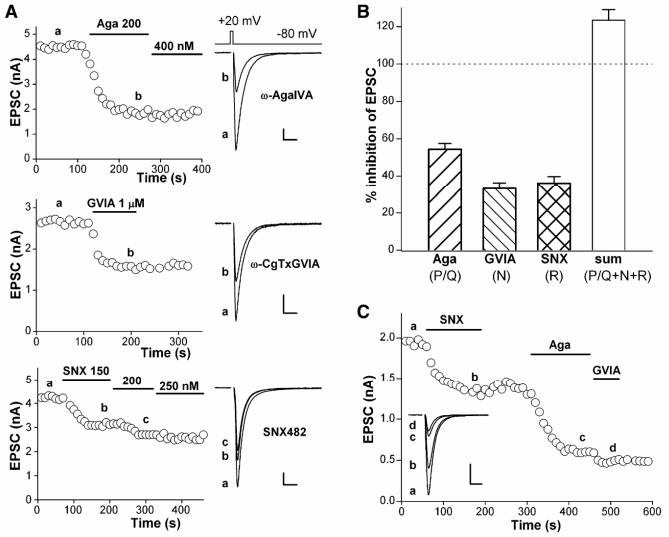

Figure 2. Multiple Types of Ca^{2+} Channels, Including P/Q-Type, Contribute to Excitatory Synaptic Transmission at Cortical Pyramidal Cells in Microculture from WT Mice

(A) Evoked EPSCs amplitudes versus time in three different WT cortical pyramidal cells in microculture before (a) and during (b and c) application of ω-AgaIVA, ω-CgTxGVIA, and SNX482, respectively. Insets: EPSC traces taken at times a, b, and c. Scale bars: 10 ms, 0.5 nA.

(B) Contribution of P/Q-, N-, and R-type Ca^{2+} channels to neurotransmission (at 8–14 DIV) evaluated from the fraction of the EPSC inhibited by Aga 200 nM (n = 18), GVIA 1 μM (n = 20), and SNX 200 nM (n = 19) in protocols like those in (A).

(C) EPSCs versus time evoked in a WT cortical pyramidal cell during sequential application of SNX 200 nM, Aga 200 nM, and GVIA 1 μM as indicated. Inset: EPSC traces taken at times a, b, c, and d. Scale bars: 10 ms, 0.5 nA.

Error bars: SEM.

To establish whether FHM1 mutations lead to increased action potential (AP)-evoked Ca^{2+} influx through presynaptic $Ca_V2.1$ channels and to increased glutamate release at cortical pyramidal cell synapses, we investigated excitatory neurotransmission in microcultures of cortical neurons from neonatal WT and R192Q KI mice. Single cortical neurons grown on glial microislands form synaptic connections onto themselves (autapses) with properties very similar to those of synapses between neurons (Bekkers and Stevens, 1991). In single cortical pyramidal cells in culture for 8–14 days (DIV), large excitatory postsynaptic currents (EPSCs) were evoked by brief depolarizing voltage steps eliciting an AP in the unclamped axonal processes (Figure 2A). As in other glutamatergic synapses, multiple types of Ca^{2+} channels contribute to synaptic transmission at cortical pyramidal cell autapses from WT mice (Figures 2A and 2B). The contribution of P/Q-, N-, and R-type Ca^{2+} channels was evaluated from the fraction of the EPSC inhibited by saturating concentrations of the specific inhibitors ω-AgaIVA (Aga, 200 nM: 54% ± 3%, n = 18), GVIA (1 μM: 33% ± 3%, n = 20), and SNX482 (SNX, 200 nM: 36% ± 4%, n = 19). Nimodipine (5 μM) was without effect (n = 5, data not shown). Since some native R-type Ca^{2+} channels are not inhibited by even higher concentrations of SNX (Sochivko et al., 2003; Tottene et al., 2000), the contribution of R-type channels may be underestimated by our protocol. Indeed, the three toxins together did not completely block synaptic transmission (residual EPSC: 14% ± 3%, n = 9) (Figure 2C), and the addition of ω-CTxMVIIC (3 μM) after the three toxins did not further inhibit the residual EPSC (n = 5, data not shown). Considering the nonlinear power relationship between presynaptic Ca^{2+} influx and neurotransmitter release (Schneggenburger and Neher, 2000), the superadditivity of the fractional EPSC inhibition by the specific blockers (Figure 2B: sum = 123% ± 6%) indicates that P/Q-, N-, and R-type Ca^{2+} channels cooperate (with overlapping local Ca^{2+} domains) in controlling release at individual synapses of cortical pyramidal cells in microculture.

If the FHM1 mutation leads to increased AP-evoked Ca^{2+} influx through $Ca_V2.1$ channels located at the active zones, the probability of vesicle release at KI synapses should be larger than that at WT synapses; one then predicts a larger AP-evoked EPSC amplitude in single cortical pyramidal neurons from KI mice accompanied by a larger contribution of P/Q-type Ca^{2+} channels to synaptic transmission. Indeed, the average EPSC amplitude was 1.7 times larger in KI than in WT mice (Figure 3A: 4.3 ± 0.3 nA [n = 111] in KI versus 2.6 ± 0.3 nA in WT [n = 114]), and a larger fraction of the EPSC was inhibited by Aga in KI neurons (Figure 3B: 78% ± 3%, n = 18), revealing a larger contribution of P/Q-type Ca^{2+} channels to neurotransmission. Accordingly, in additional experiments, a lower fraction of the EPSC was inhibited by GVIA in KI neurons (Figure 3B: 20% ± 2%, n = 22). These findings are consistent with and support the conclusion that the FHM1 mutation leads to increased AP-evoked Ca^{2+} influx through presynaptic $Ca_V2.1$ channels and, as a consequence, to increased probability of release at individual synapses on cortical pyramidal cells.

The analysis of the absolute (rather than fractional) sizes of the components of the EPSC inhibited by either Aga (Figure 3C) or GVIA (Figure 3D) indicates that the increased probability of release completely accounts for the increased EPSC amplitude in KI mice. In fact, both the amplitudes of the Aga-sensitive component (a measure of the amount of glutamate release controlled by P/Q-type channels: Figure 3C) and of the GVIA-insensitive component (a measure of the amount of release controlled by P/Q- and R-type channels: Figure 3D) were more

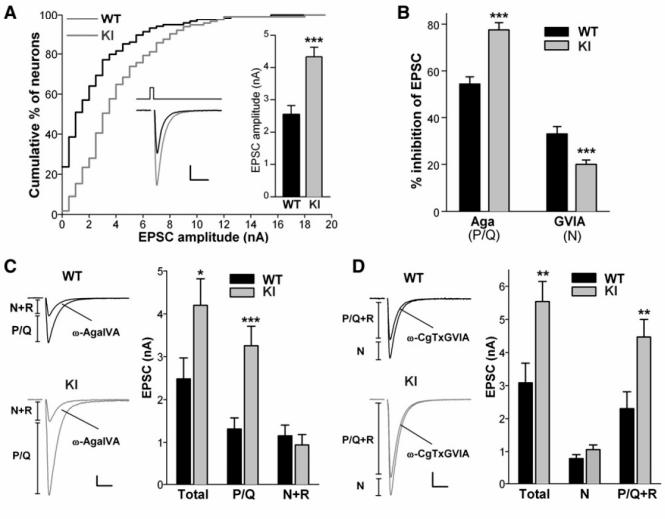

Figure 3. Increased EPSC Amplitude and Increased Contribution of P/Q-Type Ca^{2+} Channels to Excitatory Neurotransmission in Cortical Pyramidal Cell Autapses of R192Q KI Mice

(A) Cumulative distribution and average value (right inset) of evoked EPSC amplitudes from WT (n = 114) and KI (n = 111) pyramidal cells. Left inset: EPSC traces from a representative WT and KI neuron. Scale bars: 10 ms, 1 nA. The relative number of neurons recorded from WT and KI mice at different DIV were closely matched, because EPSCs amplitude continued to increase from 8 to 14 DIV in both control and KI neurons (Takada et al., 2005): WT n = 27, 43, and 44 and KI n = 29, 37, and 45 at DIV 8–9, 10–11, and 12–14, respectively.

(B) Contribution of P/Q- and N-type Ca^{2+} channels to neurotransmission evaluated from the fraction of the EPSC inhibited by Aga 200 nM and GVIA 1 μM in KI neurons (n = 18 and 22) compared to WT (n = 18 and 20) in protocols like those in Figure 2A. The relative number of neurons recorded from WT and KI mice at different DIV were closely matched.

(C) Average values of the amplitudes of the EPSC (total) and its Aga-sensitive (P/Q) and Aga-insensitive (N + R) components (same neurons as in [B]). The P/Q and N + R components for each cell were obtained as shown in the representative traces on the left, as difference of EPSC amplitude before and after Aga (P/Q) and as EPSC amplitude remaining after Aga (N + R). Scale bars: 10 ms, 1 nA.

(D) Average values of the amplitudes of the EPSC (total) and its GVIA-sensitive (N) and GVIA-insensitive (P/Q + R) components (same neurons as in [B]). The N and P/Q + R components for each cell were obtained as shown in the representative traces on the left. Scale bars: 10 ms, 1 nA.

Error bars: SEM.

than two times larger in KI than in WT mice, and the difference in size of these components between the two genotypes (P/Q: 1.9 ± 0.5 nA and P/Q + R: 2.2 ± 0.7 nA) was similar to the difference in size of the corresponding total EPSC amplitude (1.7 ± 0.8 nA and 2.5 ± 0.9 nA in Figures 3C and 3D, respectively). On the other hand, both the amplitudes of the Aga-insensitive component (a measure of the amount of glutamate release controlled by N- and R-type channels: Figure 3C) and of the GVIA-sensitive component (a measure of the amount of release controlled by N-type channels: Figure 3D) were similar in KI and WT mice. These findings are inconsistent with significant changes in the number of synapses (and/or size of the readily releasable pool of vesicles [RRP] at each synapse) in KI neurons, because changes in the number of synapses or in RRP would equally affect the toxin-sensitive and toxin-insensitive components of the EPSC. The unaltered amount of glutamate release controlled by N- and R-type Ca^{2+} channels in KI mice is also consistent with the absence of compensatory changes in the N- and R-type Ca^{2+} currents measured at the soma of dissociated cortical pyramidal cells and suggests their absence also at the active zones.

Further supporting the conclusion of an increased AP-evoked Ca^{2+} influx through presynaptic mutant $Ca_V2.1$ channels is the finding that in KI mice the Ca^{2+} dependence of the EPSC was shifted to the left with unaltered cooperativity coefficient (Figure 4A); the EPSC amplitude increased only 10% when the concentration of extracellular Ca^{2+} ions was raised above 2 mM in contrast with the more than 60% increase in WT mice. Note that the similar steepness of the Ca^{2+} dose-response curves in KI and WT synapses is also consistent with a relative homogeneous distribution of P/Q channels at individual cortical autapses (Reid et al., 1998): a nonuniform distribution would lead to a broadened dose-response curve because only synapses containing P/Q channels would have a lower EC_{50} in KI mice.

Further supporting the conclusion that the FHM1 mutation leads to an increased probability of vesicle release at individual cortical synapses are also the changes in short-term synaptic plasticity revealed in KI mice (Figure 4B). On average, WT synapses showed depression during trains of five action potentials at 50 Hz (paired-pulse ratio, PPR = 0.87 ± 0.03, n = 22, in the presence of GVIA). Short-term depression (STD) was larger in KI synapses (PPR = 0.72 ± 0.04, n = 21, $p < 0.01$), as expected for an increased probability of vesicle release in KI mice if at least part of the depression is due to vesicle depletion (and/or is anyway due to a presynaptic Ca^{2+}-dependent mechanism). Indeed, a similar relative increase in STD at these synapses was found when the probability of release was increased by raising the external Ca^{2+} concentration from 2 to 4 mM (from PPR = 0.82 ± 0.06 to 0.67 ± 0.07, n = 8, $p < 0.001$).

To investigate whether homeostatic compensatory mechanisms were present as an attempt to compensate for the increased glutamate release in KI mice (Turrigiano and Nelson, 2004), we measured miniature EPSCs (mEPSCs) from pyramidal cells in microculture and also from pyramidal cells in layer 2/3 of the somatosensory cortex in acute brain slices. In both preparations, amplitude and frequency of mEPSCs were similar in KI and WT mice (in microculture, Figure 5A: 23 ± 3 pA, 4.1 ± 0.8 Hz, n = 11 in WT and 22 ± 2 pA, 4.2 ± 0.8 Hz, n = 11 in KI; in slices,

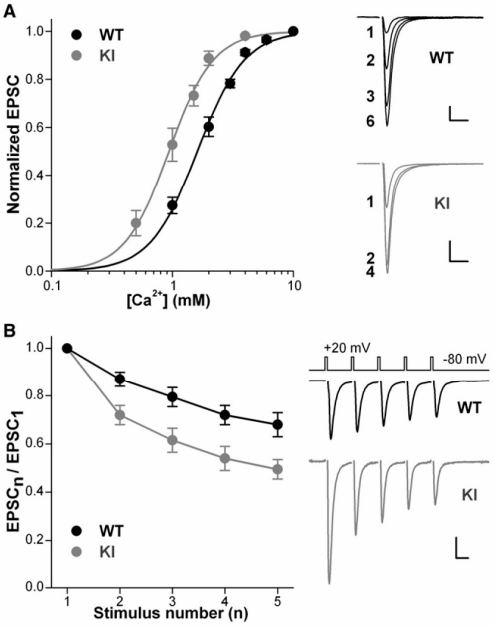

Figure 4. The Ca^{2+} Dependence of the EPSC Is Shifted to Lower Ca^{2+} Concentrations and Short-Term Depression Is Enhanced at Cortical Pyramidal Cell Autapses of R192Q KI Mice

(A) Left: evoked EPSC amplitude as a function of extracellular $[Ca^{2+}]$ in cortical pyramidal cells in microculture from WT (n = 7) and KI (n = 7) mice. In each cell, the EPSC amplitude was normalized to the maximal value. The data points were fitted according to the Hill equation: $EPSC = [Ca^{2+}]^n/\{(EC_{50})^n + [Ca^{2+}]^n\}$, with EC_{50} = 1.61 ± 0.05 mM and n = 2.21 ± 0.14 for WT and EC_{50} = 0.94 ± 0.02 mM and n = 2.37 ± 0.12 for KI. Right: EPSC traces recorded at the indicated $[Ca^{2+}]$ (in mM) from a WT and a KI neuron. Scale bars: 10 ms, 1 nA for WT; 10 ms, 0.25 nA for KI.

(B) Left: EPSC amplitudes evoked during successive depolarizing stimuli at 50 Hz (as shown on the right) normalized to the response to the first stimulus in the train, recorded after application of ω-CgTxGVIA 1 μM, in WT (n = 22) and KI (n = 21) pyramidal cells in microculture at DIV 11–14. Right: EPSC traces evoked by a 50 Hz train of stimuli in a WT and a KI neuron. Scale bars: 10 ms, 1 nA.

Error bars: SEM.

Figure 5B: 6.7 ± 0.3 pA, 6.9 ± 0.8 Hz, n = 11 in WT and 6.8 ± 0.4 pA, 6.4 ± 0.6 Hz, n = 10 in KI). Thus, there is no evidence for either postsynaptic or presynaptic homeostatic compensatory mechanisms at excitatory synapses onto pyramidal cells in KI mice. Moreover, the similar frequency of mEPSCs is consistent with and supports the absence of significant changes in either RRP or number of synapses in KI mice and also shows that mutant R192Q $Ca_V2.1$ channels do not open at voltages (−70, −80 mV) close to the resting potential of pyramidal cells.

To test the hypothesis that the gain of function of glutamate release at pyramidal cell synapses may explain the facilitation of induction and propagation of experimental CSD in R192Q KI mice (van den Maagdenberg et al., 2004), we measured the threshold for CSD induction and the velocity of CSD propagation in acute slices of somatosensory cortex of R192Q KI mice before and after application of a concentration of Aga (40 nM) that reduced glutamate release at KI pyramidal cell synapses to the value measured at WT synapses ($EPSC_{(KI+Aga\ 40)}/EPSC_{KI}$ = 0.57 ± 0.05 in Figure 6A versus $EPSC_{WT}/EPSC_{KI}$ = 0.59 ± 0.07 in Figure 3A). Pressure pulses of increasing duration were applied to a 3 M KCl-containing pipette positioned on layer 2/3 until a CSD was observed (as revealed by both the associated changes in light transmittance and the typical depolarization to almost 0 mV recorded in a pyramidal cell located 600 μm apart from the pressure-ejection pipette tip: Figure 6B). The duration of the first pulse eliciting a CSD was taken as CSD threshold, and the rate of horizontal spread of the change in intrinsic optical signal as velocity of CSD propagation. In slices from KI mice, the CSD threshold was lower than in WT slices (155 ± 7, n = 22 versus 228 ± 7 ms, n = 22, Figure 6C) and the velocity of CSD propagation was higher (3.2 ± 0.1, n = 21 versus 2.4 ± 0.1 mm/min, n = 17, Figure 6D), thus confirming in vitro the facilitation of induction and propagation of experimental CSD previously shown in KI mice in vivo. After perfusion of slices from KI mice with 40 nM Aga, the CSD threshold increased and the CSD velocity decreased to values strikingly similar to those measured in WT slices (from 148 ± 9 ms and 3.2 ± 0.2 mm/min before Aga to 208 ± 13 ms and 2.4 ± 0.1 mm/min after Aga, n = 10 and 8, Figures 6C and 6D). The fact that bringing back to WT values the $Ca_V2.1$-dependent glutamate release at pyramidal cell synapses of KI mice completely eliminates facilitation of CSD induction and propagation supports a causative link between gain of function of glutamate release at synapses onto pyramidal cells and facilitation of experimental CSD in FHM1 KI mice.

To test the hypothesis that FHM1 mutations may affect differently synaptic transmission at different cortical synapses and, as a consequence, in certain conditions may alter the balance between excitation and inhibition during cortical activity, we investigated excitatory and inhibitory neurotransmission at connected pairs of layer 2/3 pyramidal cells (PC) and multipolar fast-spiking (FS) interneurons in acute cortical slices of the somatosensory cortex of WT and KI juvenile mice, using paired patch-clamp recordings (Figure 7A and Supplemental Data available online). To study the excitatory PC-FS connection, we applied suprathreshold stimuli to the presynaptic PC neuron and measured the unitary EPSPs evoked in the postsynaptic FS interneuron; to study the inhibitory FS-PC connection, we applied suprathreshold stimuli to the presynaptic FS interneuron and measured the unitary IPSPs in the postsynaptic PC cell. The unitary PSPs were then averaged to obtain the mean PSPs (Figure 7B). In agreement with previous studies at connected pairs of layer 2/3 PC and FS neurons in rat cortical slices (Rozov et al., 2001; Zaitsev et al., 2007), saturating concentrations of Aga (400 nM) inhibited a large fraction of the EPSP at the PC-FS connection and completely inhibited the IPSP at the FS-PC connection in slices from WT mice (Figure S1).

The peak amplitude of the mean EPSP was on average two times larger in KI than in WT PC-FS connections (2.2 ± 0.4 mV in KI, n = 17, versus 1.1 ± 0.2 mV in WT, n = 16; Figure 7B). As expected, if the increased mean EPSP amplitude in the FHM1

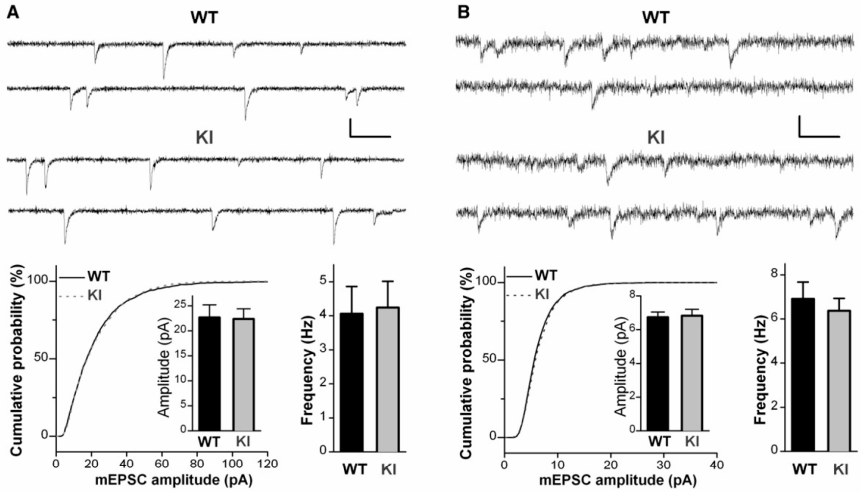

Figure 5. Amplitude and Frequency of mEPSCs in Cortical Pyramidal Cells in Microculture and in Acute Brain Slices Are Not Altered in KI Mice

(A) Representative recordings of mEPSCs at −80 mV from a WT and a KI pyramidal cell in microculture, and (left panel) cumulative distributions and average values (in inset) of mEPSC amplitudes of WT (continuous line, n = 11) and KI (dashed line, n = 11) neurons (DIV 10–13); right panel shows the corresponding average mEPSC frequencies. Amplitude analysis was made on the first 200 mEPSCs recorded from each cell. mEPSC kinetics are similar in WT and KI neurons (rise time 10%–90%: 0.62 ± 0.03 ms and 0.67 ± 0.03 ms; τ_{decay}: 3.3 ± 0.3 ms and 3.2 ± 0.2 ms in WT and KI, respectively). Scale bars: 50 ms, 20 pA.

(B) Representative recordings of mEPSCs at −65 mV from a WT and a KI layer 2/3 pyramidal cell in cortical slices, and (left panel) cumulative distributions and average values of mEPSC amplitudes of WT (continuous line, n = 11) and KI cells (dashed line, n = 10) from P16–17 mice; right panel shows the corresponding average mEPSC frequencies. Amplitude analysis was made on the first 300 mEPSCs recorded from each cell. mEPSC kinetics are similar in WT and KI cells (rise time 10%–90%: 1.01 ± 0.07 ms and 0.95 ± 0.06 ms; τ_{decay}: 4.6 ± 0.3 ms and 5.0 ± 0.4 ms in WT and KI, respectively). Scale bars: 50 ms, 10 pA.

Error bars: SEM.

mice was due to an increased probability of AP-evoked glutamate release at the synaptic contacts, both the coefficient of variation (CV) of the unitary EPSP amplitudes and the percentage of failures (i.e., the percentage of the presynaptic APs that failed to evoke an EPSP in the FS neuron) were lower in KI than in WT mice: CV = 0.26 ± 0.03 mV, failures = 0.8% ± 0.4% in KI, n = 17 versus CV = 0.45 ± 0.04 mV, failures = 9% ± 2% in WT, n = 16 (Figure 7C). Assuming a binomial model of release, the comparison of the relative values of the mean EPSP amplitude and of the inverse square of the CV in KI and WT mice confirmed the presynaptic origin of the increased excitatory neurotransmission at the PC-FS connection in KI mice and was consistent with an increased probability of vesicle release (see Supplemental Data) (Faber and Korn, 1991).

Consistent with and further supporting the conclusion that the FHM1 mutation leads to an increased probability of vesicle release at the individual synaptic contacts of the PC-FS connection are also the changes in short-term synaptic plasticity revealed in KI mice (Figure 7D). In WT mice, these synapses showed depression of the EPSPs during trains of APs at 10 Hz (PPR = 0.62 ± 0.03, n = 16). In agreement with a presynaptic mechanism of depression, percent failures increased during the train from 9% ± 2% to 29% ± 5%; as expected if depression is mainly due to vesicle depletion, analysis of single unitary events evoked by the first two pulses in the train showed an inverse correlation between the amplitudes of the first and second unitary EPSP (Figure S2) (Thomson et al., 1993). STD was larger in KI synapses (PPR = 0.42 ± 0.02, n = 17), lending strong support to the conclusion that the probability of vesicle release at the synaptic contacts between pyramidal cells and FS interneurons is larger in KI than in WT mice. Given the larger depression, the mean EPSP amplitudes elicited by the second and the following APs in the train were not significantly different between WT and KI mice.

In striking contrast with the gain of function measured at the excitatory PC-FS connection, the peak amplitudes of the evoked mean IPSPs at the inhibitory FS-PC connections were identical in slices from KI and WT mice (2.4 ± 0.4 mV in both KI, n = 16, and WT, n = 12; Figure 8A); also very similar were the CV (0.27 ± 0.02 mV in KI versus 0.31 ± 0.03 mV in WT) and the percent failures (0.9% ± 0.5% in KI versus 0.8% ± 0.5% in WT) (Figure 8B). Moreover, STD of the IPSPs during trains of APs at 10 Hz was not significantly different in the two genotypes (percent failures at the fifth AP: 10% ± 3% in KI, n = 16 versus 12% ± 4% in WT, n = 12, Figure 8C).

In summary, our analysis of cortical neurotransmission in R192Q KI mice shows that FHM1 mutations may differently affect synaptic transmission at different cortical synapses: in particular, we have shown that the FHM1 mutation leads to gain of function of excitatory neurotransmission at pyramidal

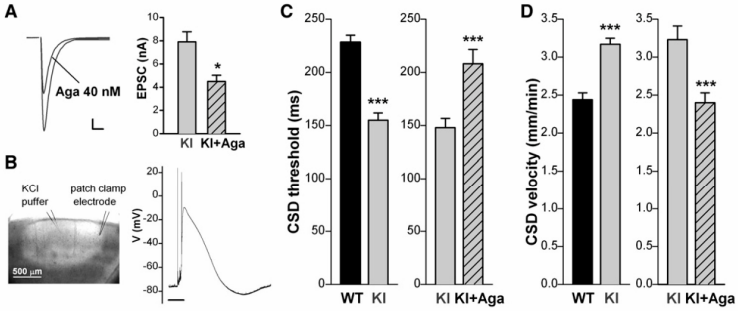

Figure 6. Facilitation of CSD Induction and Propagation in Cortical Slices of KI Mice Are Completely Eliminated after Reduction of Glutamate Release to WT Values

(A) Left: EPSCs traces recorded from a KI cortical pyramidal cell in microculture before and after application of Aga 40 nM. Scale bars: 10 ms, 1 nA. Right: average EPSC amplitudes before and after Aga 40 nM (n = 4).

(B) Left: digitalized image showing the typical changes in light transmittance associated with a spreading CSD elicited by pressure-ejection of KCl in a WT cortical slice, and the KCl application and patch-clamp recording sites (600 µm apart). Right: typical CSD depolarization of a layer 2/3 pyramidal cell recorded in current clamp. Scale bar: 1 min.

(C) Average values of CSD threshold in WT (n = 22) and KI (n = 22) slices and before and after application of Aga 40 nM in KI slices (n = 10).

(D) Average values of CSD propagation velocity in WT (n = 17) and KI (n = 21) slice and before and after application of Aga 40 nM in KI slices (n = 8).

Error bars: SEM.

cell synapses, but does not affect inhibitory neurotransmission at FS interneuron synapses.

DISCUSSION

We studied cortical neurotransmission in KI mice carrying a human FHM1 (R192Q) mutation. These mice show increased P/Q-type Ca^{2+} current density in cerebellar granule cells (van den Maagdenberg et al., 2004) and cortical pyramidal cells (Figure 1) consequent to activation of mutant $Ca_V2.1$ channels at lower voltages; they also show facilitation of induction and propagation of CSD, elicited either by electrical stimulation in vivo (van den Maagdenberg et al., 2004) or high KCl in vitro (Figure 6).

The analysis of cortical excitatory neurotransmission both in culture and in the context of functional neuronal circuits in brain slices shows that the R192Q FHM1 mutation (and presumably all the gain-of-function FHM1 mutations) leads to increased AP-evoked Ca^{2+} influx and glutamate release at cortical pyramidal cell synapses. In fact, in single cortical pyramidal cells forming autapses, both the strength of synaptic transmission and the contribution of P/Q-type Ca^{2+} channels to synaptic transmission were enhanced in KI mice; the dependence of the EPSC on the external concentration of Ca^{2+} ions was shifted to lower values and the STD of the EPSCs during a train of APs was increased. The strength of excitatory neurotransmission and STD were also increased at unitary connections between layer 2/3 pyramidal cells and FS interneurons in acute KI cortical slices. Our data indicate that a relatively small shift to lower voltages of activation of mutant $Ca_V2.1$ channels leads to a significant increase in AP-evoked Ca^{2+} influx at the active zones of pyramidal cells (assuming a similar voltage shift for presynaptic and somatic channels). Despite the gain of function of cortical excitatory neurotransmission, neither postsynaptic nor presynaptic homeostatic compensatory mechanisms (Turrigiano and Nelson, 2004) were observed at excitatory synapses onto pyramidal cells of FHM1 mice.

In apparent contrast with our findings, Cao et al. (2004) reported a decreased contribution of mutant P/Q-type Ca^{2+} channels and an unaltered overall strength of evoked excitatory neurotransmission between cultured hippocampal neurons from *cacna1a* knockout mice expressing FHM1 mutant human $Ca_V2.1\alpha_1$ subunits. As previously suggested, the different findings can be explained by the decreased number of functional mutant $Ca_V2.1$ channels in the membrane of transfected neurons (Tottene et al., 2002, 2005) in contrast with the unaltered number of functional $Ca_V2.1$ channels in neurons of FHM1 KI mice (Figure 1C) (Pietrobon, 2007; van den Maagdenberg et al., 2004).

The facilitation of induction and propagation of experimental (K^+-induced) CSD in acute slices of somatosensory cortex of R192Q KI mice was completely eliminated (both CSD threshold and velocity became similar to those in WT slices) when glutamate release at pyramidal cell synapses was brought back to WT values using subsaturating concentrations of the specific P/Q channel blocker, Aga. This finding provides direct evidence that the gain-of-function of glutamate release at synapses onto pyramidal cells may explain the facilitation of experimental CSD in FHM1 mutant mice, and thus provides novel insights into the controversial mechanisms of CSD initiation and propagation.

The interventions that can produce experimental CSD in normally metabolizing cortical tissue (such as electrical stimulation or high K^+) induce an anomalous increase in the extracellular concentration of K^+ ions and a sustained neuronal depolarization accompanied by an increase in neuronal firing. With sufficiently intense stimuli, CSD ignition occurs when the regulatory mechanisms that normally keep the extracellular $[K^+]_o$ within the physiological range are overwhelmed by the buildup of $[K^+]_o$

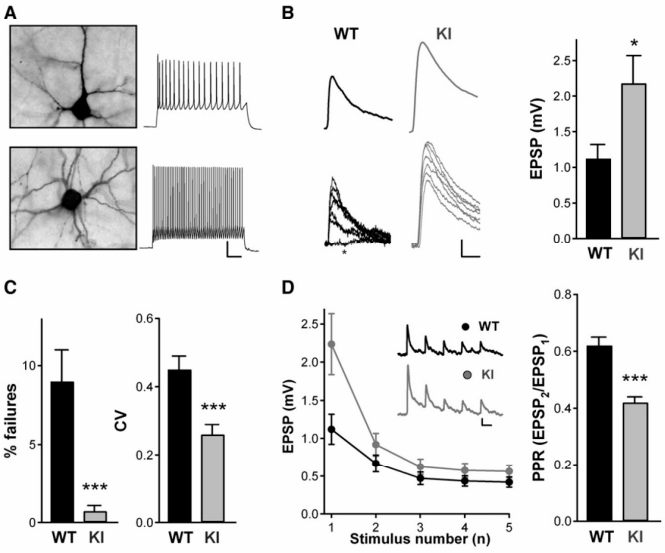

Figure 7. Increased EPSP Amplitude and Short-Term Depression at Single Excitatory Connections between Pyramidal Cells and Fast-Spiking Interneurons in Acute Cortical Slices of R192Q KI Mice

(A) Representative morphology (after biocytin staining) and firing pattern upon sustained current injection of a layer 2/3 pyramidal cell (PC, top) and fast-spiking (FS) interneuron (bottom) in slices of mice barrel cortex. Scale bars: 150 ms, 20 mV.

(B) Left: representative unitary EPSPs recorded from a layer 2/3 FS cell upon suprathreshold stimulation of a connected PC in seven successive trials in a WT and a KI slice, with on top the corresponding mean EPSPs (averaged over 63 trials in WT and 90 trials in KI). The asterisk indicates a failure in the connection, which is included for exemplification, even if their frequency was less than one in ten trials. Scale bars: 10 ms, 0.5 mV. Right: average values of mean EPSP amplitudes in 16 WT and 17 KI PC-FS connections.

(C) Average values of percent failures and CV of the unitary EPSPs (n = 16 WT; n = 17 KI).

(D) Left: average values of mean EPSP amplitudes evoked in FS cells in response to a train of five APs at 10 Hz elicited in a connected PC (n = 16 WT; n = 17 KI). Inset: representative mean EPSP responses evoked in a WT (averaged over 63 trials) and a KI (averaged over 59 trials) FS cell by the train of presynaptic APs. Scale bar: 50 ms, 0.2 mV. Right: Average values of the paired pulse ratio between the second and the first EPSP in the train (n = 16 WT; n = 17 KI).

Error bars: SEM.

via a positive feedback cycle that makes self-regenerating the initially gradual neuronal depolarization; this positive feedback cycle initiates when a sufficient number of V-dependent and/or $[K^+]_o$-dependent cationic channels are activated to generate a net inward current, with consequent further depolarization and further increase of the local $[K^+]_o$, leading to further activation of the cationic channels (Kager et al., 2002; Somjen, 2001). The nature of these cationic channels remains unclear and controversial (Somjen, 2001), although there is strong pharmacological support for a key role of NMDA receptors (Anderson and Andrew, 2002; Footitt and Newberry, 1998; Marrannes et al., 1988; Vilagi et al., 2001), and clear evidence that CSD initiates and propagates at the level of the dendrites of pyramidal cells (Kunkler et al., 2005; Somjen, 2001; Vilagi et al., 2001; Wadman et al., 1992) and involves an increased conductance in specific dendritic subregions (Canals et al., 2005). Another controversial issue is the mechanism of CSD propagation (Grafstein, 1956; Herreras, 2005; Somjen, 2001).

Our findings are consistent with and support a model of CSD initiation in which activation of presynaptic voltage-gated Ca^{2+}

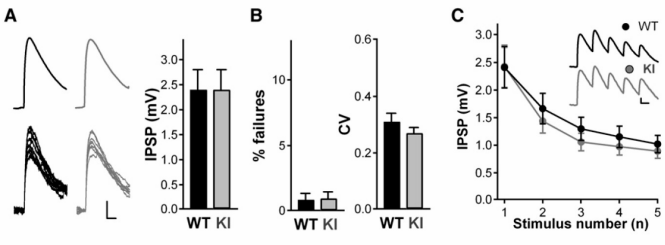

Figure 8. Unaltered IPSP Amplitude and Short-Term Depression at Single Inhibitory Connections between Fast-Spiking Interneurons and Pyramidal Cells in Acute Cortical Slices of R192Q KI Mice

(A) Left: representative unitary IPSPs recorded from a layer 2/3 PC upon suprathreshold stimulation of a connected FS cell in 8 successive trials in a WT and a KI slice, with on top the corresponding mean IPSPs (averaged over 59 trials in WT and 82 trials in KI). Scale bars: 20 ms, 1 mV. Right: Average values of mean IPSP amplitudes in 12 WT and 16 KI FS-PC connections.

(B) Average values of percent failures and CV of the unitary IPSPs (n = 12 WT; n = 16 KI).

(C) Average values of mean IPSP amplitudes evoked in PCs in response to a train of five APs at 10 Hz elicited in a connected FS cell (n = 12 WT; n = 16 KI). Inset: representative mean IPSP responses evoked in a WT (averaged over 53 trials) and a KI (averaged over 59 trials) PC by the train of presynaptic APs. Scale bar: 50 ms, 0.5 mV.

Error bars: SEM.

channels (in particular P/Q-type) with consequent release of glutamate from recurrent cortical pyramidal cell synapses and activation of NMDA receptors are key components of the positive feedback cycle that ignites CSD (Pietrobon, 2005b). Notably, the abnormal elevation of $[K^+]_o$ necessary to initiate CSD has several additional effects, besides depolarization, all favoring the opening of NMDA channels, such as shifting to higher voltages the reversal potential of both K^+ and Cl^- ions with consequent prolongation of postsynaptic APs, reduction of afterhyperpolarization and reduction of IPSPs amplitude (McCarren and Alger, 1985; Poolos and Kocsis, 1990; Traynelis and Dingledine, 1988), with the possibility that GABAergic synapses may actually become depolarizing (Marty and Llano, 2005). Regarding CSD propagation, our data are consistent with a model based on interstitial K^+ diffusion initiating in adjacent dendrites the positive feedback cycle that ignites CSD (Grafstein, 1956), rather than with the hypothesis that CSD propagates through gap junctions (Herreras, 2005; Somjen, 2001). Both the lower threshold and the increased velocity of experimental CSD in FHM1 KI mice can be explained by the proposed model, which predicts that an electrical stimulation of the cortex of lower intensity and/or a lower increase of $[K^+]_o$ are necessary to open a sufficient number of P/Q Ca^{2+} channels and release enough glutamate and open enough NMDA receptor channels to initiate the positive feedback cycle that ignites CSD and propagates it to adjacent tissue. Moreover, the enhanced release of glutamate would amplify the positive feedback; gain of function of postsynaptic P/Q channels might also reinforce the positive loop at least in the first phase. Consistent with the proposed model is also the evidence that spontaneous $Ca_V2.1$ mouse mutants with loss-of-function mutations in the $Ca_V2.1$ channel show an increased threshold for initiation and a decreased velocity of propagation of experimental CSD (Ayata et al., 2000).

In migraineurs, CSD is not induced by experimental depolarizing stimuli but arises "spontaneously" in response to specific, mostly unknown triggers; stress and intense, long-lasting sensory stimulation are among the known migraine triggers (Pietrobon and Striessnig, 2003). One must therefore admit that these triggers are able to create in the cortex of migraineurs the conditions for initiation of the positive feedback cycle that overwhelms the regulatory mechanisms controlling cortical $[K^+]_o$ and ignites CSD. Interestingly, migraineurs are hypersensitive to any kind of sensory overload and there is strong evidence for altered cortical excitability and abnormal processing of sensory information in their brain in the period between migraine attacks (Aurora and Wilkinson, 2007; Coppola et al., 2007; Pietrobon and Striessnig, 2003; Welch, 2005).

The dynamic keeping of the balance between excitation and inhibition during cortical activity is essential for preventing overexcitation and for the correct processing of sensory information (Monier et al., 2003; Shu et al., 2003). Although the mechanisms by which cortical circuits vary the strength of inhibition during ongoing changes in excitation are not well understood, recurrent inhibitory circuits appear well suited to provide dynamic regulation of the excitation-inhibition balance (Galarreta and Hestrin, 1998; Kapfer et al., 2007; Reyes et al., 1998; Silberberg and Markram, 2007). We have shown that, in contrast with the gain of function of excitatory neurotransmission, inhibitory neurotransmission at FS interneuron synapses is unaltered in FHM1 KI mice. This finding demonstrates that FHM1 mutations may differently affect synaptic transmission and short-term plasticity at different cortical synapses, and, as a consequence, very likely alter the neuronal circuits that coordinate and dynamically adjust the balance between excitation and inhibition during cortical activity. Functional alterations in these circuits may underlie the abnormal processing of sensory information of migraineurs in the interictal period; we hypothesize that these alterations may also render the cortex vulnerable to ignition of CSD in response to migraine triggers such as intense, repetitive sensory stimulation.

Considering the specific polysynaptic inhibitory subcircuit involving FS interneurons and pyramidal cells that we have investigated in the FHM1 mice, the gain of function of glutamate release at the recurrent synapses between pyramidal cells would certainly increase network excitation; in contrast, the gain of function of glutamate release at the PC-FS synapses would lead to enhanced recruitment of interneurons and enhanced inhibition. However, during high-frequency repetitive activity the enhanced recruitment of FS interneurons is expected to cease rapidly because the PC-FS synapses depress strongly during AP trains (Figure 7; much more than the recurrent PC-PC synapses: Kapfer et al., 2007), and STD is even stronger in FHM1 KI mice; already at the second AP in a 10 Hz train the EPSP amplitude becomes similar to that in WT mice (from being almost two times larger in response to the first AP). This analysis, even though restricted to a specific subcircuit, makes the important point that the differential effect of FHM1 mutations on excitatory and inhibitory neurotransmission may produce overexcitation in certain brain conditions, but may leave the excitation-inhibition balance within physiological limits in others, thus explaining the episodic nature of the disease. In the brain conditions (cf. migraine triggers) in which strong overexcitation prevails, the consequent neuronal hyperactivity might initiate the positive feedback cycle that overwhelms the $[K^+]_o$ regulation and ignites CSD.

In general, several mechanisms may contribute to a differential effect of FHM1 mutations at different synapses; these include (1) different effects on AP-evoked Ca^{2+} influx because of a different duration of the AP or a different fraction of P/Q channels (or a different P/Q isoform) at the release sites, (2) different effects of the same increase of Ca^{2+} influx on the probability of release, and (3) different mechanisms of short-term synaptic plasticity (among which there may be a differential contribution of Ca^{2+}-dependent regulation of presynaptic P/Q Ca^{2+} channels, see Mochida et al., 2008). The low CV and percentage of failures close to zero of the inhibitory FS-PC connection in WT mice (both failures and CV being similar to those of the excitatory PC-FS connection in KI mice) indicate a high probability of AP-evoked GABA release, and suggest saturation of the presynaptic Ca^{2+} sensor as a plausible explanation for the unaltered neurotransmission in FHM1 mice despite the dominant role of P/Q Ca^{2+} channels at this synapse. However, we cannot exclude that a reduced gain of function of AP-evoked Ca^{2+} influx due to the shorter AP of FS interneurons and/or to a different $Ca_V2.1$ isoform (less affected by the mutation) may contribute.

An interesting open question is why overexcitation and neuronal hyperactivity in migraine produce a CSD and not an

epileptic discharge. Indeed, local neuronal hyperactivity progressively recruiting a synchronous discharge via recurrent excitatory collaterals and $[K^+]_o$ accumulation has been proposed to initiate epileptic discharge in slice models (Jensen and Yaari, 1997; Pinto et al., 2005; Traynelis and Dingledine, 1988). A plausible hypothesis is that the initiation mechanisms of CSD and seizure are similar but the evolution is different depending on whether the neuronal hyperactivity and consequent increase in $[K^+]_o$ exceed a critical level that makes self-regenerating the depolarization; in this hypothesis, CSD represents "a poorly controlled seizure" in which $[K^+]_o$ regulation is completely disrupted (Haglund and Schwartzkroin, 1990). The involvement of similar mechanisms in initiation of CSD and seizures is consistent with (1) the established comorbidity between migraine and epilepsy, (2) the effectiveness of some antiepileptic drugs in migraine prophylaxis, (3) the fact that migraine and epilepsy have various trigger factors in common, and (4) the fact that mutations in all three known FHM genes can cause seizures (Haan et al., 2008; Welch, 2005; Pietrobon, 2007).

EXPERIMENTAL PROCEDURES

Experiments were performed using WT C57Bl6J mice and homozygous KI mice carrying the $Ca_V2.1$ R192Q FHM1 mutation with the same genetic background (van den Maagdenberg et al., 2004). All experimental procedures were carried out in accordance with the Italian Animal Welfare Act and approved by the local authority veterinary service.

Patch-clamp recordings were made at room temperature following standard techniques. Electrical signals were recorded through an Axopatch-200B or Multiclamp 700B patch-clamp amplifier and digitized using a Digidata 1440A or Digidata 1322A interface and pClamp software (Axon Instruments). The liquid junction potential (LJP) values reported below should be added to all voltages to obtain the correct membrane potentials (Neher, 1992).

Data are given as mean ± SEM; stars indicate a statistically significant difference from control assessed by the Student's t test (*$p < 0.05$, **$p < 0.01$, ***$p < 0.001$).

Ca^{2+} Current in Acutely Dissociated Cortical Pyramidal Neurons

Cortical pyramidal neurons were acutely dissociated from postnatal day (P) 13–15 mice as described in Supplemental Data. Whole-cell patch-clamp recordings of the different Ca^{2+} current components were performed as in Fletcher et al. (2001) on neurons up to 1 hr after dissociation. The pipette solution contained (in mM) 100 $CsCH_3SO_3$, 5 $MgCl_2$, 30 HEPES, 10 EGTA, 4 ATP, 0.5 GTP, 1 cAMP, pH 7.4 with CsOH. The extracellular solution contained (in mM) 5 $BaCl_2$, 148 TEA-Cl, 10 HEPES, 0.1 mg/ml cytochrome C, pH 7.4 with TEA-OH. Currents were recorded at −10 mV for KI neurons and at 0 mV for WT neurons from a holding potential of −70 mV. Compensation (typically 70%) for series resistance (Rs) was used. LJP: −12 mV.

Neurotransmission in Cortical Pyramidal Cells in Microculture

Cortical neurons from P0–2 mice were cultured on glial microislands as described in Supplemental Data. Microislands containing one or more glial cells and a single neuron with extensive processes were selected for whole-cell patch-clamp recording (sampling 5 kHz; filter 1 kHz). The pipette solution contained (in mM) 110 K-methanesulfonate, 5 $MgCl_2$, 30 HEPES, 3 EGTA, 4 ATP, 0.5 GTP, and 1 cAMP (pH 7.4 with KOH). The extracellular solution contained (in mM) 145 NaCl, 5.6 KCl, 10 HEPES, 10 glucose, 1 $MgCl_2$, 2 $CaCl_2$, 0.05 D-AP5 (pH 7.4 with NaOH). Cytochrome C (0.1 mg/ml) was added to the solutions with peptide toxins: ω-AgaIVA, SNX-482 (both from Peptide Institute Inc.), ω-CgTxGVIA, ω-CTxMVIIC (both from Bachem). Pipette resistance: 1.8–2.5 MΩ. In voltage-clamp mode, APs in the unclamped processes were induced by a 2 ms voltage pulse to +20 mV every 10 s from a holding potential of −80 mV. The currents recorded in the presence of 5 μM NBQX were subtracted to all records to obtain the AMPA-mediated EPSCs (displayed in the figures after blanking 1–3 ms around each stimulus artifact for clarity). After EPSC stabilization (typically 3 min after break-in), five to ten sweeps were averaged to obtain the EPSC amplitude. To measure short-term synaptic plasticity, the EPSCs elicited by two 50 Hz stimulus trains at a 20 s interval were averaged. EPSCs were recorded with good voltage-clamp control since EPSCs kinetics and PPR were unchanged when the size of the EPSCs was reduced using subsaturating concentrations of NBQX (50 nM; Tocris). Rs compensation (70%–80%) was used. LJP: −8 mV.

mEPSCs were acquired at −80 mV for at least 2 min (sampling 10 kHz; filter 2 kHz), and analyzed using Clampfit 10.0 (Axon Instruments); this software detects events on the basis of closeness of fit to a sliding template created (for each cell) by averaging 15–20 of its most unambiguous mEPSCs selected by eye. Each event was further visually inspected to exclude artifacts. Overlapping events were excluded from amplitude analysis.

Neurotransmission in Cortical Slices

Acute thalamocortical slices of the barrel cortex were made from P11–15 mice as described in Supplemental Data. The cells recorded were deeper than 40 μm from the surface with dendritic arborizations almost parallel to the plane of the cut. Neurons were identified based on their morphology (confirmed by postfixation inspection of the biocytin-labeled neurons) and on their firing pattern in response to current injection (Reyes et al., 1998) (Supplemental Data).

For paired patch-clamp recordings on PC and FS cells (sampling 20 kHz; filter 4 kHz), the pipette solutions contained (in mM) 105 K-gluconate, 30 KCl, 4 MgATP, 0.3 GTP, 10 phosphocreatine, 10 HEPES, and 1 mg/ml biocytin (pH 7.3 with KOH). The standard extracellular solution sACSF contained (in mM) 125 NaCl, 2.5 KCl, 25 $NaHCO_3$, 1.25 NaH_2PO_4, 1 $MgCl_2$, 2 $CaCl_2$, 25 glucose saturated with 95% O_2 and 5% CO_2. Pipette resistance: 4–6 MΩ. The two cells were patched in sequence, first the interneuron. Only cells with resting potential <−70 mV were considered (average values: −77 ± 1 mV in PC, and −73 ± 1 mV in FS cells). APs in the presynaptic cell were evoked by suprathreshold depolarizing current-injection pulses (7.5 ms duration). Once a connected pair was found, the synaptic response to a train of 5 APs at 10 Hz was recorded in the postsynaptic cell for 45–127 consecutive trials at 10 s intervals. LJP: −8 mV.

Data analysis was performed using Igor Pro. The mean peak EPSP and IPSP amplitudes and PPR for each experiment were calculated after averaging over all the sweeps recorded. The first peak amplitude was averaged over a 1 ms window (20 points) around the peak. For each consecutive response, the previous PSP was fitted with a double-exponential decay and subtracted from the trace. For quantification of the percentage of failures, each trace was visually inspected. The CV was calculated for each experiment from the scatter of the single synaptic responses (see Supplemental Data).

mEPSCs recordings (sampling 10 kHz; filter 2 kHz) were performed on acute coronal slices of the barrel cortex from P16–17 mice; the pipette solution contained (in mM) 6 KCl, 114 K-gluconate, 10 HEPES, 10 phosphocreatine, 4 MgATP, 0.3 NaGTP (pH 7.25 with KOH, osmolarity 300 mOsm with sucrose) and slices were superfused with a modified ACSF (mACSF, with 1 mM $CaCl_2$, 0.5 mM $MgCl_2$, and 3.5 mM KCl) containing (in μM) TTX 0.2, D-AP5 50, and bicuculline 20 (Tocris). mEPSCs on pyramidal cells of layer 2/3 of the barrel cortex, voltage clamped at −65 mV with no Rs compensation (Rs was below 20 MΩ with less than 20% variation), were recorded for at least 2 min and analyzed using Clampfit 10.0. LJP: −12 mV.

Cortical Spreading Depression

Acute coronal slices of the barrel cortex from P16–17 mice were perfused with mACSF at a flowing rate of 3 ml/min, and pressure-ejection pulses of 3 M KCl (0.5 bar) of increasing duration (at 8 min intervals in 20 ms steps) were applied through a glass micropipette (R = 0.19–0.25 MΩ) onto the slice surface on layer 2/3, using a PDES-02DX pneumatic drug ejection system (Npi Electronic), until a CSD was elicited. CSD was detected by monitoring the associated change in intrinsic optical signal (IOS) and/or recording in current-clamp the membrane potential of a pyramidal cell at 600 μm from the pressure-ejection pipette tip. The duration of the first pulse eliciting a CSD was taken as CSD threshold and the rate of horizontal spread of the change in IOS as CSD velocity. In

control experiments, similar CSD threshold and velocity were found when two CSD episodes were induced at a 30 min interval on the same slice (data not shown). To test the effect of ω-AgaIVA, CSD threshold and velocity were measured in control and after 30 min of perfusion with mACSF plus 40 nM ω-AgaIVA. IOS was recorded using a 12 bit monochrome digital camera (DFC 350FX, Leica) connected with a TCS SP5 confocal microscope (Leica; 10× magnification). Images were recorded at 579 ms intervals and 4.2 ms exposure time (1392 × 1040 pixel; optical resolution 3.23 μm^2/pixel). MBF ImageJ software was used for the off line analysis of the digitalized images.

SUPPLEMENTAL DATA

The Supplemental Data include Supplemental Experimental Procedures, Supplemental Results, and two figures and can be found with this article online at http://www.neuron.org/supplemental/S0896-6273(09)00094-4.

ACKNOWLEDGMENTS

This work was supported by the EU "EUROHEAD" grant (LSHM-CT-2004-504837) (to D.P., M.D.F.), the Telethon Italy grant GGP06234 (to D.P.), and the Italian Ministry of University and Research PRIN2005 (to D.P.), the Netherland Organization for Scientific Research (NWO; 425-20-403 and Vici 918·56·602 to M.D.F.), and the Centre for Medical Systems Biology (CMSB) in the framework of the Netherlands Genomics Initiative (NGI) (to M.D.F, A.M.J.M.v.d.M.). We thank Giorgio Carmignoto for critically reading the manuscript and Gabriele Losi for help with the analysis of the intrinsic optical signal.

Accepted: January 27, 2009
Published: March 11, 2009

REFERENCES

Anderson, T.R., and Andrew, R.D. (2002). Spreading depression: imaging and blockade in the rat neocortical brain slice. J. Neurophysiol. *88*, 2713–2725.

Aurora, S.K., and Wilkinson, F. (2007). The brain is hyperexcitable in migraine. Cephalalgia *27*, 1442–1453.

Ayata, C., Shimizu-Sasamata, M., Lo, E.H., Noebels, J.L., and Moskowitz, M.A. (2000). Impaired neurotransmitter release and elevated threshold for cortical spreading depression in mice with mutations in the α_{1A} subunit of P/Q type calcium channels. Neuroscience *95*, 639–645.

Ayata, C., Jin, H., Kudo, C., Dalkara, T., and Moskowitz, M.A. (2006). Suppression of cortical spreading depression in migraine prophylaxis. Ann. Neurol. *59*, 652–661.

Bekkers, J.M., and Stevens, C.F. (1991). Excitatory and inhibitory autaptic currents in isolated hippocampal neurons maintained in cell culture. Proc. Natl. Acad. Sci. USA *88*, 7834–7838.

Bolay, H., Reuter, U., Dunn, A.K., Huang, Z., Boas, D.A., and Moskowitz, M.A. (2002). Intrinsic brain activity triggers trigeminal meningeal afferents in a migraine model. Nat. Med. *8*, 136–142.

Bowyer, S.M., Aurora, K.S., Moran, J.E., Tepley, N., and Welch, K.M. (2001). Magnetoencephalographic fields from patients with spontaneous and induced migraine aura. Ann. Neurol. *50*, 582–587.

Canals, S., Makarova, I., Lopez-Aguado, L., Largo, C., Ibarz, J.M., and Herreras, O. (2005). Longitudinal depolarization gradients along the somatodendritic axis of CA1 pyramidal cells: a novel feature of spreading depression. J. Neurophysiol. *94*, 943–951.

Cao, Y.Q., Piedras-Renteria, E.S., Smith, G.B., Chen, G., Harata, N.C., and Tsien, R.W. (2004). Presynaptic Ca^{2+} channels compete for channel type-preferring slots in altered neurotransmission arising from Ca^{2+} channelopathy. Neuron *43*, 387–400.

Coppola, G., Pierelli, F., and Schoenen, J. (2007). Is the cerebral cortex hyperexcitable or hyperresponsive in migraine? Cephalalgia *27*, 1427–1439.

Faber, D.S., and Korn, H. (1991). Applicability of the coefficient of variation method for analyzing synaptic plasticity. Biophys. J. *60*, 1288–1294.

Fletcher, C.F., Tottene, A., Lennon, V.A., Wilson, S.M., Dubel, S.J., Paylor, R., Hosford, D.A., Tessarollo, L., McEnery, M.W., Pietrobon, D., et al. (2001). Dystonia and cerebellar atrophy in *Cacna1a* null mice lacking P/Q calcium channel activity. FASEB J. *15*, 1288–1290.

Footitt, D.R., and Newberry, N.R. (1998). Cortical spreading depression induces an LTP-like effect in rat neocortex in vitro. Brain Res. *781*, 339–342.

Galarreta, M., and Hestrin, S. (1998). Frequency-dependent synaptic depression and the balance of excitation and inhibition in the neocortex. Nat. Neurosci. *1*, 587–594.

Goadsby, P.J., Lipton, R.B., and Ferrari, M.D. (2002). Migraine current understanding and treatment. N. Engl. J. Med. *346*, 257–270.

Grafstein, B. (1956). Mechanism of spreading cortical depression. J. Neurophysiol. *19*, 154–171.

Haan, J., Terwindt, G.M., van den Maagdenberg, A.M., Stam, A.H., and Ferrari, M.D. (2008). A review of the genetic relation between migraine and epilepsy. Cephalalgia *28*, 105–113.

Hadjikhani, N., Sanchez del Rio, M., Wu, O., Schwartz, D., Bakker, D., Fischl, B., Kwong, K.K., Cutrer, F.M., Rosen, B.R., Tootell, R.B.H., et al. (2001). Mechanisms of migraine aura revealed by functional MRI in human visual cortex. Proc. Natl. Acad. Sci. USA *98*, 4687–4692.

Haglund, M.M., and Schwartzkroin, P.A. (1990). Role of Na-K pump potassium regulation and IPSPs in seizures and spreading depression in immature rabbit hippocampal slices. J. Neurophysiol. *63*, 225–239.

Hans, M., Luvisetto, S., Williams, M.E., Spagnolo, M., Urrutia, A., Tottene, A., Brust, P.F., Johnson, E.C., Harpold, M.M., Stauderman, K.A., and Pietrobon, D. (1999). Functional consequences of mutations in the human α_{1A} calcium channel subunit linked to familial hemiplegic migraine. J. Neurosci. *19*, 1610–1619.

Herreras, O. (2005). Electrical prodromals of spreading depression void Grafstein's potassium hypothesis. J. Neurophysiol. *94*, 3656–3657.

Jensen, M.S., and Yaari, Y. (1997). Role of intrinsic burst firing, potassium accumulation, and electrical coupling in the elevated potassium model of hippocampal epilepsy. J. Neurophysiol. *77*, 1224–1233.

Kager, H., Wadman, W.J., and Somjen, G.G. (2002). Conditions for the triggering of spreading depression studied with computer simulations. J. Neurophysiol. *88*, 2700–2712.

Kaja, S., van de Ven, R.C., Broos, L.A., Veldman, H., van Dijk, J.G., Verschuuren, J.J., Frants, R.R., Ferrari, M.D., van den Maagdenberg, A.M., and Plomp, J.J. (2005). Gene dosage-dependent transmitter release changes at neuromuscular synapses of *CACNA1A* R192Q knockin mice are non-progressive and do not lead to morphological changes or muscle weakness. Neuroscience *135*, 81–95.

Kapfer, C., Glickfeld, L.L., Atallah, B.V., and Scanziani, M. (2007). Supralinear increase of recurrent inhibition during sparse activity in the somatosensory cortex. Nat. Neurosci. *10*, 743–753.

Kunkler, P.E., Hulse, R.E., Schmitt, M.W., Nicholson, C., and Kraig, R.P. (2005). Optical current source density analysis in hippocampal organotypic culture shows that spreading depression occurs with uniquely reversing currents. J. Neurosci. *25*, 3952–3961.

Lauritzen, M. (1994). Pathophysiology of the migraine aura. The spreading depression theory. Brain *117*, 199–210.

Marrannes, R., Willems, R., De Prins, E., and Wauquier, A. (1988). Evidence for a role of the N-methyl-D-aspartate (NMDA) receptor in cortical spreading depression in the rat. Brain Res. *457*, 226–240.

Marty. A.. and Llano. I. (2005). Excitatory effects of GABA in established brain networks. Trends Neurosci. *28*, 284–289.

McCarren, M., and Alger, B.E. (1985). Use-dependent depression of IPSPs in rat hippocampal pyramidal cells in vitro. J. Neurophysiol. *53*, 557–571.

Mochida, S., Few, A.P., Scheuer, T., and Catterall, W.A. (2008). Regulation of presynaptic $Ca_V2.1$ channels by Ca^{2+} sensor proteins mediates short-term synaptic plasticity. Neuron *57*, 210–216.

Monier, C., Chavane, F., Baudot, P., Graham, L.J., and Fregnac, Y. (2003). Orientation and direction selectivity of synaptic inputs in visual cortical neurons: a diversity of combinations produces spike tuning. Neuron *37*, 663–680.

Neher, E. (1992). Correction for liquid junction potentials in patch clamp experiments. Methods Enzymol. *207*, 123–131.

Ophoff, R.A., Terwindt, G.M., Vergouwe, M.N., van Eijk, R., Oefner, P.J., Hoffman, S.M.G., Lamerdin, J.E., Mohrenweiser, H.W., Bulman, D.E., Ferrari, M., et al. (1996). Familial hemiplegic migraine and episodic ataxia type-2 are caused by mutations in the Ca^{2+} channel gene *CACNL1A4*. Cell *87*, 543–552.

Pietrobon, D. (2005a). Function and dysfunction of synaptic calcium channels: insights from mouse models. Curr. Opin. Neurobiol. *15*, 257–265.

Pietrobon, D. (2005b). Migraine: new molecular mechanisms. Neuroscientist *11*, 373–386.

Pietrobon, D. (2007). Familial hemiplegic migraine. Neurotherapeutics *4*, 274–284.

Pietrobon, D., and Striessnig, J. (2003). Neurobiology of migraine. Nat. Rev. Neurosci. *4*, 386–398.

Pinto, D.J., Patrick, S.L., Huang, W.C., and Connors, B.W. (2005). Initiation, propagation, and termination of epileptiform activity in rodent neocortex in vitro involve distinct mechanisms. J. Neurosci. *25*, 8131–8140.

Poolos, N.P., and Kocsis, J.D. (1990). Elevated extracellular potassium concentration enhances synaptic activation of N-methyl-D-aspartate receptors in hippocampus. Brain Res. *508*, 7–12.

Reid, C.A., Bekkers, J.M., and Clements, J.D. (1998). N- and P/Q-type Ca^{2+} channels mediate transmitter release with a similar cooperativity at rat hippocampal autapses. J. Neurosci. *18*, 2849–2855.

Reyes, A., Lujan, R., Rozov, A., Burnashev, N., Somogyi, P., and Sakmann, B. (1998). Target-cell-specific facilitation and depression in neocortical circuits. Nat. Neurosci. *1*, 279–285.

Rozov, A., Burnashev, N., Sakmann, B., and Neher, E. (2001). Transmitter release modulation by intracellular Ca^{2+} buffers in facilitating and depressing nerve terminals of pyramidal cells in layer 2/3 of the rat neocortex indicates a target cell-specific difference in presynaptic calcium dynamics. J. Physiol. *531*, 807–826.

Schneggenburger, R., and Neher, E. (2000). Intracellular calcium dependence of transmitter release rates at a fast central synapse. Nature *406*, 889–893.

Shu, Y., Hasenstaub, A., and McCormick, D.A. (2003). Turning on and off recurrent balanced cortical activity. Nature *423*, 288–293.

Silberberg, G., and Markram, H. (2007). Disynaptic inhibition between neocortical pyramidal cells mediated by Martinotti cells. Neuron *53*, 735–746.

Sochivko, D., Chen, J., Becker, A., and Beck, H. (2003). Blocker-resistant Ca^{2+} currents in rat CA1 hippocampal pyramidal neurons. Neuroscience *116*, 629–638.

Somjen, G.G. (2001). Mechanisms of spreading depression and hypoxic spreading depression-like depolarization. Physiol. Rev. *81*, 1065–1096.

Takada, N., Yanagawa, Y., and Komatsu, Y. (2005). Activity-dependent maturation of excitatory synaptic connections in solitary neuron cultures of mouse neocortex. Eur. J. Neurosci. *21*, 422–430.

Thomsen, L.L., Eriksen, M.K., Roemer, S.F., Andersen, I., Olesen, J., and Russell, M.B. (2002). A population-based study of familial hemiplegic migraine suggests revised diagnostic criteria. Brain *125*, 1379–1391.

Thomsen, L.L., Olesen, J., and Russell, M.B. (2003). Increased risk of migraine with typical aura in probands with familial hemiplegic migraine and their relatives. Eur. J. Neurol. *10*, 421–427.

Thomson, A.M., Deuchars, J., and West, D.C. (1993). Large, deep layer pyramid-pyramid single axon EPSPs in slices of rat motor cortex display paired pulse and frequency-dependent depression, mediated presynaptically and self-facilitation, mediated postsynaptically. J. Neurophysiol. *70*, 2354–2369.

Tottene, A., Volsen, S., and Pietrobon, D. (2000). α_{1E} subunits form the pore of three cerebellar R-type calcium channels with different pharmacological and permeation properties. J. Neurosci. *1*, 171–178.

Tottene, A., Fellin, T., Pagnutti, S., Luvisetto, S., Striessnig, J., Fletcher, C., and Pietrobon, D. (2002). Familial hemiplegic migraine mutations increase Ca^{2+} influx through single human $Ca_V2.1$ channels and decrease maximal $Ca_V2.1$ current density in neurons. Proc. Natl. Acad. Sci. USA *99*, 13284–13289.

Tottene, A., Pivotto, F., Fellin, T., Cesetti, T., van den Maagdenberg, A.M., and Pietrobon, D. (2005). Specific kinetic alterations of human $Ca_V2.1$ calcium channels produced by mutation S218L causing familial hemiplegic migraine and delayed cerebral edema and coma after minor head trauma. J. Biol. Chem. *280*, 17678–17686.

Traynelis, S.F., and Dingledine, R. (1988). Potassium-induced spontaneous electrographic seizures in the rat hippocampal slice. J. Neurophysiol. *59*, 259–276.

Turrigiano, G.G., and Nelson, S.B. (2004). Homeostatic plasticity in the developing nervous system. Nat. Rev. Neurosci. *5*, 97–107.

van den Maagdenberg, A.M., Pietrobon, D., Pizzorusso, T., Kaja, S., Broos, L.A., Cesetti, T., van de Ven, R.C., Tottene, A., van der Kaa, J., Plomp, J.J., et al. (2004). A *Cacna1a* knockin migraine mouse model with increased susceptibility to cortical spreading depression. Neuron *41*, 701–710.

Vilagi, I., Klapka, N., and Luhmann, H.J. (2001). Optical recording of spreading depression in rat neocortical slices. Brain Res. *898*, 288–296.

Wadman, W.J., Juta, A.J., Kamphuis, W., and Somjen, G.G. (1992). Current source density of sustained potential shifts associated with electrographic seizures and with spreading depression in rat hippocampus. Brain Res. *570*, 85–91.

Welch, K.M. (2005). Brain hyperexcitability: the basis for antiepileptic drugs in migraine prevention. Headache *45* (*Suppl 1*), S25–S32.

Westenbroek, R.E., Sakurai, T., Elliott, E.M., Hell, J.W., Starr, T.V., Snutch, T.P., and Catterall, W.A. (1995). Immunochemical identification and subcellular distribution of the alpha1A subunits of brain calcium channels. J. Neurosci. *15*, 6403–6418.

Zaitsev, A.V., Povysheva, N.V., Lewis, D.A., and Krimer, L.S. (2007). P/Q-type, but not N-type, calcium channels mediate GABA release from fast-spiking interneurons to pyramidal cells. J. Neurophysiol. *97*, 3567–3573.

Neuron, Volume 61

Supplemental Data

Enhanced Excitatory Transmission at Cortical Synapses as the Basis for Facilitated Spreading Depression in $Ca_V2.1$ Knockin Migraine Mice

Angelita Tottene[1,4], Rossella Conti[1,4], Alessandra Fabbro[1], Dania Vecchia[1], Maryna Shapovalova[1], Mirko Santello[1], Arn M.J.M. van den Maagdenberg[2,3], Michel D. Ferrari[2] and Daniela Pietrobon[1,*]

Supplemental Experimental Procedures

Preparation of acutely dissociated cortical pyramidal neurons

Cortical pyramidal neurons were acutely dissociated from postnatal day (P) 13-15 mice using procedures similar to those reported in Howe and Surmeier (1995) except for the following details: brain slices were cut in an ice-cold high sucrose solution continuously bubbled with 100% O_2 containing (in mM): 250 sucrose, 11 glucose, 2.5 KCl, 1 NaH_2PO_4, 2 $MgSO_4$, 2 $CaCl_2$, 15 HEPES (pH 7.4, 305 mOsm); the $NaHCO_3$-buffered holding solution also contained ascorbic acid 0.2 mM, N-nitro-L-arginine 0.1 mM and kynurenic acid 1 mM; enzymatic digestion was made using protease type XIV (Sigma) 1 mg/ml for 15 min.

Preparation of cortical neurons in microculture

Cortical neurons were isolated from P0-2 mice following the procedure of Levi et al. (1984) and cultured on glial microislands (at the density of 6000-25000 cells/ml) essentially as reported in Brody and Yue (2000) for hippocampal neurons, except for the following details: astrocytes culture medium was Basal Eagle's Medium (BME) plus 10% fetal bovine serum, 25 mM KCl, 2 mM glutamine and 50 μg/ml gentamicin; neuronal medium was Neurobasal A plus 2% B27 Supplement, 0.5 mM glutamine and 1% PSN Antibiotic mix (all from Gibco); only half volume of astrocytes medium was replaced with neuronal medium to allow the astrocytes to condition the medium before neuron plating. Every 4 days half volume of neuronal medium was changed with fresh one.

Single cortical neurons grown on glial microislands form synaptic connections onto themselves (autapses); these autaptic connections are by definition monosynaptic, offer an unusually homogeneous population of synapses producing large synaptic responses, all miniature postsynaptic currents arise from the same presynaptic cell as the evoked postsynaptic currents and solution exchanges can be fast and complete.

Slice preparation

Acute thalamocortical slices of the barrel cortex were made from P11-15 mice. Animals were anestethized with isofluoran and decapitated. The brain was quickly removed and put in an ice-cold cutting solution (in mM: 125 NaCl, 2.5 KCl, 1 $CaCl_2$, 4 $MgCl_2$, 25 glucose, pH 7.4 with 5% CO_2). The brain was dissected at the right angles to obtain thalamocortical slices, as described in Agmon and Connors (1991). 350 μm-thick slices were then cut on the vibratome. Slices were maintained at 30 °C for 30 min in standard ACSF, sACSF (in mM: 125 NaCl, 2.5 KCl, 25 $NaHCO_3$, 1.25 NaH_2PO_4, 1 $MgCl_2$, 2 $CaCl_2$, 25 glucose) saturated with 95% O_2 and 5% CO_2 and then transferred at room temperature in the same solution until use. During the experiments, the slices were put in a chamber and continuously perfused with fresh sACSF saturated with 95% O_2 and 5% CO_2. They were visually inspected with an upright microscope with IR Nomarski optics and a 60X water immersion objective. Experiments were made within 6 hours from cut.

Acute coronal slices containing the barrel cortex for mEPSCs and CSD experiments were obtained from P16-17 mice as described above, with some modifications: 50 nM minocycline was added to the sACSF, cutting was made on the coronal plane in the solution described in Dugué et al. (2005), slices were transferred for 1 min in a 95% O_2 and 5% CO_2 saturated solution containing (in mM) 225 D-mannitol, 2.5 KCl, 1.25 NaH_2PO_4, 26 $NaHCO_3$, 25 glucose, 0.8 $CaCl_2$, 8 $MgCl_2$, 2 kynurenic acid, 0.05 minocycline, then in sACSF plus 50 nM minocycline at 30 °C for 30 min and finally at room temperature.

Biocytin staining

After recording the slices were fixed in 150 mM phosphate buffer solution containing 3% paraformaldehyde for 2-5 days. After washing, quenching of endogenous peroxidase and permeabilization, the biocytin filled cells were marked by avidin and biotinylated horseradish peroxidase (Vectastain ABC elite, Vector Labs) and then colored by making them react with diaminobenzidine in the presence of hydrogen peroxide.

Identification of layer 2/3 pyramidal cells and fast-spiking interneurons for pair recordings

Neurons were first identified based on their morphology under infrared differential interference contrast microscopy (IR DIC). Fast spiking (FS) cells are characterized by their irregular shape of the soma and the absence of a main dendrite projecting towards the pia. Pyramidal cells (PCs) were instead looked for among those cells with a triangular soma, a main apical dendrite pointing towards the pia and the absence of a main dendrite in the opposite direction. The morphology of

neurons was confirmed by post-fixation staining of the biocytin introduced through the patch electrode. The characteristic AP firing induced by suprathreshold current injections of increasing amplitudes up to 400 pA in current-clamp was the main parameter used during recordings to distinguish the type of cells. The firing of pyramidal cells shows a classic spike frequency adaptation and the maximal frequency of firing is close to 20 Hz; the second AP in a series is wider than the first, and the development of an adaptive hump as the cell is further depolarized can be often observed. Fast spiking cells show almost no adaptation in their firing and can reach firing frequencies well beyond 20 Hz. Their AP is characterized by a big component of the fast afterhyperpolarization and does not change from one AP to the other in a series (Cauli et al., 2000).

CV calculation

The CV was calculated for each experiment from the scatter of the single synaptic responses. For each sweep the peak amplitude of the EPSP was taken as the difference between the peak during the 10 ms after the onset of the response and the baseline immediately before it. The standard deviation SD was calculated as in Scheuss et al. (2002). First, the differences of the amplitudes of two successive sweeps was calculated for all sweeps. The SD was then computed as the average of these differences.

$$SD^2=(1/(R-1))*\sum_i (A_i-A_{i+1})^2/2$$

with i varying from 1 to (R-1). R is the number of trials and A_i is the amplitude of the i^{th} response. We used this type of calculation to obviate possible artefacts due to long term trends or drifts of the response during recordings.

Supplemental Results

Effect of the specific P/Q-type Ca^{2+} channel inhibitor ω-AgaIVA on synaptic transmission at unitary excitatory PC-FS and inhibitory FS-PC connections in acute mouse cortical slices

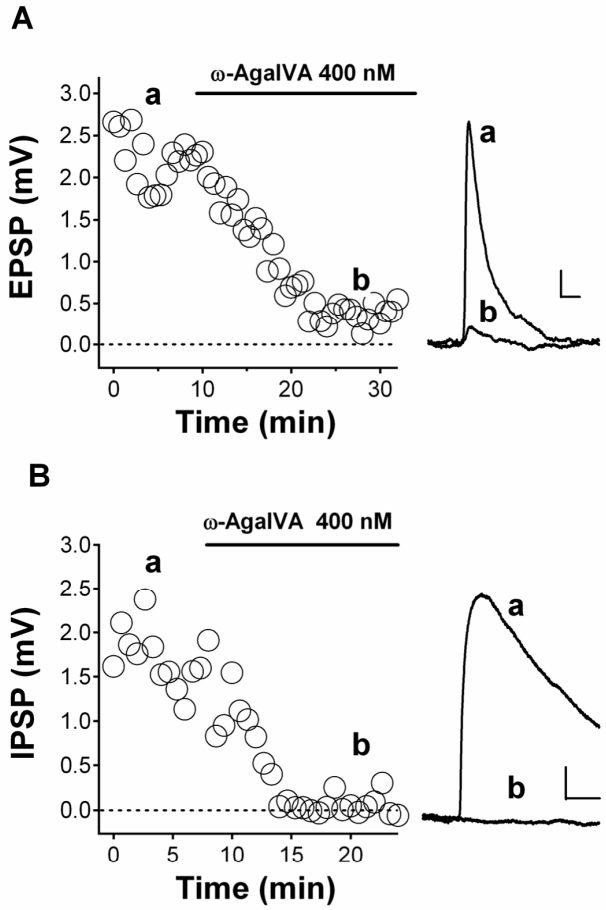

Figure S1: P/Q-type Ca^{2+} channels control both excitatory and inhibitory synaptic transmission at the PC-FS cell reciprocal connection in acute mouse cortical slices

(A) Left: EPSPs amplitudes vs time evoked in a FS cell by repeated suprathreshold stimulation of the presynaptic connected PC in an acute thalamocortical slice of a WT mouse before and during application of 400 nM ω-AgaIVA in the bath. Each data point is the average over 4 successive sweeps (40 s). Right: EPSP traces averaged over 10 min before (a) and at the end (b) of the drug application. Scale bars: 10 ms, 0.25 mV.

(B) Left: IPSPs amplitudes vs time evoked in a PC by repeated suprathreshold stimulation of the presynaptic connected FS cell in an acute thalamocortical slice of a KI mouse before and during

application of 400 nM ω-AgaIVA in the bath. Each data point is the average over 4 successive sweeps (40 s). Right: IPSP traces averaged over 8 min before (a) and at the end (b) of the drug application. Scale bars: 20 ms, 0.25 mV.

Comparison of the relative values of the mean EPSP amplitude and the square of the coefficient of variation in wild-type and FHM1 knockin mice

To further support the conclusion that the increased mean EPSP amplitude evoked in a FS interneuron in response to an action potential in the connected pyramidal cell in FHM1 knockin mice is due to a presynaptic mechanism and in particular to a change in the probability of release we used the coefficient of variation method. This method is based on the comparison of two parameters: π and ρ, which in our case are defined as:

$\pi = A_{KI}/A_{WT}$

$\rho = CV^2_{WT}/CV^2_{KI}$

where A is the amplitude of the mean EPSP and CV is the coefficient of variation of the unitary EPSP amplitudes. Assuming a binomial distribution of the unitary EPSPs, with n release sites with homogeneous probability of release p and quantal response q, the CV and average amplitude of the synaptic response can be expressed in terms of the parameters n, p and q in the following manner:

CV=[(1-p)/np]^1/2

A=npq

Consequently, if the change in amplitude is postsynaptic and hence due to a change in q, the quantity ρ shouldn't change, independently of π. If the change in amplitude is presynaptic, it could be due to a change in only n or to a change in only p or to a change in both; in the case of a change in only n, π would be equal to ρ. If only p changes, π would be smaller than ρ. From our data, $\pi = 1.99$ and $\rho = 3.00$, which is consistent with the conclusion that the increased amplitude of the mean EPSP in KI mice is due to a presynaptic change, and in particular to a change in p.

Correlation between the amplitudes of the second and the first unitary EPSP in a train at the PC-FS connection in wild-type mice

To gain insights into the mechanism of the depression of the EPSPs measured during trains of action potentials at 10 Hz at the PC-FS connection in WT mice, we investigated whether the amplitudes of the second and first unitary EPSPs in a train were correlated: Figure S2 shows an inverse correlation, as expected if depression is mainly due to vesicle depletion.

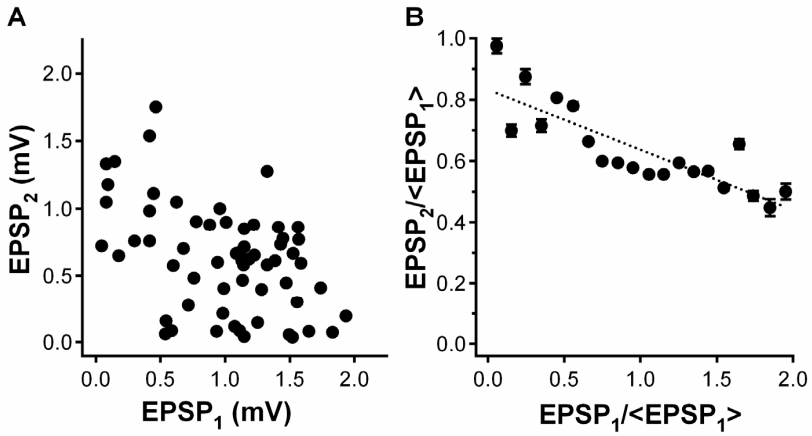

Figure S2: The paired pulse depression of the excitatory synapse onto fast-spiking interneurons is mainly attributable to vesicular depletion

(A) The peak amplitude of the second EPSP during a train is plotted for each trial as a function of the peak amplitude of the first EPSP from a representative experiment. It is evident that if the first EPSP has a big amplitude, the second EPSP is generally small. On the other hand, small responses to the first AP result in bigger responses to the second.

(B) The same analysis as in A, performed on the pooled data from all experiments with PPR<0.8 (experiments which showed clear depression; n=14). For each experiment the values of the EPSPs were normalized to the average value of the first EPSP (<$EPSP_1$>); the EPSPs data were then pooled and binned with a bin width of 0.1 mV, and the average normalized $EPSP_2$ was plotted as a function of the average normalized $EPSP_1$ in the bin. Data points were well fitted by a line (correlation coefficient r=0.87) with negative slope, indicating a clear inverse correlation between the amplitude of the first and the second EPSP in a train, as expected if the depression was due to vesicular depletion.

Supplemental References

Agmon, A. and Connors, B.W. (1991). Thalamocortical responses of mouse somatosensory (barrel) cortex in vitro. Neuroscience *41*, 365-79.

Brody, D.L. and Yue D.Y. (2000). Release-independent short-term synaptic depression in cultured hippocampal neurons. J. Neurosci. *20*, 2480-2494.

Cauli B., Porter J.T., Tsuzuki K., Lambolez B., Rossier J., Quenet B., Audinat E. (2000). Classification of fusiform neocortical interneurons based on unsupervised clustering. Proc. Natl. Acad. Sci. USA *97*, 6144-9.

Dugué, G.P., Dumoulin, A., Triller, A., and Dieudonné, S. (2005). Target-dependent use of co-released inhibitory transmitters at central synapses. J. Neurosci. *25*, 6490-6498.

Howe, A.R. and Surmeier, D.J. (1995). Muscarinic receptors modulate N-, P-, and L-type Ca^{2+} currents in rat striatal neurons through parallel pathways. J. Neurosci. *15*, 458-469.

Levi, G., Aloisi, M., Ciotti, M. and Gallo, V. (1984). Autoradiographic localization and depolarization-induced release of amino acids in differentiating granule cells cultures. Brain Res. *290*, 77-86.

Scheuss, V., Schneggenburger, R., and Neher, E. (2002). Separation of presynaptic and postsynaptic contributions to depression by covariance analysis of successive EPSCs at the calyx of held synapse. J. Neurosci. *22*, 728-739.

3. AIM OF WORK (II)

Among the FHM1 mutations, the S218L one causes a severe hemiplegic migraine syndrome associated with progressive cerebellar ataxia, seizures, and severe, sometimes fatal, cerebral oedema which can be triggered by only a trivial head trauma (Chan et al., 2008; Debiais et al., 2009; Fitzsimons and Wolfenden, 1985; Kors et al., 2001). In agreement with the more severe phenotype, the S218L mutation produces one of the largest hyperpolarized shift of activation of human $Ca_V2.1$ channels and one of the largest gain of function especially for small depolarizations (Tottene et al., 2005). Accordingly, at low voltages close to the threshold of activation of mutant channels, the gain of function of the $Ca_V2.1$ current in cerebellar granule cells was larger in homozygous S218L (SL/SL) KI mice than in homozygous R192Q (RQ/RQ) KI mice (van den Maagdenberg et al., 2004, 2010). The R192Q mutation causes a milder clinical phenotype compared to the S218L one, indeed the R192Q carriers present pure hemiplegic migraine attacks. Interestingly, the SL/SL KI mice faithfully mimic the broad spectrum of hemiplegic attacks, epileptic seizures, mild impact-triggered cerebral oedema and cerebellar ataxia seen in S218L patients, as a consequence they have a reduced life-expectancy (van den Maagdenberg et al., 2010). Moreover, these phenotypical symptoms appear to be unique to SL/SL KI as none were observed in heterozygous S218L (SL/WT) KI, nor in RQ/RQ KI mice. For these reasons S218L KI mice have been tested for the susceptibility to cortical spreading depression (CSD), the neurological phenomenon underlying migraine aura and a possible trigger of migraine headache (Pietrobon, 2005), as a lower threshold for CSD induction and an increased velocity of CSD propagation was found in RQ/RQ KI mice *in vivo* (van den Maagdenberg et al., 2004). In correlation with the more severe clinical phenotype of the S218L mutation, the facilitation of CSD induction, and especially the facilitation of CSD propagation was larger in SL/SL KI than in RQ/RQ KI mice (van den Maagdenberg et al., 2010). Moreover, homozygous S218L KI mice showed a higher incidence of recurrent CSD events upon only a single stimulus that is probably explained by the unique combination of a particularly low threshold of activation and slow inactivation, and a particularly fast rate of recovery from inactivation of mutant S218L $Ca_V2.1$ channels (Pietrobon, 2005; Tottene et al., 2005; van den Maagdenberg et al., 2010). In addition, the facilitation of CSD induction and propagation were about twice as large in homozygous compared with heterozygous S218L KI mice revealing an allele dosage-effect consistent with dominance of the mutation in FHM1 patients (van den Maagdenberg et al., 2010). The allele dosage-effect was also seen both for the

probability of experiencing successive CSD, as well as, for the increased P/Q current density in cerebellar granule cells. Interestingly, although CSD induction threshold and propagation velocity are similar in SL/WT KI and RQ/RQ KI mice, multiple CSD events were seen only rarely in the RQ/RQ KI mice (van den Maagdenberg et al., 2004, 2010). Thus the cortical susceptibility to repetitive CSD events is apparently unique to the S218L mutation, and probably underlying the severe phenotype. So investigate the mechanisms underlying the facilitation of CSD induction and propagation in both S218L KI and R192Q KI mice is important to understand the pathophysiology of FHM1 and also migraine.

Because the pivotal role of $Ca_V2.1$ channels and glutamate release in the CSD ignition (Pietrobon, 2005, 2007; see Introduction), in my laboratory has been recently studied cortical excitatory neurotransmission in homozygous R192Q KI mice to investigate the mechanisms underlying the facilitation of CSD induction and propagation in KI mice compared to wild-type (WT) mice (see pdf file attached: Tottene et al., 2009). As a consequence of the activation of mutant $Ca_V2.1$ channels at lower voltages, RQ/RQ KI mice showed gain of function of P/Q-type Ca^{2+} current density in cortical pyramidal cells that was similar to that found in cerebellar granule cells. To demonstrate if the gain of function of mutant cortical $Ca_V2.1$ channels could lead to increased action potential (AP)-evoked Ca^{2+} influx through presynaptic $Ca_V2.1$ channels and to increased glutamate release at cortical pyramidal cell synapses, cortical excitatory neurotransmission was investigated by measuring evoked excitatory postsynaptic currents in microcultures of cortical pyramidal cells and evoked excitatory postsynaptic potentials in connected pairs of layer 2/3 pyramidal cells and fast-spiking interneurons in thalamocortical slices of the somatosensory cortex. Firstly, was verified the contribution of P/Q-, N-, and R-type Ca^{2+} channels to synaptic transmission at WT cortical pyramidal cell autapses. Interestingly, it was found that all the three Ca_V2 type Ca^{2+} channels cooperate (with overlapping local Ca^{2+} domains) in controlling release at individual synapses of cortical pyramidal cells in microcoltures. After this, the increased AP-evoked Ca^{2+} and glutamate release at cortical pyramidal cell synapses from RQ/RQ KI mice was investigated. In fact, in single cortical pyramidal cells forming autapses, both the strength of synaptic transmission and the contribution of P/Q-type Ca^{2+} channels to synaptic transmission were enhanced in KI mice without compensatory changes in the N- and R-type Ca^{2+} currents. Further supporting the conclusion of an increased AP-evoked Ca^{2+} influx through presynaptic mutant $Ca_V2.1$ channels was the finding that the dependence of the EPSC on the external concentration of Ca^{2+} ions was shifted to lower values in RQ/RQ KI mice. Moreover, the short term depression (STD)

of the EPSCs during a train of action potentials was increased in RQ/RQ KI mice, indicating an increased probability of vesicle release at individual cortical synapses. The strength of excitatory neurotransmission were also increased at unitary connections between layer 2/3 pyramidal cells and fast-spiking interneurons in acute KI thalamocortical slices, where glutamate release is principally controlled by P/Q-type Ca^{2+} channels. The low percentage of the presynaptic APs that failed to evoke an EPSP in the fast-spiking interneuron and the increased STD found in RQ/RQ KI mice were consistent with an increased probability of vesicle release at the excitatory synaptic connection between pyramidal cells and fast-spiking interneurons in KI mice. These data indicate that a relatively small shift to lower voltages of activation of mutant $Ca_V2.1$ channels leads to a significant increase in AP-evoked Ca^{2+} influx at the active zones of pyramidal cells (assuming a similar voltage shift for presynaptic and somatic channels). Despite the gain of function of cortical excitatory neurotransmission, neither postsynaptic nor presynaptic homeostatic compensatory mechanisms were observed at excitatory synapses onto pyramidal cells of FHM1 mice, as both the amplitude and the frequency of miniature EPSCs recorded in microcoltures and slices were similar in RQ/RQ KI and WT mice. The development of an *in vitro* model of CSD in brain slices of somatosensory cortex, confirmed the facilitation of induction and propagation of experimental CSD in KI mice. Interestingly, a causative link between enhanced glutamate release and CSD facilitation was found, as both the CSD threshold and velocity of KI mice became similar to those of WT mice, when glutamate release at pyramidal cell synapses was brought back to WT values using subsaturating concentrations of the specific P/Q channel blocker ω-AgaIVA (40 nM). This finding, and in addition, the unaltered inhibitory neurotransmission founded at connected pairs of fast-spiking interneurons and pyramidal cells in cortical slices from KI mice, indicate that disruption of excitation-inhibition balance and neuronal hyperactivity may be basic for susceptibility of CSD ignition in KI mice and probably in migraine.

The similar gain of function of $Ca_V2.1$ current density in cerebellar granule cells and cortical pyramidal dissociated cells in RQ/RQ KI mice, as well as, a similar increased P/Q-type Ca^{2+} current density in cerebellar granule cells of SL/WT KI and RQ/RQ KI mice at voltages near the channel activation, predicts a similar increased $Ca_V2.1$ current density in cortical pyramidal cells from heterozygous S218L KI mice (Tottene et al., 2009; van den Maagdenberg et al., 2004, 2010).Because the increased excitatory neurotransmission in RQ/RQ KI mice, the causative link between enhanced glutamate release and susceptibility to CDS, as well as, the a similar facilitation to CSD in SL/WT KI and RQ/RQ KI mice, one would predict a similar increased action

potential-evoked Ca^{2+} influx through cortical SL/WT $Ca_V2.1$ channels at the active zone and a consequent similar increased of glutamate release in SL/WT KI and RQ/RQ KI mice (Tottene et al., 2009; van den Maagdenberg et al., 2004, 2010). As a consequence the gain of function of excitatory neurotransmission should be larger in homozygous S218L KI mice, since the allele dosage effect founded in SL/WT and SL/SL KI mice for both the facilitation of CSD, and the increased P/Q current density in cerebellar granule cells (van den Maagdenberg et al., 2010). The supposed larger enhanced glutamate release should explain the larger facilitation of CSD in homozygous S218L KI mice and the more severe clinical phenotype.

To demonstrate these hypothesis, I have studied cortical excitatory neurotransmission measuring AP-evoked excitatory postsynaptic current in microcultures of cortical pyramidal cells from neonatal wild-type and heterozygous S218L KI mice. The use of heterozygous S218L KI mice was preferred to that of homozygous S218L KI mice because, as above reported, adult SL/SL KI mice have a reduce life expectancy that causes a decrease number of successfully breed compared to heterozygous S218L KI mice (van den Maagdenberg et al., 2010). In addition, FHM1 is a autosomic dominant disease, so the mutation in humans is expressed in heterozygous (Ophoff et al., 1996). For this reason the study of the functional consequences of the S218L mutation in heterozygous KI mice is interestingly.

4. RESULTS (II)

4.1 Cortical excitatory neurotransmission in heterozygous S218L knock-in mice

I investigated cortical excitatory neurotransmission in heterozygous knock-in (KI) mice carrying the $Ca_V2.1$ S218L FHM1 mutation to understand the mechanisms underlying the greater facilitation of induction and propagation of cortical spreading depression (CSD) in S218L KI mice compared to KI mice carrying the human R192Q FHM1 mutation. I studied glutamatergic neurotransmission in heterozygous S218L (SL/WT) KI mice because FHM1 is an autosomal dominant disease and the allelic disorder is presented in heterozygosis in humans (Ophoff et al., 1996). Moreover, the life expectancy and the number of successfully breeds are higher in SL/WT KI compared to homozygous S218L (SL/SL) KI mice (van den Maagdenberg et al., 2010). In addition, an allele dosage in SL/SL and SL/WT was reported both for the gain of function of $Ca_V2.1$ current density in cerebellar granule cells and for facilitation of CSD, so one predicts an allele dosage effect also for cortical neurotransmission.

To investigate cortical excitatory neurotransmission, I measured action potential (AP)-evoked excitatory postsynaptic currents (EPSCs) in microcultures of cortical pyramidal cells from neonatal wild-type (WT) and SL/WT KI mice. Single cortical

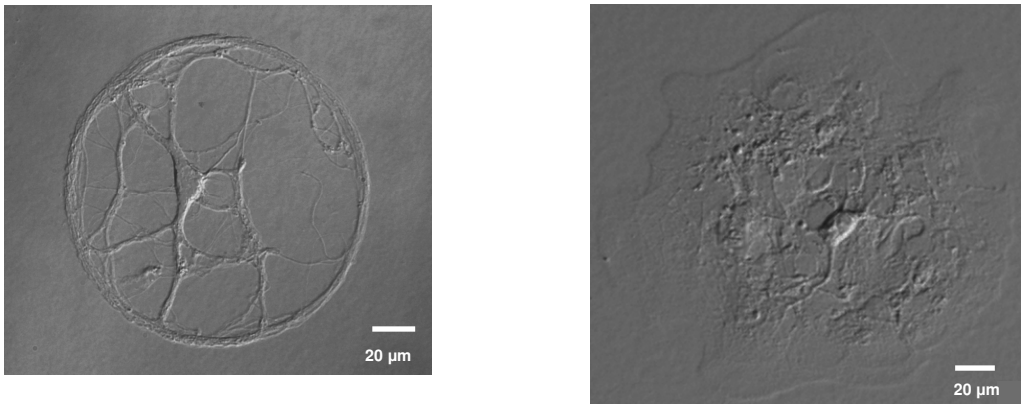

Figure 4.1. Examples of single cortical pyramidal neurons grown on substrate or glial microislands
Left: Example of a single pyramidal cortical cell grown on a microisland of substrate for 10 days *in vitro*. In this preparation astrocytes were not presented in order to clearly see the autapses formation.
Right: Example of a single pyramidal cortical cell grown on a glial microisland for 10 days *in vitro*. This is the typical single cortical neuron grown on a glial microisland selected for patch-clamp recordings.

neurons grown on glial microislands form synaptic connections onto themselves (autapses) with properties very similar to those of synapses between neurons (Bekkers and Stevens, 1991; Figure 4.1, right). In single cortical pyramidal cells in culture, large EPSC was evoked by a 2 ms depolarizing voltage step to +20 mV from the holding potential of -80 mV, which elicited an action potential in the unclamped axonal processes. The action potential propagated to synaptic terminals where it induced glutamate release. The AP-evoked excitatory postsynaptic current was recorded at -80 mV for 100 ms. Since the fast excitatory neurotransmission is mediated by the AMPA-type glutamate receptors, NMDA receptors were blocked by the specific NMDA receptors inhibitor D-AP5 (0.05 mM), added to the recording solution. The average current (obtained from 4-5 traces) recorded in the presence of saturating concentration of the specific AMPA receptors inhibitor, NBQX (5 µM), was subtracted to all records to obtain the pure AMPA-mediated EPSCs (Figure 4.2).

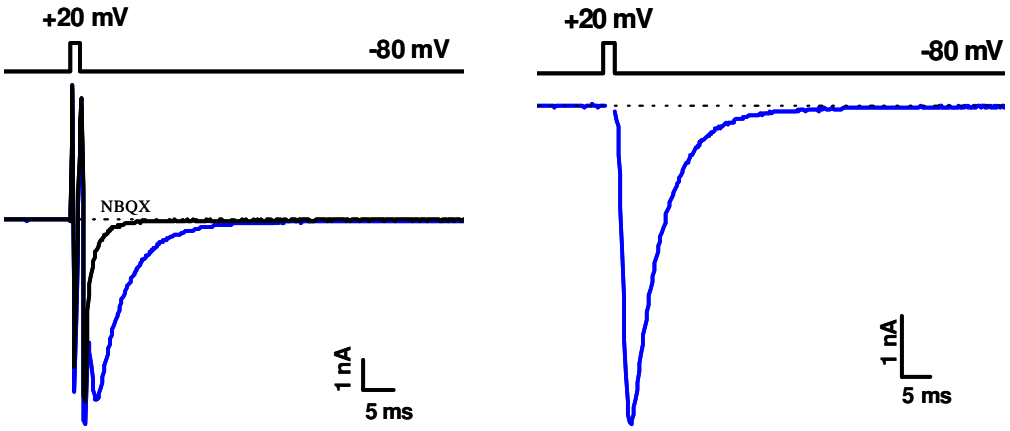

Figure 4.2. Example of excitatory postsynaptic current (EPSC) before and after subtraction of trace recorded in NBQX

Left: Example of EPSC recorded before (blue trace) and after (black trace) NBQX application.

Right: Example of the pure AMPA-mediated EPSC after subtraction of the EPSC trace recorded in NBQX, represented in the left panel.

The brief depolarizing voltage step was applied every 10 s and the average EPSC amplitude of each experiment was calculated from the peak EPSC of 5-6 recordings obtained 3 minutes after break-in and, in case, after the EPSC stabilization (experiments in which an EPSC amplitude run-down more than 40 % was observed during the first 3 minutes, were discarded). This was the standard method used to measure the mean EPSC amplitude; for particular cases (analysis of the Ca^{2+} dependence of EPSC and of the short-term plasticity) see details in below paragraphs.

The amplitude of the AMPA-mediated EPSC from neurons grown on glial microcultures increased with days *in vitro* (Figure 4.3) for an increased number of functional autapses (Takada et al., 2005). To accurately compare the results obtained from WT and SL/WT KI mice the number of recordings for days *in vitro* (DIV) were closely matched for every typology of experiment.

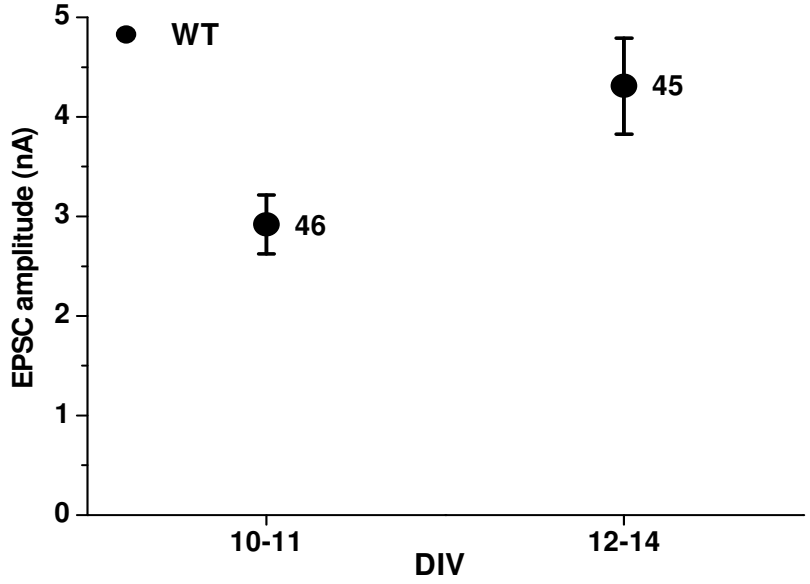

Figure 4.3. Increased average amplitude of action potential-evoked excitatory postsynaptic current in wild-type mice with days *in vitro* (DIV)

The average evoked EPSC amplitudes recorded from WT pyramidal cells were plotted as a function of DIV (2.9 ± 0.3 nA, n = 46 at DIV 10-11; 4.3 ± 0.5 nA, n = 45 at DIV 12-14, respectively). The EPSC amplitude recorded in neurons in autaptic cultures continued to increase with DIV (Takada et al., 2005). For this reason it was necessary to closely match the number of neurons recorded from WT and SL/WT KI mice at different DIV.

4.1.1 Amplitude of action potential-evoked excitatory postsynaptic current in wild-type and heterozygous S218L knock-in mice

I recorded action potential-evoked excitatory postsynaptic current in WT and heterozygous S218L pyramidal cells to compare the results obtained for R192Q KI mice. If the S218L FHM1 mutation, as demonstrated for the R192Q one (Tottene et al., 2009), leads to an increased AP-evoked Ca^{2+} influx through $Ca_V2.1$ channels located at the active zones, the probability of vescicle release at SL/WT KI synapses should be larger than the one at WT synapses. Therefore a larger AP-evoked EPSC amplitude in single cortical pyramidal neurons from SL/WT KI mice should be expected. Indeed, I

observed that the average value of AP-evoked EPSC amplitude recorded at 10-14 DIV was 1.76 times larger in heterozygous SL/WT KI mice than in WT mice (Figure 4.4B: 6.3 ± 0.5 nA, n = 95 in SL/WT KI versus 3.6 ± 0.3 nA, n = 91 in WT mice). Figure 4A shows the cumulative distribution of AP-evoked EPSC amplitudes from WT and SL/WT KI pyramidal cells, representing the fraction of neurons with an EPSC amplitude equal or lower than the value reported on the X-axis. Both the cumulative distribution and the average value of AP-evoked EPSC amplitudes demonstrate an increased glutamate release in heterozygous S218L KI mice compared to WT mice, in agreement with an increased probability of vesicle release due to an increased AP-evoked Ca^{2+} influx through mutant presynaptic P/Q-type Ca^{2+} channels at the active zones.

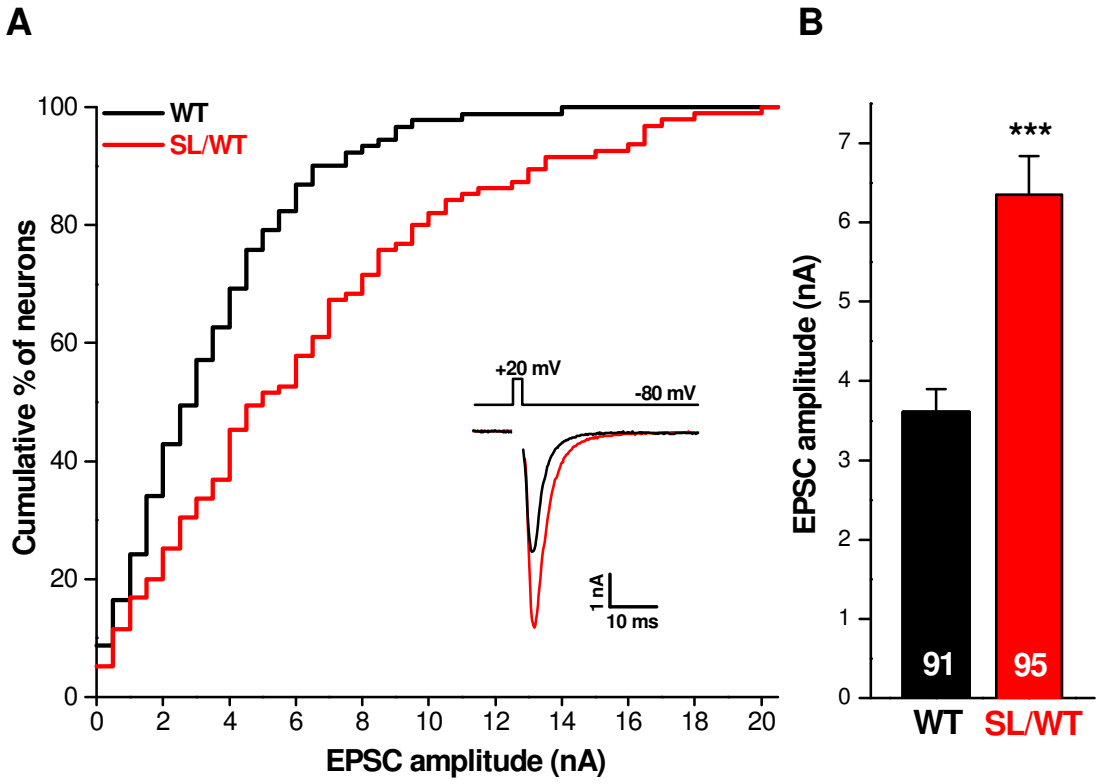

Figure 4.4. Increased action potential-evoked excitatory postsynaptic current in heterozygous S218L KI mice

A: Cumulative distribution (bin 0.5) of AP-evoked EPSC amplitudes from WT (n = 91) and SL/WT KI (n = 95) pyramidal cells.

Inset: EPSC traces from a representative WT and SL/WT KI neuron.

B: Average value of AP-evoked EPSC amplitudes from WT (3.6 ± 0.3 nA, n = 91) and SL/WT KI (6.3 ± 0.5 nA, n = 95) pyramidal cells.

The relative number of neurons recorded from WT and SL/WT KI mice at different DIV were closely matched as represented in Figure 4.5: WT n = 46, 45 and SL/WT KI n = 48, 47 at DIV 10-11 and 12-14, respectively. As it is shown, the

difference in the average value of the AP-evoked EPSC amplitudes from WT and SL/WT KI pyramidal cells was statistically significant at both DIV ranges.

The analysis of the AP-evoked EPSC amplitude indicates that the glutamate release at cortical pyramidal autapses is larger in heterozygous S218L KI than in WT mice.

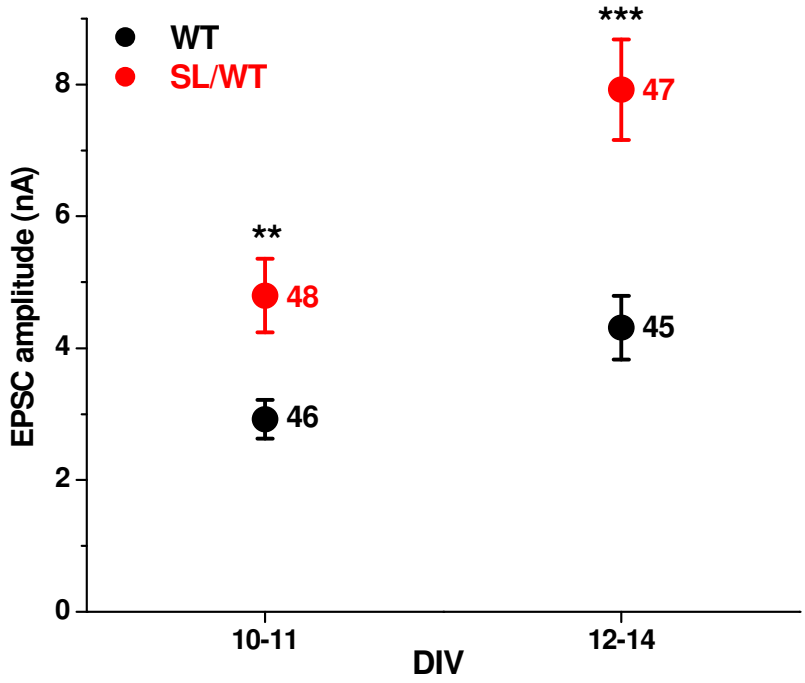

Figure 4.5. Developmental increase in the amplitude of action potential-evoked excitatory postsynaptic current from wild-type and heterozygous S218L knock-in pyramidal cells
The average evoked EPSC amplitudes were plotted as a function of DIV. WT mice: 2.9 ± 0.3 nA, n = 46 at DIV 10-11; 4.3 ± 0.5 nA, n = 45 at DIV 12-14, respectively. SL/WT KI mice: 4.8 ± 0.6 nA, n = 48 at DIV 10-11; 7.9 ± 0.8 nA, n = 47 at DIV 12-14, respectively.

4.1.2 Contribution of $Ca_V2.1$ channels to cortical excitatory neurotransmission in wild-type and heterozygous S218L knock-in mice

The increased action potential-evoked excitatory postsynaptic current found in heterozygous S218L KI mice was in agreement with the results previous reported for the R192Q mutation (Tottene et al., 2009). In R192Q KI mice we have demonstrated that the increased of glutamate release at KI synapses is exclusively due to an increased probability of release as a consequence of an increased AP-evoked Ca^{2+} influx through mutant $Ca_V2.1$ channels located at the active zones. Further supporting this conclusion, in R192Q KI mice compensatory mechanisms are not present: neither a change in the contribution of N- and R-type Ca^{2+} channels to cortical excitatory neurotransmission nor a change in the number of synaptic vesicles and/or in the size of the ready releasable

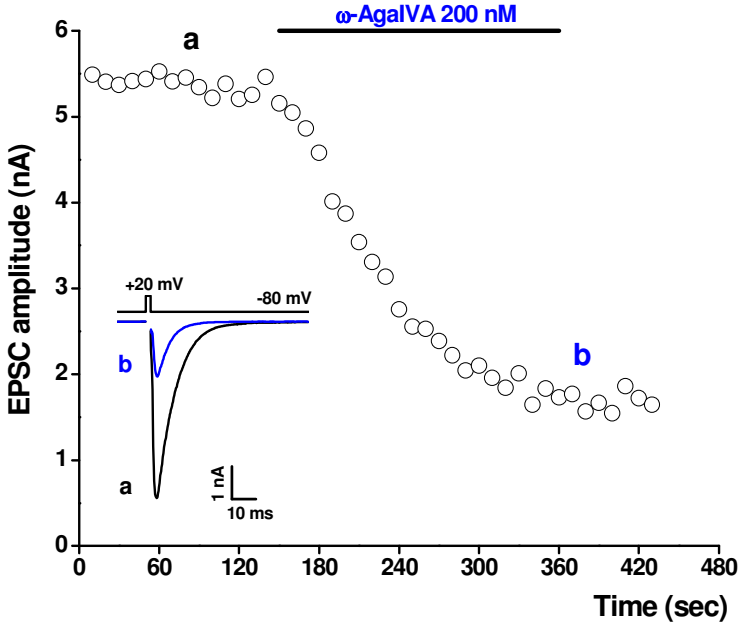

Figure 4.6. Action potential-evoked EPSCs amplitudes versus time in a SL/WT KI pyramidal neuron before (a) and during (b) application of the specific $Ca_V2.1$ channel inhibitor ω-AgaIVA (200 nM)

Inset: Representative EPSC traces taken at times a and b in a SL/WT KI pyramidal neuron.

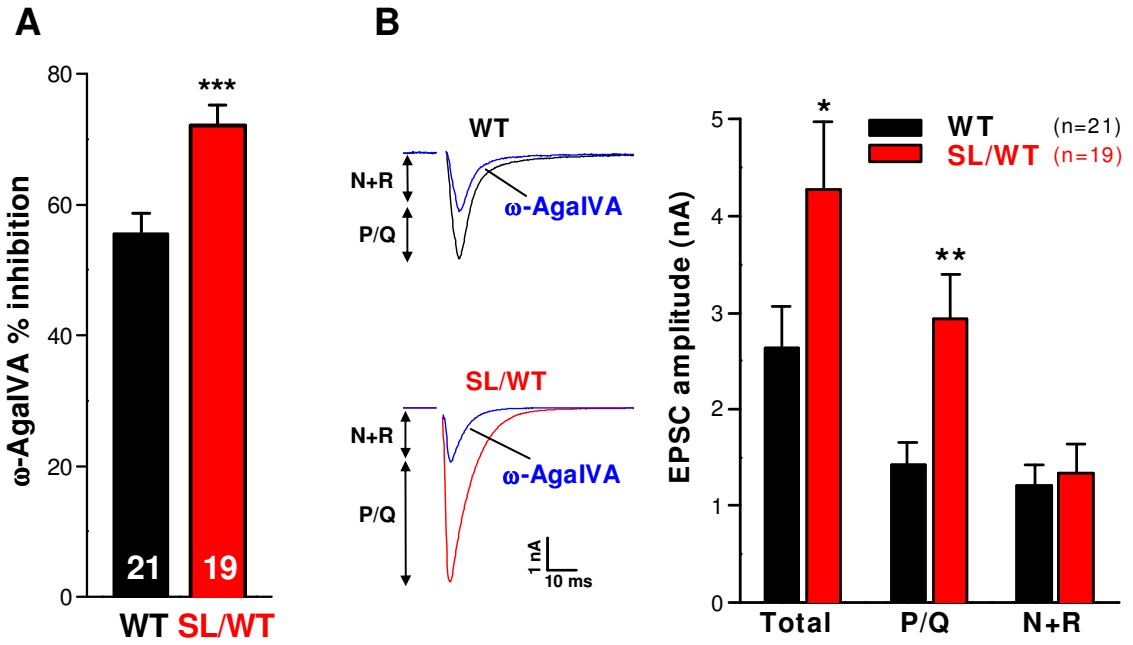

Figure 4.7. Increased contribution of $Ca_V2.1$ channels to excitatory neurotransmission in cortical pyramidal cells autapses of heterozygous S218L knock-in mice

A: Contribution of P/Q-type Ca^{2+} channels to neurotransmission evaluated from the fraction of the EPSC inhibited by ω-AgaIVA 200 nM in SL/WT KI (72 ± 3 %, n = 19) compared to WT neurons (56 ± 3 %, n = 21), using a protocol like in Figure 4.6.

B: Average values of the amplitudes of the total EPSC and its ω-AgaIVA-sensitive (P/Q) and ω-AgaIVA-insensitive (N + R) components. The P/Q and N+R components for each neuron were obtained as shown in the representative traces on the left, as the difference between the EPSC amplitude before and after ω-AgaIVA application (P/Q) and as EPSC amplitude remaining after ω-AgaIVA application (N + R).

pool (RRP) were found in KI mice. If this would be true also for the S218L FHM1 mutation, one would predict that the larger AP-evoked EPSC amplitude was due to a larger contribution of P/Q-type Ca^{2+} channels to synaptic transmission in SL/WT KI mice. To demonstrate this hypothesis I evaluated the P/Q-type Ca^{2+} channels contribution to synaptic transmission by measuring the fraction of the EPSC inhibited by a saturating concentration of the specific $Ca_V2.1$ inhibitor ω-AgaIVA (200nM), with a protocol like the one represented in Figure 4.6. A larger fraction of the EPSC was inhibited by ω-AgaIVA in SL/WT KI pyramidal neurons when compared to WT cells (Figure 4.7A: 72 ± 3 %, n = 19 in SL/WT KI versus 56 ± 3 %, n = 21 in WT mice). As previously observed, in this set of experiments I confirmed that the total evoked EPSC amplitude in SL/WT KI neurons was larger (1.62 times) that in WT neurons (Figure 4.7B, left: 4.3 ± 0.7 nA in SL/WT KI versus 2.6 ± 0.4 nA in WT mice). Moreover, I closely matched the number of cells recorded from 8 to 14 days *in vitro* (in SL/WT KI n = 3, 6, 10 and in WT mice n = 5, 8, 8 at DIV 8-9, 10-11, 12-14 respectively) and I added 3 new recordings to the 18 WT experiments reported in Tottene et al. (2009) done in the same period of the SL/WT ones, to accurately compare WT and SL/WT KI mice.

The analysis of the absolute size of the EPSC component inhibited by ω-AgaIVA indicated that the increased probability of release completely accounted for the increased EPSC amplitude in SL/WT KI mice. In fact, the absolute size of the ω-AgaIVA-sensitive component (a measure of the amount of glutamate release controlled by P/Q-type channels) was two times larger in SL/WT KI mice than in WT mice (Figure 4.7B, middle: 2.9 ± 0.5 nA in SL/WT KI versus 1.4 ± 0.2 nA in WT mice). Moreover, the difference in size of this component between the two genotypes (1.5 ± 0.5 nA) was similar to the difference in size of the corresponding total EPSC amplitude (1.6 ± 0.8 nA in Figure 4.7B, left). On the other hand, the absolute size of the ω-AgaIVA-insensitive component (a measure of the amount of glutamate release controlled by N- and R-type channels) was similar in SL/WT KI mice and WT mice (Figure 4.7B, right: 1.3 ± 0.3 nA in SL/WT KI versus 1.2 ± 0.2 nA in WT mice), indicating the absence of compensatory changes in the contribution of N- and R-type Ca^{2+} channels to neurotransmission in SL/WT KI mice. This result was also in agreement with the similar N- and R-type Ca^{2+} current densities found in cerebellar granule neurons in heterozygous S218L KI mice and WT mice (van den Maagdenberg et al., 2010). The findings that in SL/WT KI mice the amount of glutamate release controlled by P/Q-type channels was larger than in WT mice, despite an unaltered contribution of N- and R-type Ca^{2+} channels to neurotransmitter release, were inconsistent with significant changes in the number of synapses and/or in the size of the

RRP of vesicles at each synapse of SL/WT KI neurons. Indeed, any change in the number of synapses or in the RRP would have equally affected the ω-AgaIVA-sensitive and ω-AgaIVA-insensitive components of the EPSC.

Overall, these data indicate that the S218L FHM1 mutation causes an increased action-potential evoked Ca^{2+} influx through presynaptic $Ca_V2.1$ channels and, as a consequence, an increased probability of glutamate release at individual synapses on SL/WT cortical pyramidal cells.

4.1.3 Ca^{2+} dependence of the action potential-evoked excitatory postsynaptic current and short-term depression in wild-type and heterozygous S218L knock-in mice

To support the conclusion that the S218L FHM1 mutation leads to an increased action potential-evoked Ca^{2+} influx through presynaptic mutant P/Q channels I studied the extracellular Ca^{2+} dependence of the EPSC. If for every Ca^{2+} concentration there is an increased Ca^{2+} influx through presynaptic SL/WT $Ca_V2.1$ channels, the Ca^{2+} dependence of the EPSC in heterozygous S218L KI mice would be expected to shift to lower extracellular Ca^{2+} concentrations relative to WT mice (as reported for R192Q mutation in Tottene et al., 2009). To study the Ca^{2+} dependence of the EPSC, postsynaptic currents were evoked perfusing neurons with extracellular solution with different Ca^{2+} concentrations. Every extracellular solution with a different Ca^{2+} concentration was applied for at least one minute and for Ca^{2+} concentration higher than 2 mM the EPSC was evoked every 20 seconds to avoid vesicle depletion. If vesicle depletion in high extracellular Ca^{2+} concentration was present, or if less than 5-6 stable evoked postsynaptic current were recorded for every Ca^{2+} concentration tested, the experiment was discarded. In each cell, the EPSC amplitude was normalized to the maximal value obtained by fitting the data points according to the Hill equation: $EPSC = EPSC_{max} \times [Ca^{2+}]^n/\{(EC_{50})^n + [Ca^{2+}]^n\}$. Subsequently, the average normalized data points were fitted according to the Hill equation: $EPSC = [Ca^{2+}]^n/\{(EC_{50})^n + [Ca^{2+}]^n\}$, with $EC_{50} = 1.61 \pm 0.05$ mM and $n = 2.21 \pm 0.14$ for WT mice (n = 7, as reported in Tottene et al., 2009) and $EC_{50} = 0.81 \pm 0.02$ mM and $n = 2.16 \pm 0.10$ for SL/WT KI mice (n = 9, Figure 4.8); in SL/WT KI mice the EPSC amplitude increased by only 10% when the concentration of extracellular Ca^{2+} ions was raised above 2 mM in contrast with the more than 60% increase in WT mice. These data revealed that in heterozygous S218L KI mice the dependence of the EPSC on the external concentration of Ca^{2+} ions

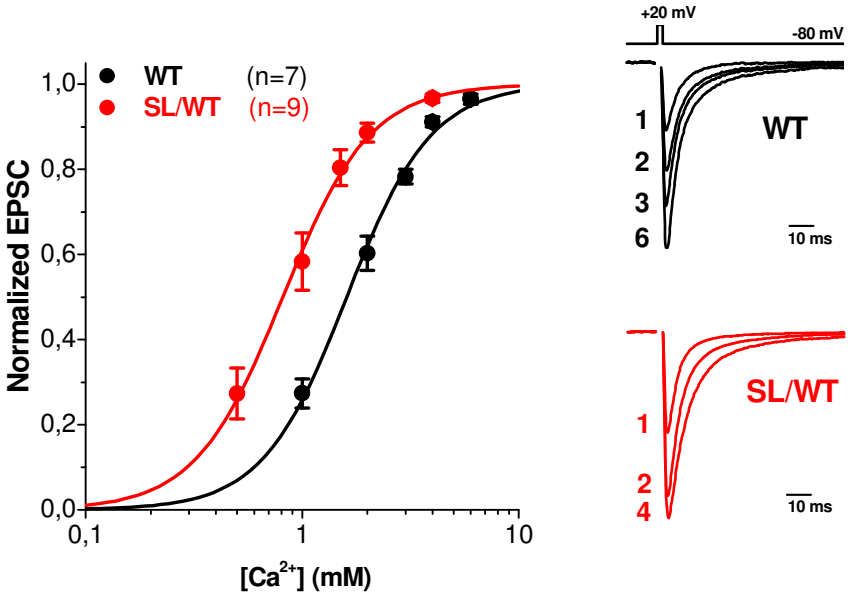

Figure 4.8. The Ca^{2+} dependence of the excitatory postsynaptic current is shifted to lower Ca^{2+} concentrations at cortical pyramidal cell autapes of heterozygous S218L knock-in mice

Left: evoked EPSC amplitude as a function of extracellular [Ca^{2+}] in autaptic cortical pyramidal neurons from WT (n = 4 and 3 at DIV 10-11, 12-14) and SL/WT KI mice (n = 6 and 3 at DIV 10-11, 12-14). The total evoked EPSC amplitude in SL/WT KI cells (4.5 ± 0.9 nA) was larger that in WT cells (3.0 ± 0.4 nA).

Right: Representative EPSC traces recorded at the indicated [Ca^{2+}] (mM) from a WT and a SL/WT neuron.

was shifted to lower values with unaltered cooperativity coefficient, indicating that the S218L FHM1 mutation causes an increased action potential-evoked Ca^{2+} influx through presynaptic SL/WT P/Q-type Ca^{2+} channels. As for R192Q KI synapses also in SL/WT KI synapses the Ca^{2+} dose-response curve had a similar steepness compared to the WT one, indicating a relative homogeneous distribution of P/Q channels at individual cortical autapses (Reid et al., 1998). Indeed, in the case of a non-uniform distribution of $Ca_V2.1$ channels, SL/WT KI mice dose-response curve would have been broadened, because only synapses containing P/Q channels would have had a lower EC_{50}.

To support the conclusion that the S218L FHM1 mutation leads to an increased probability of vesicle release at individual cortical pyramidal synapses as a consequence of the increased action potential-evoked Ca^{2+} influx through presynaptic P/Q-type Ca^{2+} channels, I compared the short-term depression (STD) in heterozygous S218L KI and WT mice. The phenomenon of STD is present when the amplitude of the second EPSC or of successive in a series, elicited by a series of APs, is smaller than that of the first one, so the paired pulse ratio (PPR, the ratio between the amplitude of the second or successive EPSC and the first EPSC) is lower than one. STD is mainly due to vesicle

depletion or to a presynaptic Ca^{2+}-dependent mechanism (Catteral and Few, 2008). If at least part of STD was due to vesicle depletion and if SL/WT KI mice had an increased probability of vesicle release, one predicted in heterozygous SL/WT KI mice a decreased of PPR compared to WT mice. To study STD the EPSCs evoked by two 50 Hz APs stimuli, applied five times at a 10 s interval, were averaged. Only neurons between 11 and 14 days *in vitro* were recorded to decrease the PPR variability as PPR value increased with DIV in autaptic cultures (Takada et al., 2005).

I found that the average PPR was decreased in SL/WT KI mice (0.72 ± 0.03, n = 36) compared to WT mice (0.89 ± 0.05, n = 38; Figure 4.9A, left). This result supports the conclusion that the S218L FHM1 mutation leads to an increased probability of vesicle release at individual cortical pyramidal synapses. Moreover, I verified that the amplitudes of both the first and the second EPSC evoked by two APs (50 Hz) in SL/WT

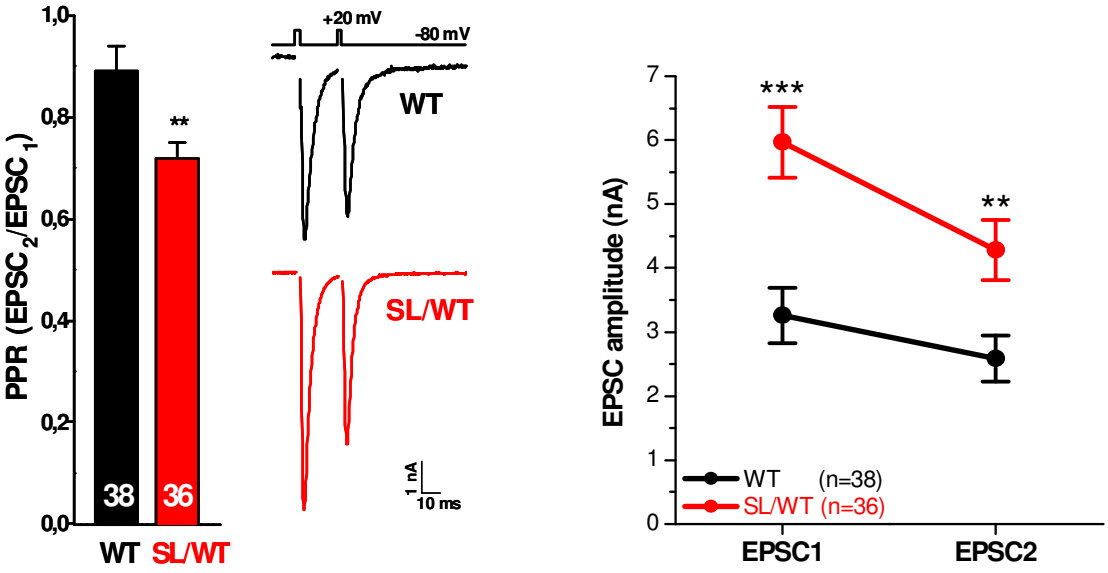

Figure 4.9. The short-term depression is enhanced at cortical pyramidal cell autapses of heterozygous S218L KI mice

A Left: Paired pulse ratio value in WT cells (0.89 ± 0.05, n = 38 at DIV 11-14) and SL/WT KI neurons (0.72 ± 0.03, n = 36 at DIV 11-14).

A Right: Average EPSCs traces evoked by two 50 Hz action potentials stimuli, applied five times every 10 seconds in a WT and a SL/WT KI neuron.

B: Average absolute EPSC amplitudes in WT (n = 38 at DIV 11-14) and SL/WT KI cells (n =36 at DIV 11-14) evoked by two 50 Hz action potentials stimuli, applied five times every 10 seconds. The mean EPSC amplitudes were: EPSC1 = 3.3 ± 0.4 nA and 6 ± 1 nA in WT and SL/WT KI neurons, respectively. EPSC2 = 2.6 ± 0.4 nA and 4.3 ± 0.5 nA in WT and SL/WT KI neurons, respectively.

KI neurons were larger than in WT neurons and that this difference remains statistically different between the two genotypes even if STD was enhanced in SL/WT KI mice (Figure 4.9B).

These experiments demonstrate that heterozygous S218L KI mice show an increased probability of vesicle release at individual cortical pyramidal cell synapses, due to an increased action potential-evoked Ca^{2+} influx through presynaptic P/Q-type Ca^{2+} channels.

4.2 Modulation of cortical excitatory synaptic transmission in heterozygous S218L knock-in and homozygous R192Q knock-in mice by $GABA_B$ receptors

I have also studied the modulation of neurotransmission due to activation of $GABA_B$ receptors. It is known from literature that these receptors modulate neurotransmission through the activation of G proteins, with a mechanism of presynaptic inhibition due, at least in part, to inhibition of presynaptic Ca^{2+} channels (Bettler et al., 2004; Bettler and Tiao, 2006). Experiments performed in a heterologous expression system demonstrated that FHM1 mutations affect the modulation of $Ca_V2.1$ channels mediated by G protein-coupled receptors (de Vries et al., 2009). In particular S218L, R192Q and Y1245C FHM1 mutations promote accelerated Gβγ dissociation from human recombinant $Ca_V2.1$ channels (Melliti et al., 2003; Weiss et al., 2008; Serra et al., 2009). Because this phenomenon may contribute to cortical hyperexcitability due to enhanced $Ca_V2.1$-dependent glutamate release and, as a consequence, to the greater facilitation to CSD found in both S218L and R192Q KI mice, I investigated if FHM1 mutations altered the $GABA_B$ modulation of the cortical excitatory synaptic transmission. To do this I evaluated the fraction of the AP-evoked EPSC inhibited by a saturating concentration of the specific $GABA_B$ agonist baclofen (10 μM, applying in a protocol like the one represented in Figure 4.10A, top) in WT, heterozygous S218L KI and homozygous R192Q (RQ/RQ) KI mice. Excitatory postsynaptic current were evoked with the same protocol described in the previous sections and the number of experiments conducted for days *in vitro* (between DIV 10 and DIV 14) were closely matched. I found that both SL/WT KI and RQ/RQ KI mice were less susceptible to presynaptic inhibition by activation of $GABA_B$ receptors; indeed, the fraction of EPSC inhibited by baclofen was lower in SL/WT KI and RQ/RQ KI mice compared to WT

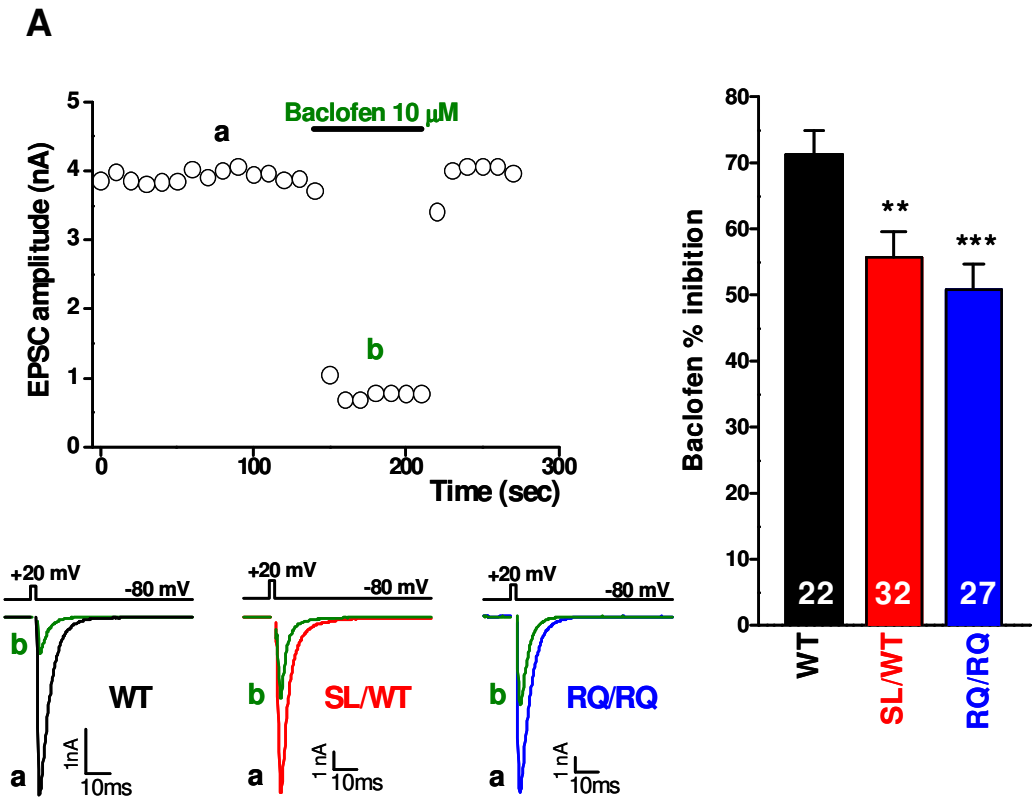

Figure 4.10. Decreased inhibition of cortical excitatory neurotransmission due to $GABA_B$ receptors activation in cortical pyramidal cell autapses of heterozygous S218L and homozygous R192Q knock-in mice

A, top: Action potential-evoked EPSC amplitudes versus time in a WT pyramidal neuron before (a) and during (b) application of the specific $GABA_B$ agonist baclofen (10 µM).

A, bottom: Representative EPSC traces taken at times a and b in a WT, SL/WT KI and RQ/RQ KI pyramidal neuron.

B: Inhibition of cortical excitatory neurotransmission by $GABA_B$ receptors activation evaluated from the fraction of the EPSC inhibited by baclofen 10 µM in SL/WT KI (56 ± 4 %, n = 16, 16 at DIV 10-11 and 12-14), RQ/RQ KI (51 ± 4 %, n = 14, 13 at DIV 10-11 and 12-14) compared to WT neurons (71 ± 4 %, n = 10, 12 at DIV 10-11 and 12-14) in protocol like the one in A, top.

mice (Figure 4.10B: 71 ± 4 %, n = 22 versus 56 ± 4 %, n = 32 versus 51 ± 4 %, n = 27 in WT, SL/WT and RQ/RQ KI mice). As a consequence of the lower inhibition of EPSC by $GABA_B$ receptors activation, cortical excitatory synaptic transmission, during G protein modulation, was further facilitated in SL/WT KI and RQ/RQ KI mice compared to WT mice, as shown by a larger difference between KI EPSC and WT EPSC amplitude during application of the $GABA_B$ agonist compared to the control condition (Figure 4.11). Indeed, the ratio between average KI EPSC and WT EPSC amplitude was enhanced during baclofen application (2.88 ± 0.84 and 3.59 ± 0.96 for

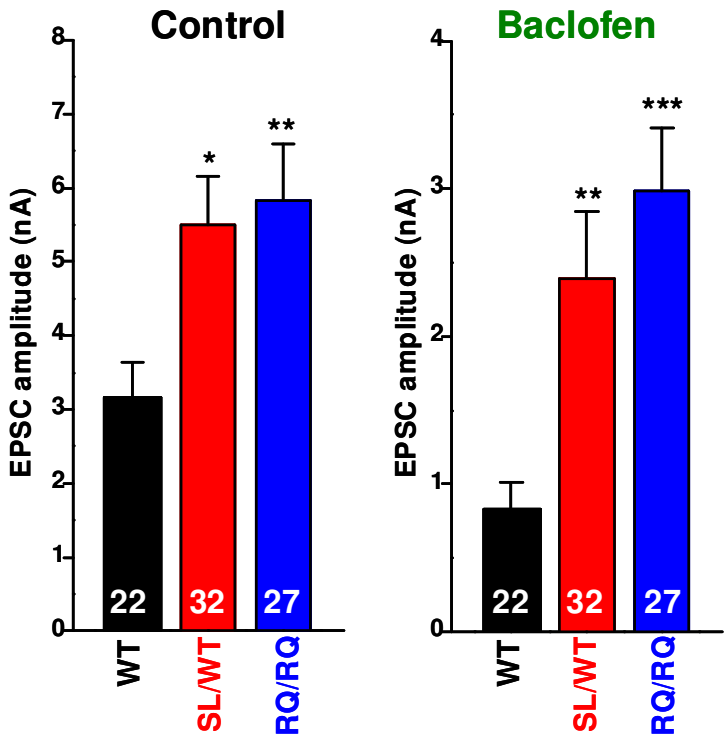

Figure 4.11. Increased facilitation of cortical excitatory synaptic transmission, during G protein modulation, in heterozygous S218L and homozygous R192Q knock-in mice

Left: Average value of total AP-evoked EPSC amplitudes from WT (3.2 ± 0.5 nA, n = 10, 12 at DIV 10-11 and 12-14), SL/WT KI (5.5 ± 0.7 nA, n = 16, 16 at DIV 10-11 and 12-14) and RQ/RQ KI pyramidal neurons (5.8 ± 0.8 nA, n = 14, 13 at DIV 10-11 and 12-14).

Rigth: Average value of AP-evoked EPSC amplitudes in the presence of baclofen 10 µM, in the same experiments reported in the left histogram from WT (0.8 ± 0.2 nA), SL/WT KI (2.4 ± 0.5 nA) and RQ/RQ KI pyramidal neurons (3.0 ± 0.4 nA).

SL/WT KI and RQ/RQ KI mice, respectively; data elaborated from Figure 4.11, right) compared to the control condition (1.74 ± 0.34 and 1.84 ± 0.38 for SL/WT KI and RQ/RQ KI mice, respectively; data elaborated from Figure 4.11, left). To verify that the lower inhibition by baclofen found in KI mice was really due to a specific effect of FHM1 mutations, and not to the fact that, as the SL/WT KI and RQ/RQ KI Ca^{2+} sensors were nearly saturated, an inhibitor would have been a lower effect in KI compared to WT neurons, I applied nickel 200 µM to inhibit the same proportion of P/Q-, N-, and R-type Ca^{2+} channels in WT, SL/WT KI and RQ/RQ KI mice. I found that a similar fraction of EPSC was inhibited by nickel in WT, SL/WT KI and RQ/RQ KI mice (40 ± 5 %, n = 2 and 6 ; 43 ± 5 %, n = 3 and 6; 33 ± 5 %, n = 5 and 7 in WT, SL/WT KI and RQ/RQ KI neurons at DIV 10-11 and 12-14, respectively). In contrast, in the same experiments the fraction of EPSC inhibited by baclofen in KI mice was lower than in WT mice (71 ± 8 %, n = 8; 51 ± 7 %, n = 9; 53 ± 5 %, n = 12 in WT, SL/WT KI and

RQ/RQ KI neurons, respectively). Even if the number of these experiments was low, the percentage of baclofen inhibition found in these experiments was similar to that reported in Figure 4.10B. These findings demonstrate that S218L and R192Q FHM1 mutations affect the G protein modulation of cortical excitatory neurotransmission mediated by $GABA_B$ receptors.

4.3 Comparison of the results from the study of cortical excitatory neurotransmission in heterozygous S218L knock-in and homozygous R192Q knock-in mice

S218L KI and R192Q KI mice presented a facilitation of induction and propagation of cortical spreading depression (CSD) *in vivo* (van den Maagdenberg et al., 2010). As the CSD threshold and velocity were similar in heterozygous S218L KI and homozygous R192Q KI mice, and considering the causative link between enhanced glutamate release and facilitation of CSD in R192Q KI mice (Tottene et al., 2009), one would have expected to find a similar gain of function of cortical glutamatergic synaptic transmission in SL/WT KI and RQ/RQ KI mice. For this reason, I compared the findings obtained from my study of cortical excitatory neurotransmission in SL/WT KI mice to the results reported in Tottene et al. (2009) for RQ/RQ KI mice; except for the new experiments of short-term plasticity and neuromodulation by G protein-coupled receptors. I found that the increase in AP-evoked EPSC amplitude, reported as the ratio between average evoked EPSC in KI and WT mice (Figure 4.12A: 1.76 ± 0.20 for SL/WT KI and 1.67 ± 0.22 for RQ/RQ KI neurons) and the contribution of $Ca_V2.1$ channels to neurotransmission (Figure 4.12B: 72 ± 3 %, n = 19 in SL/WT KI and 78 ± 3 %, n = 18 in RQ/RQ KI neurons) were similar in SL/WT KI and RQ/RQ KI mice. The similar increased AP-evoked EPSC amplitude accompanied by a larger and similar contribution of P/Q Ca^{2+} channels to synaptic transmission may have been due to a similar increased AP-evoked Ca^{2+} influx through presynaptic $Ca_V2.1$ channels and as a consequence to a similar enhanced probability or vesiscle release at SL/WT KI and RQ/RQ KI cortical pyramidal synapses. Indeed, this conclusion was supported by the findings that the Ca^{2+} dependence of the EPSC (Figure 4.12C: EC_{50} = 0.81 ± 0.02 mM and n = 2.16 ± 0.10, n = 9 for SL/WT KI versus EC_{50} = 0.94 ± 0.02 mM and n = 2.37 ± 0.12, n = 7 for RQ/RQ KI cells) and the decrease in PPR relative to WT (Figure 4.12D: 0.81 ± 0.06 for SL/WT KI and 0.73 ± 0.05 for RQ/RQ KI cells) were similar in SL/WT KI and RQ/RQ KI mice. These data demonstrated that heterozygous S218L KI and

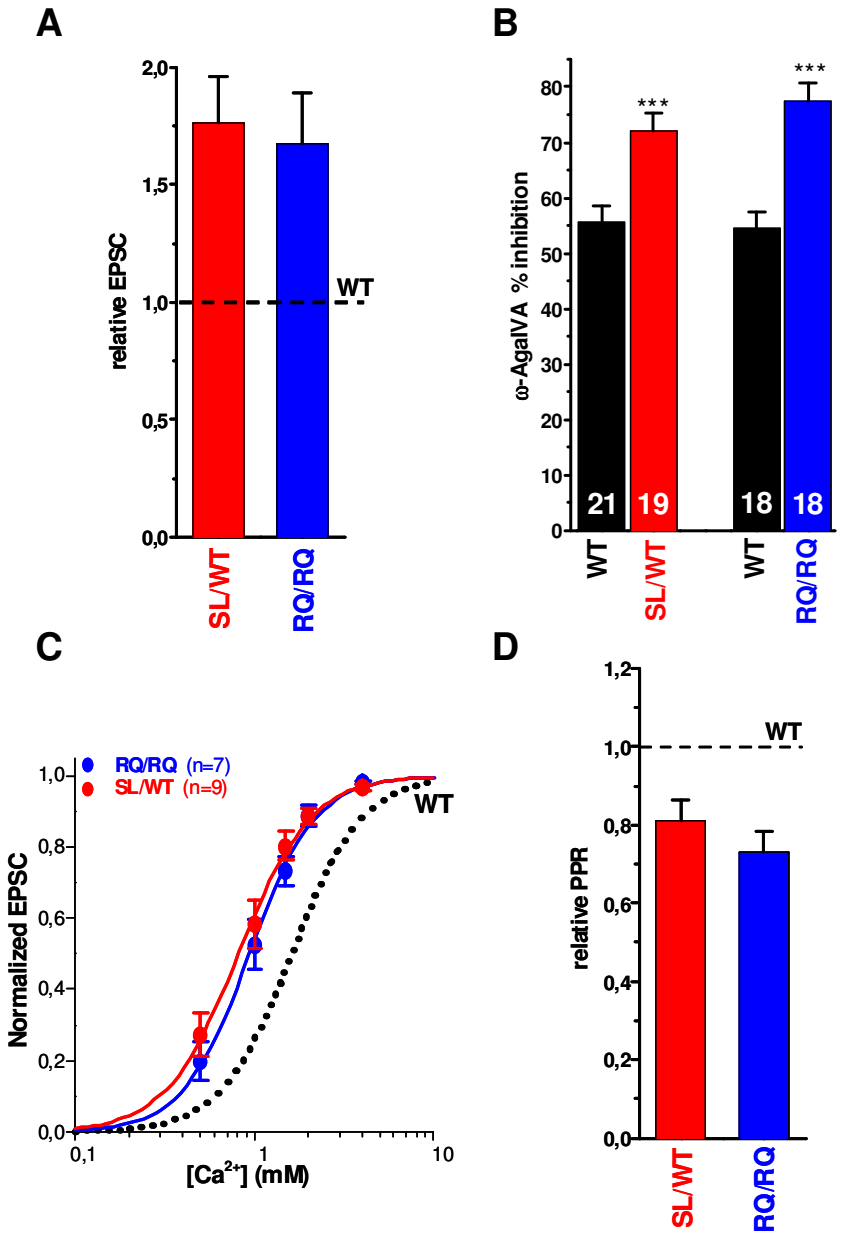

Figure 4.12. Cortical excitatory neurotransmission in SL/WT KI and RQ/RQ KI mice
A: Ratio between average AP-evoke EPSC amplitude in KI and WT mice. For SL/WT KI mice: ratio 1.76 ± 0.20 from data reported in Figure 4.4B. For RQ/RQ KI mice: ratio 1.67 ± 0.22 from elaborated data in Tottene et al. (2009) [3.0 ± 0.3 nA, n = 87 for WT and 5.0 ± 0.4 nA, n = 82 for RQ/RQ KI cells]. DIV were closely matched (WT n = 43, 44 and RQ/RQ KI cells n = 37, 45 at DIV 10-11 and 12-14, respectively).
B: Contribution of P/Q-type Ca^{2+} channels to neurotransmission evaluated from the fraction of the EPSC inhibited by ω-AgaIVA 200nM in SL/WT KI (72 ± 3 %, n = 3, 6 and 10 at DIV 8-9, 10-11 and 12-14, respectively) compared to WT neurons (56 ± 3 %, n = 5, 8 and 8 at DIV 8-9, 10-11 and 12-14, respectively) and RQ/RQ KI (78 ± 3 %, n = 4, 6 and 8 at DIV 8-9, 10-11 and 12-14, respectively) compared to WT neurons (54 ± 3 %, n = 5, 6 and 7 at DIV 8-9, 10-11 and 12-14, respectively) in protocol like the one in Figure 4.6. Data for RQ/RQ KI and corrispective WT mice were from Tottene et al. (2009).
C: evoked EPSC amplitude as a function of extracellular $[Ca^{2+}]$ in autaptic cortical pyramidal from WT (n = 4 and 3 at DIV 10-11, 12-14), SL/WT KI (n = 6 and 3 at DIV 10-11, 12-14) and RQ/RQ KI mice (n = 4 and 3 at DIV 10-11 and 12-14).
D: Ratio between PPR in KI and WT mice in neurons recorded at DIV 11-14. For SL/WT KI: ratio 0.81 ± 0.06 from data reported in Figure 4.9A, left. For RQ/RQ KI: ratio 0.73 ± 0.05 from 0.65 ± 0.03, n = 36 for RQ/RQ KI and 0.89 ± 0.05, n = 38 for WT neurons.

homozygous R192Q KI mice present a similar enhanced action potential-evoked Ca^{2+} influx and glutamate release at cortical pyramidal cell synapses. Moreover, also the presynaptic inhibition mediated by $GABA_B$ receptors is similar in the two KI compared to WT mice (Figure 4.10B).

Assuming an allele dosage effect not only for P/Q current density, and for facilitation of CSD induction and propagation, as reported in van den Maagdenberg et al. (2010) but also for glutamate release, it can be concluded that the severe S218L mutation causes a larger gain of function of cortical glutamatergic synaptic transmission than the milder R192Q FHM1 mutation. The larger gain of function of excitatory transmission produced by S218L compared to R192Q is further enhanced during neuromodulation by G protein-coupled receptors. This larger gain of function may explain the greater susceptibility to CSD induced by the S218L mutation, and possibly its dramatic clinical phenotype.

5. DISCUSSION (II)

I studied cortical excitatory neurotransmission in microcoltures of cortical pyramidal neurons from neonatal heterozygous S218L (SL/WT) KI mice carrying the human S218L FHM1 mutation. I found that the mutation S218L in the P/Q-type Ca^{2+} channel, that in patients causes a severe hemiplegic migraine syndrome, leads to an increased action potential (AP)-evoked Ca^{2+} influx and to an increased glutamate release at single cortical pyramidal cell autapses in SL/WT KI mice. In fact, both the strength of synaptic transmission and the contribution of P/Q-type Ca^{2+} channels to synaptic transmission were enhanced in SL/WT KI mice; the dependence of the excitatory postsynaptic current (EPSC) on the external concentrations of Ca^{2+} ions was shifted to lower values and the short term synaptic depression of the EPSCs during pair pulses of APs was increased. The contribution of N-, and R-type Ca^{2+} channels was unaltered at excitatory synapses onto pyramidal cells of SL/WT KI mice.

These findings indicate that a similar shift to lower voltages of activation of mutant $Ca_V2.1$ channels leads to a similar increase in AP-evoke Ca^{2+} influx at the active zones of pyramidal cells in both SL/WT KI and RQ/RQ KI mice. A similar gain of function of SL/WT and RQ/RQ $Ca_V2.1$ current density in cortical pyramidal cells is supposed since the increased $Ca_V2.1$ current density is similar in cerebellar granule cells and cortical pyramidal neurons in RQ/RQ KI mice, and in cerebellar granule cells from both RQ/RQ KI and SL/WT KI mice (Tottene et al., 2009; van den Maagdenberg et al., 2004, 2010). Further supporting the conclusion that the similar gain of function of $Ca_V2.1$ current density leads to a similar AP-evoked glutamate release, is the finding that SL/WT KI and RQ/RQ KI mice present a similar facilitation of cortical spreading depression (CSD) as in my laboratory has been demonstrated a causative link between enhanced glutamate release and facilitation of CSD in RQ/RQ KI mice (Tottene et al., 2009; van den Maagdenberg et al., 2010). On the other hand, the finding that another FHM1 KI mouse presents facilitation of excitatory synaptic transmission, as a consequence of the shift to lower voltages of $Ca_V2.1$ channels activation, is consistent with the hypothesis that hyperactivity of cortical circuits may render the cortex of FHM patients vulnerable to CSD ignition in response to specific migraine triggers (Pietrobon, 2005; Tottene et al., 2009). Moreover, SL/WT KI and RQ/RQ KI mice are, to a same extent, less susceptible to presynaptic inhibition by activation of G protein-coupled $GABA_B$ receptors. As a consequence, during G protein-coupled neuromodulation, cortical excitatory synaptic transmission may be further facilitated by FHM1 mutations. The reduced inhibition of neurotransmission, by $GABA_B$ receptors activation, found in

FHM1 KI mice may lead to an increase hyperactivity of cortical circuits and may further explain the facilitation of CSD in these KI mice. The FHM1 mutations reduce the G protein inhibition of human recombinant $Ca_V2.1$ channels accelerating the Gβγ dissociation from the channel during step-voltage depolarization (Melliti et al., 2003; Weiss et al., 2008). However, $GABA_B$ receptors inhibit neurotransmission also through a mechanism Ca_V channels-independent. Indeed, it has been proposed that $GABA_B$ receptors inhibit neurotransmitter release via a direct modulation of synaptic vesicle priming (Sakaba and Neher, 2003; Ulritch and Bettler, 2007). Moreover, recent findings demonstrate that the $GABA_B$ activation decreases the fusion willingness of synaptic vesicles by directly interfering with the release machinery at ippocampal autapses (Rost et al., 2009). Indeed, our preliminary data demonstrate that $GABA_B$ receptors activation induces also a decrease in frequency of mEPSCs which in our conditions are independent from the Ca^{2+} influx through presynaptic Ca_V channels (data not shown). However, the reduction of the mEPSC frequency is similar in WT and RQ/RQ KI mice and cannot account for the reduced in the EPSC amplitude.

How do the data explain the larger facilitation of CSD in homozygous S218L KI mice and the more severe phenotype caused by the S218L mutation? In humans this mutation causes a severe hemiplegic migraine syndrome associated with fever, seizures, progressive cerebellar ataxia, coma (even fatal), and long lasting cerebral oedema triggered by mild head trauma (Kors et al., 2001). Interestingly, homozygous S218L KI mice which faithfully resemble the human clinical phenotype, present a larger gain of function of $Ca_V2.1$ current density in cerebellar granule cells and a larger facilitation of CSD induction and propagation *in vivo* compared to KI mice carrying the milder R192Q mutation (van den Maagdenberg et al., 2004, 2010). Moreover, heterozygous and homozygous S218L KI mice present an allele dosage effect, consistent with dominance of the mutation in FHM1 patients, for both gain of function of $Ca_V2.1$ current density and facilitation of CSD (van den Maagdenberg et al., 2010). These findings and the similar gain of function of cortical excitatory neurotransmission in SL/WT KI and RQ/RQ KI mice support the conclusion that the severe S218L mutation causes a larger gain of function of cortical glutamatergic synaptic transmission than the mild R192Q FHM1 mutation. Given the recent evidence of a causative link between enhanced glutamate release and facilitation of CSD in homozygous R192Q KI mice, this may explain the greater susceptibility to CSD induced by the S218L mutation, and possibly its dramatic clinical phenotype. In addition, S218L KI mice show a much higher incidence of recurrent CSDs (van den Maagdenberg et al., 2010). The unique combination of a particularly low CSD threshold and a high propensity for multiple

CSD events may, at least in part, explain the high sensitivity of the S218L brain to even mild stimuli. Moreover, recurrent CSDs might open the blood-brain barrier and explain the delayed cerebral oedema (Pietrobon, 2007). Indeed, CSD causes prolonged activation and up-regulation of brain metalloproteinases that lead to impairment of the blood-brain barrier and vascular leakage (Dalkara et al., 2006; Pietrobon, 2005). Even if the exact mechanism for recurrent CSD events following a single stimulus remain to be determined, the unique combination of a particularly low threshold of activation and slow inactivation, and a particularly fast rate of recovery from inactivation of mutant S218L $Ca_V2.1$ channels, suggests the involvement of a process that is particularly sensitive to Ca^{2+} influx at rest, channel inactivation, or both (Pietrobon, 2007; van den Maagdenberg et al., 2010). The higher incidence of repetitive CSD seen in SL/SL KI, with an allele dosage effect in SL/WT KI, but only rarely in RQ/RQ KI mice may be also due to an increased spontaneous neurotransmitter release at cortical synapses at resting potential. Indeed, at neuromuscular junction (NMJ) was found a much larger increase in spontaneous neurotransmitter release in SL/SL KI compared to RQ/RQ KI mice (van den Maagdenberg et al., 2004, 2010). Even if SL/WT KI and RQ/RQ KI mice showed a quantitatively similar gain of function effects in Ca^{2+} current density and CSD threshold and velocity, spontaneous neurotransmitter release at NMJ was much larger in SL/WT KI mice, suggesting a larger Ca^{2+} influx at rest in the nerve terminal. Interestingly, in preliminary data I found that the frequency of mEPSC at rest, at single cortical pyramidal autapses of SL/SL KI mice, decreases after application of saturating concentration of ω-AgaIVA, indicating a Ca^{2+} influx through SL/SL $Ca_V2.1$ channels at resting. In contrast, the frequency of mEPSCs was unaltered after block of P/Q-type Ca^{2+} channels in WT and RQ/RQ KI mice. The activation of SL/SL and probably SL/WT $Ca_V2.1$ channels at resting potential could lead to an increased spontaneous glutamate release and to a further cortical hyperexcitability that may explain the higher incidence of recurrent CSDs in these KI mice.

Homozygous S218L KI mice display mild permanent cerebellar ataxia, accompanied by reduced arborisation solely of proximal, primary dendrites of cerebellar Purkinje neurons (van den Maagdenberg et al., 2010). Although it is unclear how the S218L mutation may cause cerebellar ataxia, recent findings from Gao et al. (2009) points to an irregular Purkinje cell firing patterns due to the gain of function of S218L $Ca_V2.1$ channels. Indeed, authors found that neurotransmitter release from parallel fibers was increased. In addition, the Ca^{2+} channel activation curve in Purkinje cells is shifted to negative voltages and, as a consequence, Purkinje cells fire Ca^{2+}-spikes at lower current injections, which together with the subsequent pauses disrupt AP firing

patterns. The authors concluded that the gain of function of S218L $Ca_V2.1$ channels leads to irregular action potential firing in Purkinje cells and thus minimizes cerebellar information coding.

As yet, it is unclear how the S218L mutation causes coma and epilepsy. Recently Eikermann-Haerter et al. (2009b) found a facilitated propagation of CSD in subcortical regions in SL/SL KI mice. Indeed, in both SL/SL KI and RQ/RQ KI but never in WT mice, CSD was recorded in cortex, and striatum pointing to propagation of CSD until striatum as the basis for hemiparesis in humans and motor deficits after CSD in KI mice (Eikermann-Haerter et al., 2009a, 2009b). Instead, thalamic and hippocampal propagation of CSD only in SL/SL KI mice may underlie coma and seizures in S218L carriers (Eikermann-Haerter et al., 2009a).

6. AIM OF WORK (III)

In Tottene et al. (2009) was investigated cortical excitatory and inhibitory neurotransmission at connected pairs of layer 2/3 pyramidal cells and multipolar fast-spiking (FS) interneurons in acute thalamocortical slices of the somatosensory cortex of wild type (WT) and homozygous R192Q (RQ/RQ) KI juvenile mice. This was done to verify if FHM1 mutations might affect differently synaptic transmission at different cortical synapses and, as a consequence, in certain conditions might alter the balance between excitation and inhibition during cortical activity. FS interneurons were identified for the heterogeneous and irregular shape of the soma and the absence of a main dendrite projecting towards the pia and for the characteristic action potential (AP) firing pattern. Indeed, FS interneurons, upon depolarizing current injection, discharge action potentials continuously at high rates (over 20 APs per second) without frequency adaptation (Markram et al., 2004; Reyes et al., 1998). Their single action potentials are very brief, and are characterized by a deep fast afterhyperpolarization that does not change from one AP to the other in a series (Cauli et al., 2000; Markram et al., 2004). These characteristics permit to distinguish FS cells from bitufted interneurons. The latter interneurons are characterized by ovoid somata from which one to four tufts of dendrites extended only in the apical and basal directions, in contrast with multiple dendrites that extended radially from the soma of multipolar interneurons (Reyes et al., 1998). Moreover, bitufted interneurons have a AP firing with amplitude and frequency accommodation (Cauli et al., 2000; Reyes et al., 1998). A further physiological criterion for classification of multipolar FS and bitufted interneurons is the frequency-dependent change in unitary excitatory postsynaptic potential (EPSP) amplitudes evoked by stimulation in the connected pyramidal cell, as reported in Reyes et al. (1998). Authors reported that EPSPs depressed in multipolar FS cells, whereas EPSPs facilitated in bitufed cells. In addition, many of bitufted interneurons were immunopositive for the neuropeptide somatostatin. In contrast, all the multipolar interneurons were immunonegative for somatostatin, but many of which expressed the calcium-binding proteins parvalbumin.

Once defined the criterions to recognized FS interneurons, the cortical excitatory and inhibitory neurotransmission was investigated from synaptically connected pyramidal cells and FS neurons. The strength of excitatory neurotransmission was increased at unitary connections between layer 2/3 pyramidal cells and multipolar fast-spiking interneurons in acute RQ/RQ KI thalamocortical slices of somatosensory cortex. Firstly was controlled that the glutamate release at WT pyramidal cell and fast-spiking

connections was mainly controlled by P/Q-type Ca^{2+} channels, as saturating concentration of ω-AgaIVA inhibited a large fraction of the evoked EPSP. The peak amplitude of the mean EPSP evoked by a single presynaptic AP was on average two times larger in RQ/RQ KI than in WT pyramidal cells and fast-spiking interneurons connections. The low percentage of the presynaptic APs that failed to evoke an EPSP in the fast-spiking interneuron and the increased short term depression (STD) found in KI mice were consistent with an increased probability of vesicle release at the excitatory synaptic connections between pyramidal cells and fast-spiking interneurons in RQ/RQ KI mice. This finding was in agreement with the increased AP-evoked Ca^{2+} influx and glutamate release found at single cortical pyramidal cell autapses.

In striking contrast, inhibitory neurotransmission at FS interneuron synapses was unaltered in RQ/RQ FHM1 KI mice. Indeed, the peak amplitudes of the evoked mean inhibitory postsynaptic potentials (IPSPs) at the inhibitory FS interneuron and pyramidal cell connections were identical in slices from RQ/RQ KI and WT mice, despite a dominant role of $Ca_V2.1$ channels in controlling neurotransmitter GABA release, as saturating concentration of ω-AgaIVA completely inhibited the evoked IPSP. Moreover, STD and percentage of failures were very similar in RQ/RQ KI and WT mice.

The analysis of cortical neurotransmission in RQ/RQ KI mice shows that FHM1 mutations may affect differently synaptic transmission at different cortical synapses: in particular, the R192Q FHM1 mutation leads to gain of function of excitatory neurotransmission at pyramidal cell synapses, but does not affect inhibitory neurotransmission at FS interneuron synapses. On one hand the increased glutamate release at pyramidal cells synapses explains the major susceptibility to CSD in KI mice, as in Tottene et al. (2009) was found a causative link between enhanced glutamate release and facilitation of CSD. On the other hand the different effect of R192Q FHM1 mutation on excitatory and inhibitory synaptic transmission at cortical synapses indicate that R192Q mutation, but presumably all FHM1 mutations, alter the neuronal circuits that coordinate and dynamically adjust the balance between excitation and inhibition during cortical activity. These alterations may further increase cortex hyperexcitability and, as a consequence, render the cortex vulnerable to ignition of CSD in response to specific migraine triggers.

To understand why inhibitory neurotransmission at these synapses was not influenced by FHM1 mutation, despite being also initiated by $Ca_V2.1$ channels, I studied inhibitory synaptic transmission in cortical multipolar fast-spiking interneurons grown on glial microislands from WT and RQ/RQ KI mice.

7. RESULTS (III)

In Tottene et al. (2009) was demonstrated that, in striking contrast with the enhanced strength of cortical excitatory synaptic transmission, inhibitory neurotransmission at fast-spiking (FS) interneuron synapses was unaltered in homozygous R192Q FHM1 KI mice, despite a dominant role of $Ca_V2.1$ channels in controlling neurotransmitter GABA release. To understand why inhibitory neurotransmission at these synapses was not influenced by FHM1 mutation, despite being also initiated by $Ca_V2.1$ channels, I studied inhibitory synaptic transmission in cortical multipolar fast-spiking interneurons grown on glial microislands from WT and homozygous R192Q KI mice. I measured the AP-evoked inhibitory postsynaptic current (IPSC) depolarizing, every 10 seconds, the multipolar cell with a voltage step to +20 mV delivered to the soma from the holding potential of -80 mV. The fast IPSC due to activation of the $GABA_A$-type receptors by GABA release as a consequence of the propagated AP to synaptic terminals was recorded for 150 ms at -90 mV. The mean current (4-5 traces) recorded in the presence of saturating concentration of a specific $GABA_A$ receptors inhibitor, bicuculline (20 μM), was subtracted to all records to obtain the pure $GABA_A$-mediated IPSCs. As for excitatory neurotransmission, the IPSC amplitude for each experiment was calculated by averaging the peak amplitude of IPSCs from 5-6 traces after 3 minutes from break-in and, if it was the case, after the IPSC stabilization (discarding all experiments in which the IPSC amplitude run-down was more than 40 % during 3 minutes from break-in). Multipolar fast-spiking interneurons were recognized by the soma heterogeneous and irregular morphology, and by extensive asymmetrical processes emanating from the soma, which clearly differentiate them from bitufted and classical bipolar interneurons (fusiform soma shape and symmetrical processes) (Markram et al., 2004; Reyes et al., 1998). To further recognize FS interneurons from the other interneuron types I recorded, in current-clamp mode, their typical AP firing, well described in literature (Cauli et al., 2000; Markram et al., 2004). In particular, I verified that the interneurons I patched were FS interneurons by studying the firing induced by 1s – long suprathreshold current injections of increasing amplitude up to 400 pA, holding the neuron near -70 mV (Figure 7.1). All the AP firing that I recorded had similar properties: a non accommodating firing frequency higher than 30 Hz, a fast AP afterhyperpolarization that does not change from one AP to the other in a series. All these AP firing properties are characteristic of fast-spiking interneurons (Cauli et al., 2000).

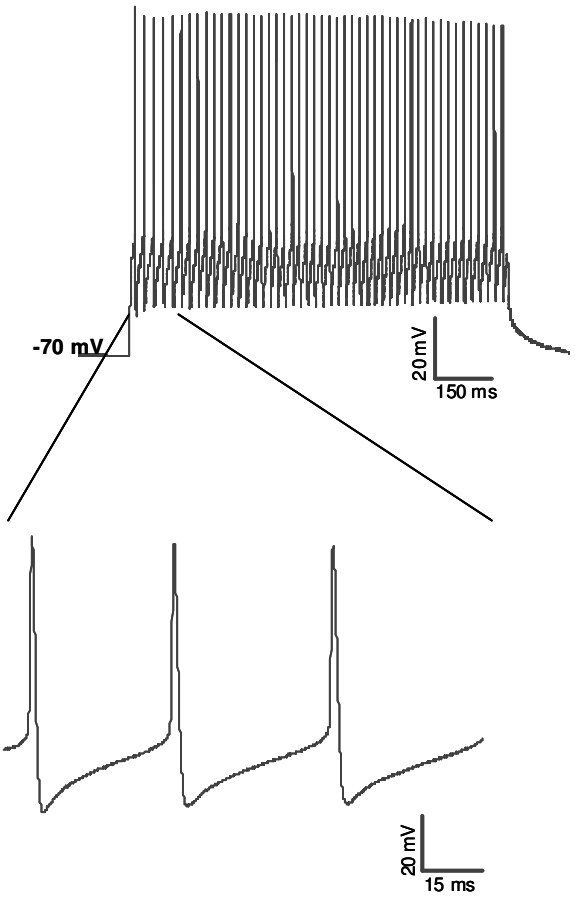

Figure 7.1. Action potential firing induced by a 1 s-long suprathreshold injection current of 320 pA in a wild-type multipolar fast-spiking interneuron

To be sure that the multipolar FS interneurons in microislands had the same characteristics of that in slices, I checked that also in cultures GABA release was controlled by P/Q Ca^{2+} channels in both WT and RQ/RQ KI mice at single FS interneuron synapses. Indeed, the fraction of the IPSC inhibited by a saturating concentration of the specific $Ca_V2.1$ inhibitor ω-AgaIVA (200 nM) in a protocol like that represented in Figure 7.2A was large and similar in WT and RQ/RQ KI mice (Figure 7.2B: 71 ± 5 %, n = 8 in RQ/RQ KI and 78 ± 6, n = 8 in WT cells). This result demonstrated that also in autaptic cultures inhibitory neurotransmission at FS interneurons synapses was mostly initiated by $Ca_V2.1$ channels and that these channels equally contributed to GABA-mediated neurotransmission in WT and RQ/RQ KI mice. However, I found that in a 20 % of WT and RQ/RQ KI interneurons P/Q-type Ca^{2+} channels controlled only a 20 % of GABA release, raising the possibility that in a subgroup of multipolar interneurons inhibitory neurotransmission is initiated by N-type Ca^{2+} channels. Indeed, in another group of experiments the fraction of the IPSC inhibited by a saturating concentration of the specific $Ca_V2.2$ inhibitor ω-GVIA (1 μM)

was measured. I found that in the greatest part of the cases the toxin inhibited no more than the 25 % of the EPSC but in the 35 % of the cases it inhibited the 70% of the EPSC in both WT and RQ/RQ KI mice. More pharmacological experiments will be done to clearly understand the contribution of P/Q and N-type to inhibitory neurotransmission

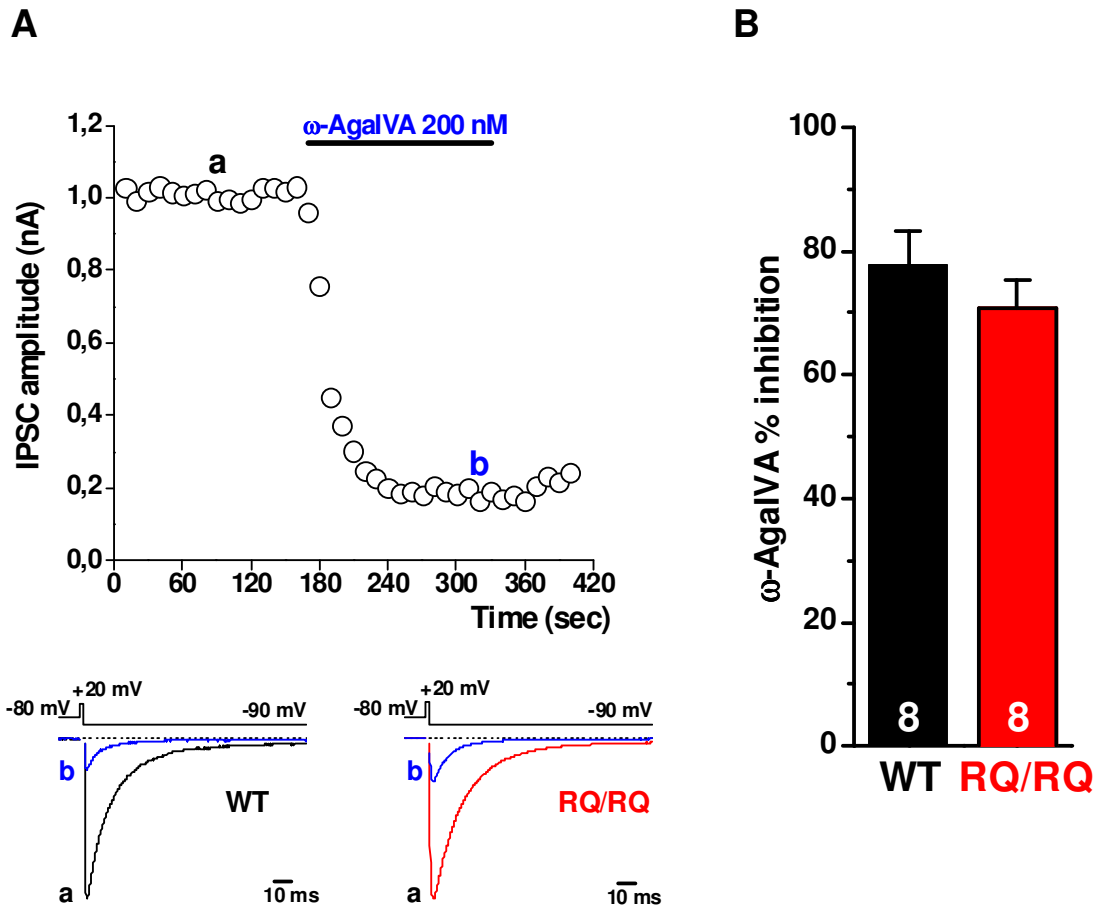

Figure 7.2. GABA release was controlled by $Ca_V2.1$ channels at single multipolar fast-spiking interneuron synapses of both WT and homozygous R192Q KI mice

A top: Action potential-evoked IPSC amplitudes versus time in a WT pyramidal neuron before (a) and during (b) application of a specific $Ca_V2.1$ channel inhibitor ω-AgaIVA (200 nM).

A bottom: Representative IPSC traces taken at times a and b in a WT and RQ/RQ KI multipolar FS interneuron.

B: Contribution of P/Q-type Ca^{2+} channels to inhibitory neurotransmission evaluated from the fraction of the IPSC inhibited by ω-AgaIVA 200nM in RQ/RQ KI (71 ± 5 %, n = 6, 2 at DIV 10-11 and 12-14, respectively) compared to WT multipolar FS interneurons (78 ± 6 %, n = 4, 4 at DIV 10-11 and 12-14, respectively).

and to investigate if the conflicting data are due to the presence in cultures of multipolar fast-spiking interneurons from different type of cortex and different cortical layers (see Discussion). However, as only in a 20 % of both WT and RQ/RQ KI cells a small fraction of EPSC was inhibited by ω-AgaIVA, I can conclude that neurotransmission at

multipolar FS interneurons synapses is mainly initiated by $Ca_V2.1$ channels and that these channels equally contribute to GABA-mediated neurotransmission in WT and RQ/RQ KI mice.

If the contribution of P/Q channels was the same in WT and RQ/RQ KI mice one would predict to find a similar GABA release at WT and RQ/RQ KI multipolar FS interneurons synapses as reported in Tottene et al. (2009). Indeed, the average amplitude of AP-evoked IPSC at DIV 10-14 was the same in WT and RQ/RQ KI mice (Figure 7.3B: 1.2 ± 0.1 nA, n = 63 and 1.1 ± 0.1 nA, n = 53 in WT and RQ/RQ KI mice, respectively).

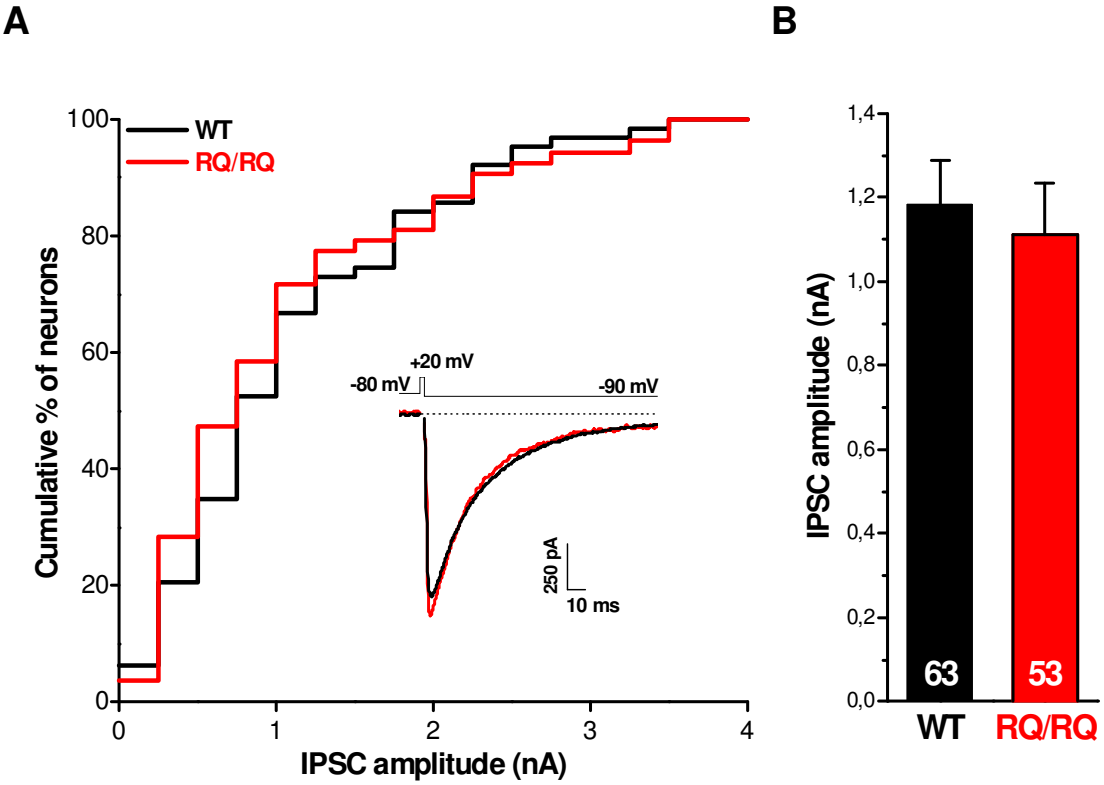

Figure 7.3. Unaltered action potential-evoked inhibitory postsynaptic current in homozygous R192Q KI mice

A: Cumulative distribution (bin 0.25) of AP-evoked IPSC amplitudes from WT (n = 63) and RQ/RQ KI (n = 53) cortical multipolar FS interneurons.

Inset: IPSC traces from a representative WT and RQ/RQ KI cortical multipolar FS interneuron.

B: Average value of AP-evoked IPSC amplitudes from WT (1.2 ± 0.1 nA, n = 63) and RQ/RQ KI (1.1 ± 0.1 nA, n = 53) cortical multipolar FS interneurons.

Both the cumulative distribution and the average value of AP-evoked IPSC amplitudes (Figure 7.3A and B) demonstrate an unaltered GABA release in homozygous R192Q KI mice compared to WT mice, despite a pivotal role of presynaptic P/Q Ca^{2+} channels in

initiating inhibitory neurotransmission. The amplitude of the $GABA_A$-mediated IPSC, as for the AMPA-mediated EPSC, from neurons grown on glial microcultures increased with DIV (Figure 7.4); for this reason I tried to closely match the number of recordings for DIV for all types of experiments. Even if the relative number of neurons recorded from WT and RQ/RQ KI mice at DIV 12-14 were not perfectly matched, I included them in the mean as the average evoked IPSC amplitudes were very similar between WT and RQ/RQ KI mice at DIV 10-11 (0.9 ± 0.1 nA, n = 35 for WT and 1.1 ± 0.1 nA, n = 36 for RQ/RQ KI cells) where the number of experiments were closely matched.

The data confirmed that inhibitory neurotransmission is unaltered at single multipolar fast-spiking interneuron synapses of homozygous R192Q KI mice also in

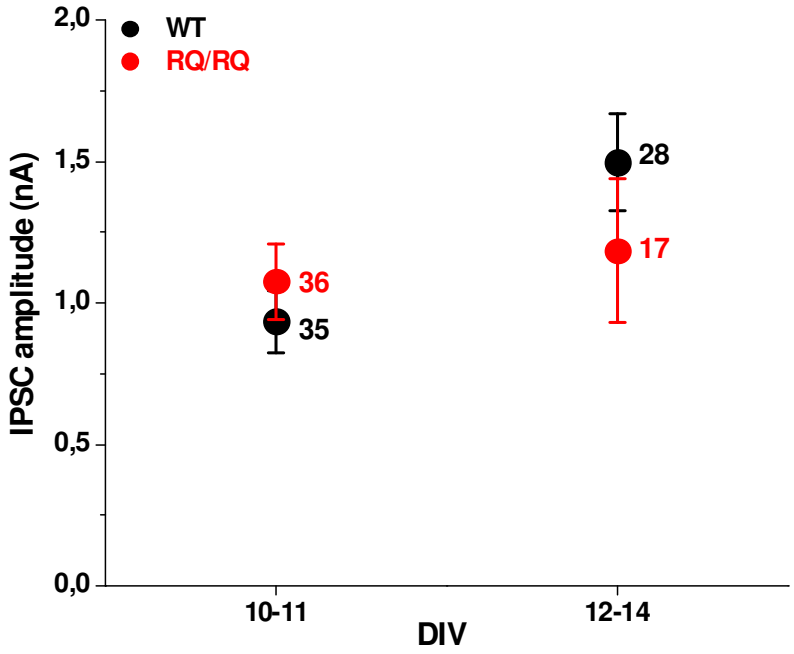

Figure 7.4. Developmental increase in the amplitude of action potential-evoked inhibitory postsynaptic current from wild-type and homozygous R192Q knock-in multipolar fast-spiking interneurons

The average evoked IPSC amplitudes were plotted as a function of DIV. WT mice: 0.9 ± 0.1 nA, n = 35 at DIV 10-11; 1.5 ± 0.2 nA, n = 28 at DIV 12-14, respectively. RQ/RQ KI mice: 1.1 ± 0.1 nA, n = 36 at DIV 10-11; 1.2 ± 0.3 nA, n = 17 at DIV 12-14, respectively.

microcultures, despite being initiated by $Ca_V2.1$ channels. There are three reasons which might explain why FHM1 mutation may differently affect excitatory and inhibitory synaptic transmission. The first is that the FHM1 mutation could determine an increased AP-evoked Ca^{2+} influx through mutant presynaptic P/Q channels, but the presynaptic Ca^{2+} sensor for vesicle exocytosis is already saturated. The second is that the FHM1 mutation does not induce an increased action potential-evoked Ca^{2+} influx either as a

consequence of the shorter action potential in FS interneurons with respect to pyramidal cells (Cauli et al., 2000) or because FS interneurons express a different splice variant of α_{1A} subunit than pyramidal neurons, and that the mutation does not affect its biophysical properties. Recently, Adams et al. (2009) reported that two splice variants of human recombinant FHM1 $Ca_V2.1$ channels exhibit different biophysical properties. To discriminate between these three possibilities, I studied the extracellular Ca^{2+} dependence of the IPSC in WT and RQ/RQ KI mice by perfusing neurons with different Ca^{2+} concentrations in the extracellular solution; experiments and analysis were performed in the same way previous described for the Ca^{2+} dependence of evoked EPSC. I found that in WT interneurons the Ca^{2+} sensor was nearly saturated at physiological Ca^{2+} concentration, in contrast with the Ca^{2+} dependence of EPSC in WT pyramidal cells, as shown by the EC_{50} values, with unaltered cooperativity coefficient

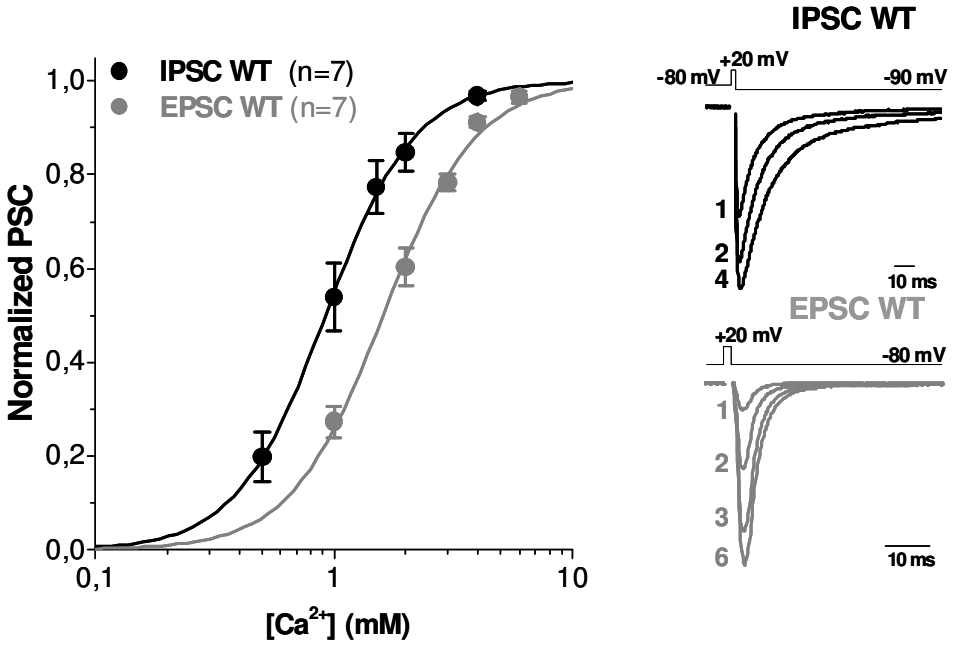

Figure 7.5. The Ca^{2+} dependence of the inhibitory postsynaptic current is shifted to lower Ca^{2+} concentrations at cortical wild-type fast-spiking interneuron autapses

Left: evoked IPSC amplitude as a function of extracellular $[Ca^{2+}]$ in WT cortical multipolar FS interneurons (n = 4 and 3 at DIV 10-11, 12-14) and WT cortical pyramidal neurons (n = 4 and 3 at DIV 10-11, 12-14).

Right: Representative IPSC and EPSC traces recorded at the indicated $[Ca^{2+}]$ (mM) from a WT multipolar FS interneuron and a WT pyramidal cell.

resulting from fit of the mean normalized data points according to Hill equation: $IPSC = [Ca^{2+}]^n/\{(EC_{50})^n + [Ca^{2+}]^n\}$ (Figure 7.5: $EC_{50} = 0.92 \pm 0.01$ mM and $n = 2.32 \pm 0.07$ for

WT cortical FS interneurons [n = 7] and EC_{50} = 1.61 ± 0.05 mM and n = 2.21 ± 0.14 for WT cortical pyramidal cells [n = 7, as reported in Tottene et al., 2009]). In WT pyramidal neurons the Ca^{2+} sensor was not saturated at physiological Ca^{2+} concentration, indeed when the extracellular Ca^{2+} concentration was raised above 2 mM the EPSC amplitude increased of about 60 %, in contrast with only a 12 % increased in IPSC amplitude. The nearly saturated Ca^{2+} sensor in FS interneurons was in agreement with the higher probability of release at FS interneuron synapses than at pyramidal synapses revealed by the percentage of failure (the % of the presynaptic APs in FS interneurons that failed to evoke an IPSP in the pyramidal neuron) close to zero at FS-pyramidal cells synapses in slices (Tottene et al., 2009).

If the similar mean IPSC amplitude in WT and RQ/RQ KI mice was due to the close saturation of the Ca^{2+} sensor at the terminals of WT interneurons, one would have expected to find a different IPSC amplitude in WT and RQ/RQ KI mice at Ca^{2+} concentrations far from the saturation and so one would predict that the Ca^{2+} dependence of IPSC in RQ/RQ KI mice was shifted to lower calcium concentrations compared to that of WT mice. In contrast with this prediction, I found that the Ca^{2+} dependence of the IPSC was unaltered at individual cortical multipolar FS interneuron synapses of RQ/RQ KI mice (Figure 7.6: EC_{50} = 0.88 ± 0.01 mM and n = 2.43 ± 0.05 for RQ/RQ KI [n = 8] and EC_{50} = 0.92 ± 0.01 mM and n = 2.32 ± 0.07 for WT mice [n = 7]). These findings demonstrate that the R192Q FHM1 mutation does not alter inhibitory neurotransmission at multipolar fast-spiking interneuron autapses, in agreement with the results reported at connected pair of multipolar fast-spiking interneurons and pyramidal cells in acute thalamocortical slices (Tottene et al., 2009). The different effect of the mutation on neurotransmission at cortical excitatory and inhibitory synapses is largely due to a different effect on AP-evoked Ca^{2+} influx through mutant presynaptic P/Q Ca^{2+} channels at pyramidal cell and multipolar interneuron synapses: in contrast with the gain-of-function effect at the glutamatergic synapses, the FHM1 mutation does not significantly increase AP-evoked P/Q Ca^{2+} influx at the GABAergic synapses, possibly as a consequence of the shorter action potential and/or the expression of a different slice variant of α_{1A} subunit. Further investigations will be necessary to discriminate between the two hypothesis.

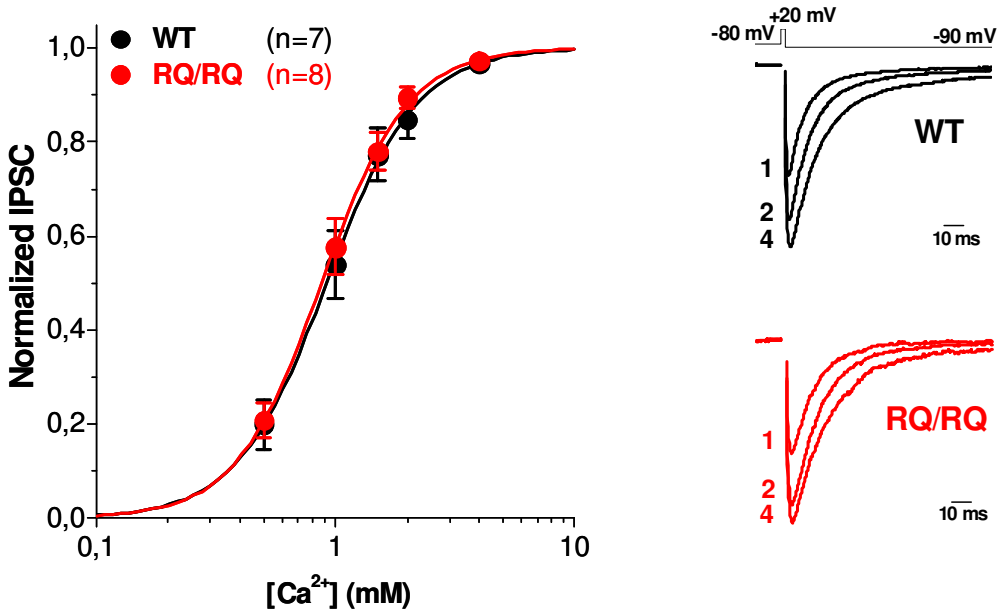

Figure 7.6. Unaltered Ca^{2+} dependence of the inhibitory postsynaptic current at cortical multipolar FS interneuron autapses of homozygous R192Q knock-in mice

Left: evoked IPSC amplitude as a function of extracellular [Ca^{2+}] in autaptic cortical multipolar FS interneurons from WT (n = 4 and 3 at DIV 10-11, 12-14) and RQ/RQ KI mice (n = 4 and 4 at DIV 10-11, 12-14). The total evoked IPSC amplitude in RQ/RQ KI cells (1.0 ± 0.3 nA, n = 8) was similar to that in WT cells (1.3 ± 0.4 nA, n = 7).

Right: Representative IPSC traces recorded at the indicated [Ca^{2+}] (mM) from a WT and a RQ/RQ KI multipolar FS interneuron.

To confirm that not only the R192Q but all the FHM1 mutations may differentially affect excitatory and inhibitory neurotransmission, I measured the AP-evoked IPSC at DIV 10-14 also at single cortical multipolar fast-spiking autapses from heterozygous S218L KI mice. Even if these results are only preliminary, I found that the average AP-evoked IPSC was unaltered in SL/WT KI mice, despite a high contribution of P/Q Ca^{2+} channels in controlling GABA release (64 ± 3 %, fraction of IPSC inhibited by ω-AgaIVA 200 nM, n = 9, data not shown), compared to RQ/RQ KI and WT mice (Figure 7.7, left: 1.2 ± 0.2 nA, n = 30 in SL/WT KI; 1.1 ± 0.1 nA, n = 53 in RQ/RQ KI and 1.2 ± 0.1 nA, n =63 in WT cells). This finding demonstrates that probably all FHM1 mutations may differently affect synaptic transmission at different cortical synapses, and, as a consequence, very likely alter the balance between excitation and inhibition during cortical activity.

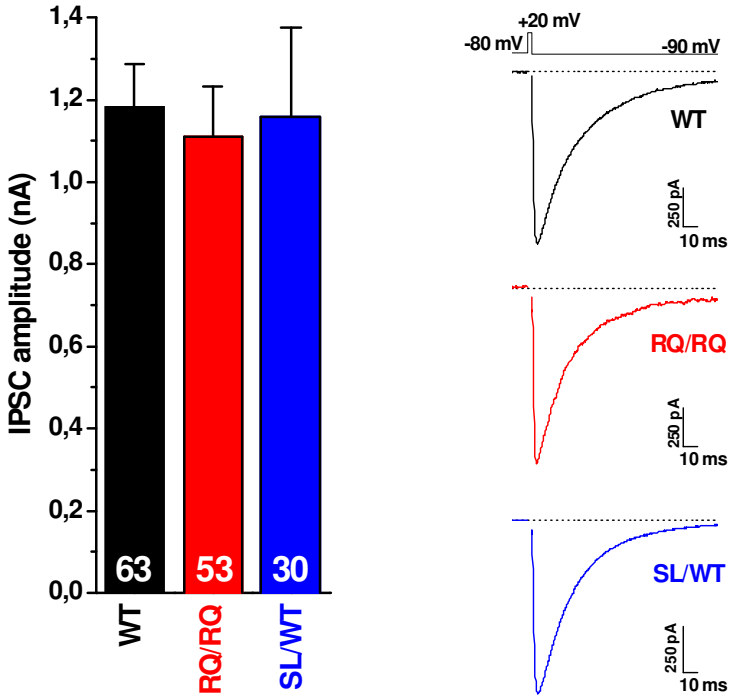

Figure 7.7. Unaltered action potential-evoked inhibitory postsynaptic current in heterozygous S218L KI mice

Left: Average value of AP-evoked IPSC amplitudes from WT (1.2 ± 0.1 nA, n = 35, 28 at DIV 10-11 and 12-14, respectively), RQ/RQ KI (1.1 ± 0.1 nA, n = 36, 17 at DIV 10-11 and 12-14, respectively) and SL/WT KI (1.2 ± 0.2 nA, n = 14, 16 at DIV 10-11 and 12-14, respectively) cortical multipolar FS interneurons.

Inset: IPSC traces from a representative WT, RQ/RQ KI and SL/WT cortical multipolar FS interneuron.

8. DISCUSSION (III)

I studied inhibitory synaptic transmission in cortical multipolar fast-spiking interneurons grown on glial microislands from WT and homozygous R192Q (RQ/RQ) KI mice to understand why at layer 2/3 fast-spiking interneurons and pyramidal cells connections in acute thalamocortical slices of the somatosensory cortex from RQ/RQ KI mice inhibitory neurotransmission is unaltered, despite being initiated by $Ca_V2.1$ channels (Tottene et al., 2009).

Multipolar fast-spiking interneurons in microcoltures were first identified based on their morphology. Indeed, the heterogeneous and irregular soma shape and the asymmetrical processes distributions permitted to distinguish them from bitufted and classical bipolar interneurons (Reyes et al., 1998). Moreover, all the interneurons I analysed for action potential firing pattern shown the characteristic high frequency non accommodating firing with a deep and constant afterhyperpolarization typical of fast-spiking interneurons, as reported in literature (Cauli et al., 2000; Markram et al., 2004). In addition, inhibitory synaptic transmission at fast-spiking autapses was mostly mediated by P/Q-type Ca^{2+} channels in agreement with studies at connected pairs of layer 2/3 fast-spiking and pyramidal neurons in cortical slices of prefrontal (Zaitsev et al., 2007) and barrel cortex (Rozov et al., 2001; Tottene et al., 2009). However, I found that in 20 % of multipolar interneurons, inhibitory synaptic transmission was affected for only a 20 % by application of ω-AgaIVA (200 nM) and, on the other hand, in some interneurons application of saturating concentration of ω-GVIA (1μM) inhibited a large fraction of AP-evoked IPSCs. These results rise the possibility that inhibitory neurotransmission in this group of multipolar fast-spiking interneurons was mainly mediated by N-type Ca^{2+} channels as reported at connected pairs of layer 5 fast-spiking and pyramidal neurons in cortical slices of motor cortex (Ali and Nelson., 2006). Because *in vitro* is impossible to distinguish between neurons of different cortical layers, the conflicting pharmacological results may be due to a heterogeneous population of multipolar interneurons. Indeed, in one multipolar interneuron with a typical fast-spiking AP firing I found that P/Q-type Ca^{2+} channels contributed for only a 25 % to GABA release. However, the fast-spiking AP firing recorded in all the neurons tested, the low and similar percentage of cells in which ω-AgaIVA inhibited a small fraction of the IPSC in both WT and RQ/RQ KI mice, and the similar contribution of $Ca_V2.1$ channels to inhibitory synaptic transmission in both WT and RQ/RQ KI mice, support the conclusion that the results from the two mice came from a homogenous population of cells.

I found that, in agreement with that reported in Tottene et al. (2009), the cortical inhibitory neurotransmission is unaltered at multipolar fast-spiking interneuron autapses in RQ/RQ KI mice, despite the dominant role of $Ca_V2.1$ channels in controlling GABA release. Indeed, the average AP-evoked IPSC peak amplitude was similar in WT and RQ/RQ KI mice. The same result was obtained, in preliminary data, also for heterozygous S218L KI mice. A possible explanation for this finding was that the FHM1 mutation determines an increased AP-evoked Ca^{2+} influx through presynaptic $Ca_V2.1$ channels but the presynaptic Ca^{2+} sensor for vesicle exocytosis is already saturated in WT mice. The study of the extracellular Ca^{2+} dependence of the IPSC peak amplitude revealed that in WT interneurons the Ca^{2+} sensor is nearly saturated at physiological Ca^{2+} concentration, as increase the external Ca^{2+} concentration above 2 mM resulted in only 12 % of increase in IPSC peak amplitude. However, if the similar IPSC amplitude in WT and RQ/RQ KI mice was due to the near saturation of the Ca^{2+} sensor at the terminals of WT interneurons one would expect to find a different IPSC amplitude in WT and RQ/RQ KI mice at Ca^{2+} concentration far from the saturation. Instead I found that the extracellular Ca^{2+} dependence of the IPSC peak amplitude was unaltered in RQ/RQ KI mice. The data support the conclusion that the unaltered inhibitory neurotransmission at cortical multipolar fast-spiking synapses is due to unaltered AP-evoked Ca^{2+} influx through presynaptic $Ca_V2.1$ channels in RQ/RQ KI mice. The absence of gain of function of mutant $Ca_V2.1$ current may be the consequence of the shorter action potential in fast-spiking interneurons than in pyramidal cell (Cauli et al., 2000). Moreover, in my laboratory has been demonstrated that the gain of function of AP-evoked Ca^{2+} current in RQ/RQ KI trigeminal neurons decreases with decreasing duration of the action potential (Fioretti and Pietrobon, unpublished data).

Another possible explanation for unaltered AP-evoked Ca^{2+} influx through presynaptic RQ/RQ $Ca_V2.1$ channels is that multipolar FS interneurons express a different $Ca_V2.1$ splice variant than pyramidal neurons, and that the FHM1 mutation does not affect its biophysical properties. In a subtype of trigeminal neurons, for example, the R192Q FHM1 mutation does not influence P/Q current in contrast with the gain of function found in the central nervous system neurons (Fioretti and Pietrobon, unpublished data).

Given the evidence that the magnitude (or even the presence) of the negative shift in activation of human $Ca_V2.1$ channels produced by FHM1 mutations may depend on the particular recombinant $Ca_V2.1$ α1 splice variant and/or $Ca_V2.1\beta$ subunit (Mullner et al, 2004; Adams et al, 2009), a possible explanation for the unaltered inhibitory

transmission may be a $Ca_V2.1$ isoform that is little affected by the mutation at FS interneuron synapses.

Moreover, different splicing variants of rat α_{1A} subunit generates cerebral variant of P/Q-type Ca^{2+} channels with different physiological properties in voltage-dependent activation and inactivation and inactivation kinetics, as well as different sensitivity to ω-AgaIVA (Bourinet et al., 1999). In addition, recently Adams et al. (2009) showed that different splice variants of human recombinant $Ca_V2.1$ α_1 subunits carrying the R192Q, and S218L FHM1 mutations exhibit different physiological properties. Furthermore, the magnitude of the negative shift in activation of human $Ca_V2.1$ channels produced by FHM1 mutations may depend on the particular recombinant $Ca_V2.1$ β subunit, as reported in Mullner et al. (2004).

The result of the Ca^{2+} dependence of the IPSC peak amplitude at WT cortical multipolar fast-spiking synapses is the first direct evidence that at these cortical synapses the Ca^{2+} sensors is nearly saturated. Instead, at rat ippocampal fast-spiking basket cell and granule cell connections the Ca^{2+} sensor operates in a subsaturating regime, as reported in Bucurenciu et al. (2008). This finding is in agreement with that reported in Ikeda et al. (2008) for rat ippocampal inhibitory autapses, even if in this case were patched all type of interneurons. Is not surprising that the same synapses studied in different brain regions from different animals present different physiological properties.

9. MATERIALS AND METHODS

Experiments were performed using WT C57Bl/6J mice and the corresponding KI strains carrying the $Ca_V2.1$ R192Q or S218L FHM1 mutations as described in van den Maagdenberg et al. (2004) and in van den Maagdenberg et al. (2010). In particular, homozygous R192Q KI and heterozygous S218L KI mice were used. All experimental procedures were carried out in accordance with the Italian Animal Welfare Act and approved by the local authority veterinary service.

9.1 Cell cultures

Cortical neurons were cultured on glial microislands essentially as reported in Brody and Yue (2000b) for hippocampal neurons with some differences. Briefly, 13 mm diameter glass coverslip (VWR International) were ethanol-sterilized and placed in 35 mm culture dishes (Falcon). A 0.15% agarose solution was spread uniformly on the slips to provide a hydrophobic, nonadhesive background. After drying and UV-sterilization a solution containing 1 mg/ml poly-D-lysine and 2.5 mg/ml collagen (both from Sigma Aldrich) dissolved in 8.5 mM acetic acid was sprayed onto the plates using an homemade airbrush to make 150-300 µm diameter islands of adhesive substrate. After drying and UV-sterilization, cultured astrocytes left over from a previous preparation were trypsinized and plated at the range density of 12500-50000 cells/ml in BME media. BME media was Basal Eagle's Medium (BME; Gibco-Invitrogen) plus 10% fetal bovine serum, 25 mM KCl, 2 mM glutamine and 50 µg/ml gentamicin. After 4-5 days at 37°C in 5% CO_2, the astrocytes spread out to cover the microislands without grow on the agarose and a millilitre of BME was replaced with a millilitre of neuronal medium Neurobasal A plus 2% B27 Supplement, 0.5 mM glutamine and 1% PSN Antibiotic mix (all from Gibco-Invitrogen) to allow the astrocytes to condition the medium before neuron plating. The next day cortical neurons were isolated from P0-2 mice following the procedure of Levi et al. (1984) and plated onto the astrocytes microislands at the range density of 6000-25000 cells/ml. Astrocytes and cortical neurons were plated at range of densities to increase the probability to find a significant number of microislands containing a single cortical neuron. The day after neuronal plating half medium was replaced with a millilitre of fresh Neurobasal A medium containing 35 µM 5-fluoro-2-deoxyuridine and 75 µM uridine (both from Sigma-Aldrich). After three days half medium was replaced with a millilitre of fresh Neurobasal A medium containing 17.5

µM 5-fluoro-2-deoxyuridine and 32.5 µM uridine. 5-fluoro-2-deoxyuridine and uridine were added to neuronal medium to block astrocytes proliferation.

9.2 Patch-clamp technique

The principle of patch-clamp recordings is to isolate from the extracellular solution a membrane patch through the formation of a seal (seal resistance > 10 GΩ) between the membrane and the pipette tip. In order to get a good seal it is necessary to filter all the solution used, and to fire polish the pipette tip. At last to avoid contact of the tip with impurities present in the bath solution, a positive pressure is applied inside the pipette.

A silver electrode covered with silver chloride is placed in the pipette; this is connected with a feedback amplifying system which allows the control of the voltage difference across the membrane patch after seal formation (Figure 9.1). The same electrical circuit allows current measurements through the membrane patch while voltage is controlled (voltage-clamp) or, alternatively, to measure voltage difference after current injections (current-clamp) (Molleman, 2003). In voltage-clamp mode the measured potential is compared with the potential set by the experimenter (holding potential). Any deviation of the recorded potential from the holding potential is instantly corrected by compensatory current injection. This current is then an accurate representation (but opposite in sign) of the ionic current over the membrane under investigation. In current-clamp mode the voltage is not clamped and a fixed amount of current is injected by the experimenter.

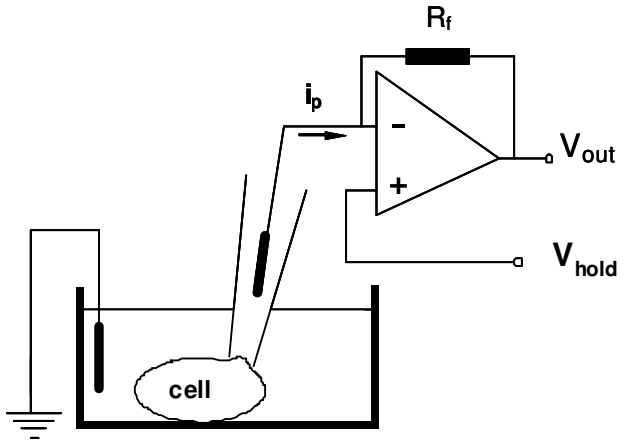

Figure 9.1. Simplified scheme of the feedback amplifying system in a patch-clamp amplifier

9.2.1 Patch-clamp configurations

One of the features of patch-clamp that makes the method so powerful is that it can be used in different configurations, which enables the experimenter to: study ion channels at different levels, either whole-cell (activity of all ion channels added up) or individual ion channels; manipulate easily the fluid on the extracellular or the intracellular side of the membrane during a recording. Indeed, when the tip of the recording pipette touches the plasma membrane and the seal is formed four different experimental configurations can be obtained: cell-attached, whole-cell, inside-out, and outside-out (Molleman, 2003).

Cell-attached.

In this configuration the pipette is positioned against the cell membrane where the glass makes a very strong connection, resulting in a tight (high resistance) seal (Figure 9.2A). This configuration allows measurements of single channel current (if a channel is present in the patch) without altering cytosolic environment. Because the pipette is on the extracellular side of the membrane, it is usually filled with bathing solution.

Whole-cell.

In this configuration, if a suction is applied to the pipette tip, the patch of membrane under the pipette tip in cell-attached patch configuration is ruptured, then the pipette solution and the electrode make direct electrical contact with the cytoplasm (Figure 9.2C). In this configuration the patch electrode is on one side of the plasma membrane and the ground electrode is on the other, therefore the membrane potential can be recorded directly. As patch pipette tip is sufficiently wide to allow washout of the cytoplasm by the pipette-filling solution, the composition of the intracellular fluid can be considered equal to that of the pipette filling solution. Usually to obtain a physiological situation the pipette is filled with a solution of ionic composition that resembles the cytoplasm as closely as possible. This configuration allows the measurement of the current flowing through all the channel expressed in the plasma membrane. In the whole-cell configuration the experimenter can manipulate the intracellular composition changing the ionic composition of the intracellular filling solution, but unknown cytosolic factors relevant to the subject of study can be unwittingly washed out. To avoid the latter, perforated patch-clamp was used, where electrical contact with the cytosol is established by adding a membrane-perforating agent to the pipette solution. The agent (nystatin or amphoteracin B) perforates the membrane so that only small molecules such as ions can pass through, leaving the cytoplasm's organic composition largely intact.

Inside-out and outside-out are two single-channel configurations that do away with the cell altogether by excising a patch of membrane from the cell and studying it in isolation. This provides the experimenter with ultimate control over the environment of the patch and any ion channels in it, both electrically and chemically. 'Outside' and 'inside' refer to the extracellular and intracellular side of the membrane, respectively, and 'out' refers to the bath.

Inside-out

This configuration is obtained from a cell-attached patch configuration, where the pipette is pulled away. The result is now a vesicle attached to the pipette tip. The vesicle can be destroyed by exposure to air, i.e. the pipette is briefly lifted above the bath. This leaves a patch with the cytosolic side facing the bath (Figure 9.2B). Inside-out patches are useful for studying the effects of cytosolic factors on channels but to do this the bath solution must be replaced with intracellular solution in each experiment.

Outside-out

This configuration is obtained by simply pulling away the patch pipette from a whole-cell configuration. The membrane will eventually break and, owing to the properties of the phospholipids, fold back on itself into a patch covering the pipette (Figure 9.2D). For obtain a physiological situation the pipette solution should resemble the intracellular ionic environment because it is facing the intracellular side of the membrane. Outside-out patches can be used to study the effects of extracellular factors on the channels, because the bath composition can be altered easily during recording.

9.2.2 Patch-clamp set up and recordings

Patch-clamp recording were performed in whole-cell configuration, both in voltage-clamp or current-clamp mode.

Recordings of excitatory and inhibitory postsynaptic currents were made between 8 and 14 days *in vitro* because, as reported in Bekkers and Stevens (1991), functional autaptic contacts start to be found after 8 days *in vitro*. Microislands containing one or more glial cells and a single neuron with extensive processes were selected for whole-cell patch-clamp recording. Patch-clamp recordings were made at room temperature following standard techniques. Electrical signals were recorded through an Axopatch-200B and digitized using a Digidata 1440A interface and pClamp software (Axon Instruments). The liquid junction potential (LJP) value (-8 mV) should be added to all voltages to obtain the correct membrane potentials (Neher, 1992).

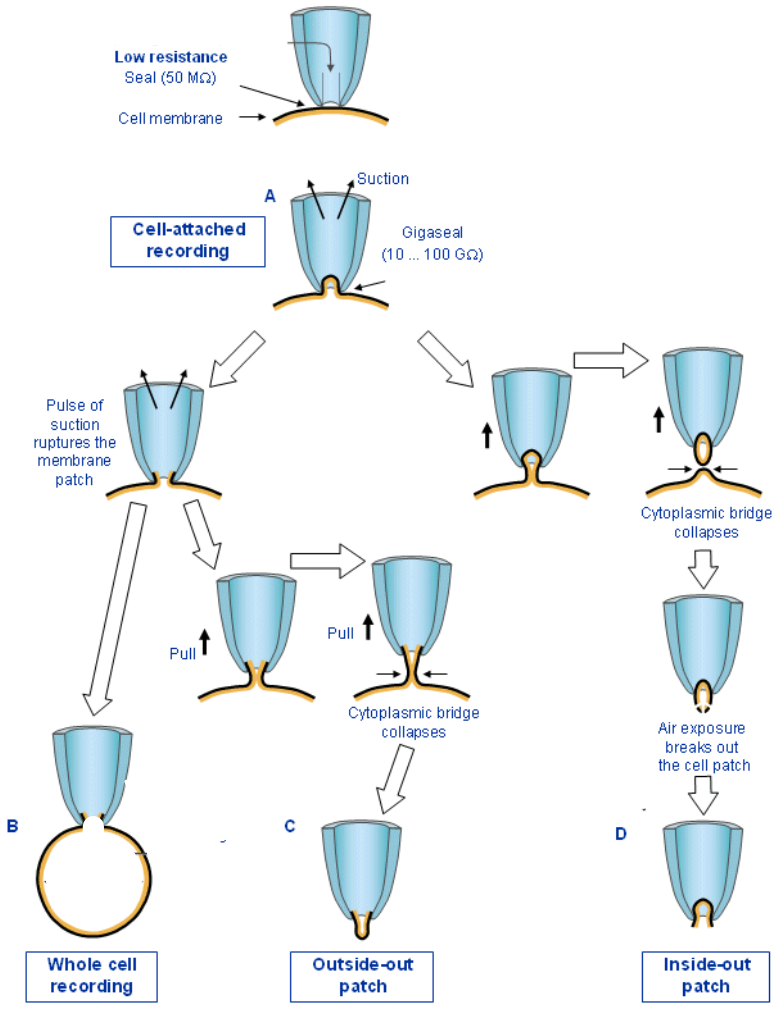

Figure 9.3. Representation of the four patch-clamp configurations, adapted from Hamill et al. (1981)

Whole-cell patch-clamp pipettes with a resistance of 1.8-2.5 MΩ were pulled from borosilicate glass, lightly fire-polished and filled with (in mM): 110 K-methanesulfonate, 5 $MgCl_2$, 30 HEPES, 3 EGTA, 4 ATP, 0.5 GTP and 1 cAMP (pH 7.4 with KOH). The extracellular solution contained (in mM): 145 NaCl, 5.6 KCl, 10 HEPES, 10 glucose, 1 $MgCl_2$, 2 $CaCl_2$ (pH 7.4 with NaOH). In whole-cell patch-clamp recordings on pyramidal cells 0.05 mM D-AP5 was added to all the solutions to block NMDA receptors. Cytochrome C (0.1 mg/ml) was added to the solution with peptide toxin ω-AgaIVA.

In voltage-clamp mode, action potentials in the unclamped processes were induced by a 2 ms voltage pulse to +20 mV every 10 s from a holding potential of -80 mV for EPSCs or -90 mV for IPSCs. Both for pyramidal cells or fast-spiking multipolar interneurons the postsynaptic current was recorded at -80 mV. To study the Ca^{2+}-

dependence of EPSC and IPSC, the extracellular solution was applied for at least one minute for every Ca^{2+} concentration and for $[Ca^{2+}]_{ext}$ above 2 mM the postsynaptic currents were evoked every 20 seconds to avoid vesicle depletion. If phenomenon of vesicle depletion in high extracellular Ca^{2+} concentration were present or if, for every Ca^{2+} concentration, at least 5-6 stable evoked postsynaptic current were not recorded the experiment was discarded. In each cell, the EPSC or IPSC (PSC) amplitude was normalized to the maximal value obtained by fitting the data points according to the Hill equation: $PSC = PSC_{max} \times [Ca^{2+}]^n/\{(EC_{50})^n + [Ca^{2+}]^n\}$. After, the mean normalized data points were fitted according to the Hill equation: $PSC = [Ca^{2+}]^n/\{(EC_{50})^n + [Ca^{2+}]^n\}$. To measure short-term synaptic plasticity the EPSCs elicited by two 50 Hz action potentials stimuli, applied five times at a 10 seconds interval, were averaged. The excitatory postsynaptic currents recorded in the presence of 5 μM NBQX were subtracted to all records to obtain the AMPA-mediated EPSCs. The inhibitory postsynaptic currents recorded in the presence of 20 μM Bicuculline were subtracted to all records to obtain the $GABA_A$-mediated IPSCs. In the Figures EPSC or IPSC are represented after blanking 1-3 ms around each stimulus artefact for clarity. For each experiment, after EPSC or IPSC stabilization (typically 3 min after break-in), 5-6 sweeps were averaged to obtain the mean EPSC or IPSC amplitude. Filtering was at 1 kHz, sampling was at 5 kHz and series resistance compensation (70-80%) was used.

For current-clamp recordings, the fast mode of the Axonpatch 200B was used. Baseline current injection was typically applied and adjusted to maintain a resting potential near –70 mV. The action potential firing was induced by 1 s – long suprathreshold current injections of increasing amplitude up to 400 pA. Filtering was at 2 kHz, sampling was at 10 kHz and capacitance neutralization was carefully adjusted.

9.2.3 Analysis and statistics

Patch-clamp experiments were analysed using the Clampfit 10.0 software (Axon Instruments). All averages were calculated with Microsoft Excel. Graphs and statistical comparison were obtained with the Origin software (Microcal Software, Inc.). Data are given as mean ± SEM; stars indicate a statistically significant difference from control assessed by the Student's t test (*$p < 0.05$, **$p < 0.01$ and ***$p < 0.001$).

9.2.4 Drugs and toxin

Cytochrome C was form Sigma-Aldrich; D-AP5, NBQX and Bicuculline were from Ascent-Scientific; R-Baclofen was from Tocris and ω-AgaIVA was from Peptide Institute Inc..

10. REFERENCES

Adams, P.J., Garcia, E., David, L.S., Mulatz, K.J., Spacey, S.D., and Snutch, T.P. (2009). $Ca_V2.1$ P/Q-type calcium channel alternative splicing affects the functional impact of familial hemiplegic migraine mutations: implications for calcium channelopathies. Channels (Austin) *3*, 110-121.

Ali, A.B., and Nelson, C. (2006). Distinct Ca^{2+} channels mediate transmitter release at excitatory synapses displaying different dynamic properties in rat neocortex. Cereb. Cortex *16*, 386-393.

Arikkath, J., and Campbell, K.P. (2003). Auxiliary subunits: essential components of the voltage-gated calcium channel complex. Curr. Opin. Neurobiol. *13*, 298-307.

Aurora, S.K., and Wilkinson, F. (2007). The brain is hyperexcitable in migraine. Cephalalgia *27*, 1442-1453.

Ayata, C., Shimizu-Sasamata, M., Lo, E.H., Noebels, J.L., and Moskowitz, M.A. (2000). Impaired neurotransmitter release and elevated threshold for cortical spreading depression in mice with mutations in the α_{1A} subunit of P/Q type calcium channels. Neuroscience *95*, 639-645.

Ayata, C., Jin, H., Kudo, C., Dalkara, T., and Moskowitz, M.A. (2006). Suppression of cortical spreading depression in migraine prophylaxis. Ann. Neurol. *59*, 652-661.

Bekkers, J.M., and Stevens, C.F. (1991). Excitatory and inhibitory autaptic currents in isolated hippocampal neurons maintained in cell culture. Proc. Natl. Acad. Sci. USA *88*, 7834-7838.

Bettler, B., Kaupmann, K., Mosbacher, J., and Gassmann, M. (2004). Molecular structure and physiological functions of $GABA_B$ receptors. Physiol. Rev. *84*, 835-867.

Bettler, B., and Tiao, J.Y. (2006). Molecular diversity, trafficking and subcellular localization of $GABA_B$ receptors. Pharmacol. Ther. *110*, 533-543.

Birnbaumer, L., Campbell, K.P., Catterall, W.A., Harpold, M.M., Hofmann, F., Horne, W.A., Mori, Y., Schwartz, A., Snutch, T.P., Tanabe, T., and et al. (1994). The naming of voltage-gated calcium channels. Neuron *13*, 505-506.

Bolay, H., Reuter, U., Dunn, A.K., Huang, Z., Boas, D.A., and Moskowitz, M.A. (2002). Intrinsic brain activity triggers trigeminal meningeal afferents in a migraine model. Nat. Med. *8*, 136-142.

Bourinet, E., Soong, T.W., Sutton, K., Slaymaker, S., Mathews, E., Monteil, A., Zamponi, G.W., Nargeot, J., and Snutch, T.P. (1999). Splicing of alpha 1A subunit gene generates phenotypic variants of P- and Q-type calcium channels. Nat. Neurosci. *2*, 407-415.

Bowery, N.G., Bettler, B., Froestl, W., Gallagher, J.P., Marshall, F., Raiteri, M., Bonner, T.I., and Enna, S.J. (2002). International Union of Pharmacology. XXXIII. Mammalian gamma-aminobutyric acid(B) receptors: structure and function. Pharmacol. Rev. *54*, 247-264.

Bowyer, S.M., Aurora, K.S., Moran, J.E., Tepley, N., and Welch, K.M. (2001). Magnetoencephalographic fields from patients with spontaneous and induced migraine aura. Ann. Neurol. *50*, 582-587.

Brody, D.L., and Yue, D.T. (2000a). Relief of G-protein inhibition of calcium channels and short-term synaptic facilitation in cultured hippocampal neurons. J. Neurosci. *20*, 889-898.

Brody, D.L., and Yue, D.T. (2000b). Release-independent short-term synaptic depression in cultured hippocampal neurons. J. Neurosci. *20*, 2480-2494.

Brown, D.A., and Sihra, T.S. (2008). Presynaptic signaling by heterotrimeric G-proteins. Handb. Exp. Pharmacol. *184*, 207-270.

Bucurenciu, I., Kulik, A., Schwaller, B., Frotscher, M., and Jonas,P. (2008). Nanodomain coupling between Ca^{2+} channels and Ca^{2+} sensors promotes fast and efficient transmitter release at cortical GABAergic synapse. Neuron *57*, 536-545.

Canals, S., Makarova, I., Lopez-Aguado, L., Largo, C., Ibarz, J.M., and Herreras, O. (2005). Longitudinal depolarization gradients along the somatodendritic axis of CA1 pyramidal cells: a novel feature of spreading depression. J. Neurophysiol. *94*, 943-951.

Cannon, S.C. (2006). Pathomechanisms in channelopathies of skeletal muscle and brain. Annu. Rev. Neurosci. *29*, 387-415.

Catterall, W.A. (1998). Structure and function of neuronal Ca2+ channels and their role in neurotransmitter release. Cell Calcium *24*, 307-323

Catterall, W.A., Few, A.P. (2008). Calcium channel regulation and presynaptic plasticity. Neuron *59*, 882-901.

Catterall, W.A., Perez-Reyes, E., Snutch, T.P., and Striessnig, J. (2005). International Union of Pharmacology. XLVIII. Nomenclature and structure-function relationships of voltage-gated calcium channels. Pharmacol. Rev. *57*, 411-425.

Cauli, B., Porter, J.T., Tsuzuki, K., Lambolez, B., Rossier, J., Quenet, B., and Audinat, E. (2000). Classification of fusiform neocortical interneurons based on unsupervised clustering. Proc. Natl. Acad. Sci. U S A *97*, 6144-6149.

Chan, Y., Burgunder, J., Wilder-Smith, E., Chew, S., Lam-Mok-Sing, K.M.J., Sharma, V., Ong, B.K.C. (2008). Electroencephalographic changes and seizures in familial hemiplegic migraine patients with the *CACNA1A* gene S218L mutation. J. Clin. Neurosci. *15*, 891-894.

Charles, A. (2009). Advances in the basic and clinical science of migraine. Ann. Neurol. *65*, 491-498.

Charles, A., and Brennan, K. (2009). Cortical spreading depression-new insights and persistent questions. Cephalalgia *29*, 1115-1124.

Coppola, G., Pierelli, F., and Schoenen, J. (2007). Is the cerebral cortex hyperexcitable or hyperresponsive in migraine? Cephalalgia *27*, 1427-1439.

Couve, A., Moss, S. J., and Pangalos, M.N. (2000). $GABA_B$ receptors: a new paradigm in G protein signaling. Mol. Cell. Neurosci. *16*, 296-312.

Dalkara, T., Zervas, N.T., and Moskowitz, M.A. (2006). From spreading depression to the trigeminovascular system. Neurol. Sci. *27 Suppl 2*, S86-90.

de Vries, B., Frants, R.R., Ferrari, M.D., and van den Maagdenberg, A.M. (2009). Molecular genetics of migraine. Hum. Genet. *126*, 115-132.

De Waard, M., and Campbell, K.P. (1995). Subunit regulation of the neuronal alpha 1_A Ca^{2+} channel expressed in Xenopus oocytes. J. Physiol. *485 (Pt 3)*, 619-634.

De Waard, M., Gurnett, C.A., and Campbell, K.P. (1996). Structural and functional diversity of voltage-activated calcium channels. Ion Channels *4*, 41-87.

De Waard, M., Hering, J., Weiss, N., and Feltz, A. (2005). How do G proteins directly control neuronal Ca^{2+} channel function? Trends Pharmacol. Sci. *26*, 427-436.

Debiais, S., Hommet, C., Bonnaud, I., Barthez, M.A., Rimbaux, S., Riant, F., and Autret, A. (2009). The FHM1 mutation S218L: a severe clinical phenotype? A case report and review of the literature. Cephalalgia *29*, 1337-1339.

Ducros, A., Denier, C., Joutel, A., Cecillon, M., Lescoat, C., Vahedi, K., Darcel, F., Vicaut, E., Bousser, M. G., and Tournier-Lasserve, E. (2001). The clinical spectrum of familial hemiplegic migraine associated with mutations in a neuronal calcium channel. N. Engl. J. Med. *345*, 17-24.

Eikermann-Haerter, K., Dilekoz, E., Kudo, C., Savitz, S. I., Waeber, C., Baum, M.J., Ferrari, M.D., van den Maagdenberg, A.M., Moskowitz, M.A., and Ayata, C. (2009a). Genetic and hormonal factors modulate spreading depression and transient hemiparesis in mouse models of familial hemiplegic migraine type 1. J. Clin. Invest. *119*, 99-109.

Eikermann-Haerter, K., Wang, Y., Yuzawa, I., Waeber, C., Hoffmann, U., Ferrari, M., van den Maagdenberg, A.M., Moskowitz, M.A, and Ayata, C. (2009b). Facilitated subcortical propagation of cortical spreading depression in mice expressing the S218L, R192Q mutations causing familial hemiplegic migraine type 1. 39th Annual Meeting, Chicago, USA. Soc. Neurosci. Abstracts *521.6*.

Ertel, E.A., Campbell, K.P., Harpold, M.M., Hofmann, F., Mori, Y., Perez-Reyes, E., Schwartz, A., Snutch, T.P., Tanabe, T., Birnbaumer, L., et al. (2000). Nomenclature of voltage-gated calcium channels. Neuron *25*, 533-535.

Fitzsimons, R.B., and Wolfenden, W.H. (1985). Migraine coma. Meningitic migraine with cerebral oedema associated with a new form of autosomal dominant cerebellar ataxia. Brain *108 (Pt 3)*, 555-577.

Gao, Z., Todorov, B., Barrett, C.F., Frants, R.R., Ferrari, M.D., van den Maagdenberg, A.M., De Zeeuw, C.I., and Hoebeek, F.E. (2009). Increased calcium influx in *CACNA1A* S218L knock-in mice induces irregular Purkinje cell firing patterns. 39th Annual Meeting, Chicago, USA. Soc. Neurosci. *Abstract 660.1*.

Gasparini, S., Kasyanov, A.M., Pietrobon, D., Voronin, L.L., and Cherubini, E. (2001). Presynaptic R-type calcium channels contribute to fast excitatory synaptic transmission in the rat hippocampus. J. Neurosci. *21*, 8715-8721.

Haan, J., Kors, E.E., Vanmolkot, K.R., van den Maagdenberg, A.M., Frants, R.R., and Ferrari, M.D. (2005). Migraine genetics: an update. Curr. Pain Headache Rep. *9*, 213-220.

Hadjikhani, N., Sanchez del Rio, M., Wu, O., Schwartz, D., Bakker, D., Fischl, B., Kwong, K.K., Cutrer, F.M., Rosen, B.R., Tootell, R.B.H., et al. (2001). Mechanisms of migraine aura revealed by functional MRI in human visual cortex. Proc. Natl. Acad. Sci. USA *98*, 4687-4692.

Hamill, O.P., Marty, A., Neher, E., Sakmann, B., and Sigworth, F.J. (1981). Improved patch-clamp techniques for high-resolution current recording from cells and cell-free membrane patches. Pflugers Arch. *391*, 85-100.

Hans, M., Luvisetto, S., Williams, M.E., Spagnolo, M., Urrutia, A., Tottene, A., Brust, P.F., Johnson, E.C., Harpold, M.M., Stauderman, K.A., and Pietrobon, D. (1999). Functional consequences of mutations in the human α_{1A} calcium channel subunit linked to familial hemiplegic migraine. J. Neurosci. *19*, 1610-1619.

Hille, B. (2001). Ionic channels of excitable membranes. Sutherland MA: Sinauer

Ikeda, K., Yanagawa, Y., and Bekkers, J.M. (2008). Distinctive quantal properties of neurotransmission at excitatory and inhibitory autapses revealed using variance-mean analysis. J. Neurosci. *28*, 13563-13573.

Iwasaki, S., Momiyama, A., Uchitel, O.D, and Takahashi, T. (2000). Developmental changes in calcium channel types mediating central synaptic transmission. J. Neurosci. *20*, 59-65.

Jen, J.C. (2008). Hereditary episodic ataxias. Ann. N. Y. Acad. Sci. *1142*, 250-253.

Jen, J.C., Graves, T.D., Hess, E.J., Hanna, M.G., Griggs, R.C., and Baloh, R.W. (2007). Primary episodic ataxias: diagnosis, pathogenesis and treatment. Brain *130*, 2484-2493.

Jones, L.P., Patil, P.G., Snutch, T.P., and Yue, D.T. (1997). G-protein modulation of N-type calcium channel gating current in human embryonic kidney cells (HEK 293). J. Physiol. *498 (Pt 3)*, 601-610.

Klugbauer, N., Lacinova, L., Marais, E., Hobom, M., and Hofmann, F. (1999). Molecular diversity of the calcium channel alpha2delta subunit. J. Neurosci. *19*, 684-691.

Koester, H.J., and Sakmann, B. (2000). Calcium dynamics associated with action potentials in single nerve terminals of pyramidal cells in layer 2/3 of the young rat neocortex. J. Physiol. *529 Pt 3*, 625-646.

Kordasiewicz, H.B., Thompson, R.M., Clark, H.B., and Gomez, C.M. (2006). C-termini of P/Q-type Ca^{2+} channel alpha1A subunits translocate to nuclei and promote polyglutamine-mediated toxicity. Hum. Mol. Genet. *15*, 1587-1599.

Kors, E.E., Terwindt, G.M., Vermeulen, F.L., Fitzsimons, R.B., Jardine, P.E., Heywood, P., Love, S., van den Maagdenberg, A.M., Haan, J., Frants, R.R., and Ferrari, M.D. (2001). Delayed cerebral edema and fatal coma after minor head trauma: role of

the *CACNA1A* calcium channel subunit gene and relationship with familial hemiplegic migraine. Ann. Neurol. *49*, 753-760.
Kruglikov, I., and Rudy, B. (2008). Perisomatic GABA release and thalamocortical integration onto neocortical excitatory cells are regulated by neuromodulators. Neuron *58*, 911-924.

Lauritzen, M. (1994). Pathophysiology of the migraine aura. The spreading depression theory. Brain *117 (Pt 1)*, 199-210.

Levi, G., Alosi, M., Ciotti, M., and Gallo, V. (1984). Autoradiographic localization and depolarization-induced release of amino acids in differentiating granule cells cultures. Brain Res. *290*, 77-86.

Li, L., Bischofberger, J., and Jonas, P. (2007). Differential gating and recruitment of P/Q-, N-, and R-type Ca^{2+} channels in hippocampal mossy fiber boutons. J. Neurosci. *27*, 13420-13429.

Llinas, R.R., Choi, S., Urbano, F.J., and Shin, H.S. (2007). Gamma-band deficiency and abnormal thalamocortical activity in P/Q-type channel mutant mice. Proc. Natl. Acad. Sci. U S A *104*, 17819-17824.

Markram, H., Toledo-Rodriguez, M., Wang, Y., Gupta, A., Silberberg, G., and Wu, C. (2004). Interneurons of the neocortical inhibitory system. Nat. Rev. Neurosci. *5*, 793-807.

Melliti, K., Grabner, M., and Seabrook, G.R. (2003). The familial hemiplegic migraine mutation R192Q reduces G-protein-mediated inhibition of P/Q-type ($Ca_V2.1$) calcium channels expressed in human embryonic kidney cells. J. Physiol. *546*, 337-347.

Mintz, I. M., Sabatini, B.L., and Regehr, W.G. (1995). Calcium control of transmitter release at a cerebellar synapse. Neuron *15*, 675-688.

Molemman, A. (2003). Patch Clamping: an introductory guide to patch clamp electrophysiology. John Wiley & Sons, Ltd.

Mullner, C., Broos, L.A., van den Maagdenberg, A.M., and Striessnig, J. (2004). Familial hemiplegic migraine type 1 mutations K1336E, W1684R, and V1696I alter $Ca_V2.1$ Ca^{2+} channel gating: evidence for beta-subunit isoform-specific effects. J. Biol. Chem. *279*, 51844-51850.

Neher, E. (1992). Correction for liquid junction potentials in patch clamp experiments. Methods Enzymol. *207*, 123-131.

Ophoff, R.A., Terwindt, G.M., Vergouwe, M.N., van Eijk, R., Oefner, P.J., Hoffman, S.M.G., Lamerdin, J.E., Mohrenweiser, H.W., Bulman, D.E., Ferrari, M., et al. (1996). Familial hemiplegic migraine and episodic ataxia type-2 are caused by mutations in the Ca^{2+} channel gene *CACNL1A4*. Cell *87*, 543-552.

Pietrobon, D. (2002). Calcium channels and channelopathies of the central nervous system. Mol. Neurobiol. *25*, 31-50.

Pietrobon, D. (2005). Migraine: new molecular mechanisms. Neuroscientist *11*, 373-386.

Pietrobon, D. (2007). Familial hemiplegic migraine. Neurotherapeutics *4*, 274-284.

Pietrobon, D., and Striessnig, J. (2003). Neurobiology of migraine. Nat. Rev. Neurosci. *4*, 386-398.

Qian, J., and Noebels, J.L. (2000). Presynaptic Ca^{2+} influx at a mouse central synapse with Ca^{2+} channel subunit mutations. J. Neurosci. *20*, 163-170.

Reid, C.A., Bekkers, J.M., and Clements, J.D. (1998). N- and P/Q-type Ca^{2+} channels mediate transmitter release with a similar cooperativity at rat hippocampal autapses. J. Neurosci. *18*, 2849-2855.

Reyes, A., Lujan, R., Rozov, A., Burnashev, N., Somogyi, P., and Sakmann, B. (1998). Target-cell-specific facilitation and depression in neocortical circuits. Nat. Neurosci. *1*, 279-285.

Rost, B.R., Breustedt, J., Nicholson, P., Rosenmund, C., and Schmitz, D. (2009). Mechanisms of presynaptic inhibition by GABAb receptors. 39th Annual Meeting, Chicago, USA. Soc. Neurosci. *Abstract 615.6*.

Rozov, A., Burnashev, N., Sakmann, B., and Neher, E. (2001). Transmitter release modulation by intracellular Ca^{2+} buffers in facilitating and depressing nerve terminals of pyramidal cells in layer 2/3 of the rat neocortex indicates a target cell-specific difference in presynaptic calcium dynamics. J. Physiol. *531*, 807-826.

Sakaba, T., and Neher, E. (2003). Direct modulation of synaptic vesicle priming by $GABA_B$ receptor activation at a glutamatergic synapse. Nature *424*, 775-778.

Scanziani, M. (2000). GABA spillover activates postsynaptic $GABA_B$ receptors to control rhythmic hippocampal activity. Neuron *25*, 673-681.

Serra, S.A., Fernandez-Castillo, N., Macaya, A., Cormand, B., Valverde, M.A., and Fernandez-Fernandez, J.M. (2009). The hemiplegic migraine-associated Y1245C

mutation in *CACNA1A* results in a gain of channel function due to its effect on the voltage sensor and G-protein-mediated inhibition. Pflugers Arch. *458*, 489-502.
Somjen, G.G. (2001). Mechanisms of spreading depression and hypoxic spreading depression-like depolarization. Physiol. Rev. *81*, 1065-1096.

Stam, A.H., Luijckx, G.J., Poll-The, B.T., Ginjaar, I.B., Frants, R.R., Haan, J., Ferrari, M.D., Terwindt, G.M., and van den Maagdenberg, A.M. (2009). Early seizures and cerebral oedema after trivial head trauma associated with the *CACNA1A* S218L mutation. J. Neurol. Neurosurg. Psychiatry *80*, 1125-1129.

Takada, N., Yanagawa, Y., and Komatsu, Y. (2005). Activity-dependent maturation of excitatory synaptic connections in solitary neuron cultures of mouse neocortex. Eur. J. Neurosci. *21*, 422-430.

Tedford, H.W., and Zamponi, G.W. (2006). Direct G protein modulation of Ca_V2 calcium channels. Pharmacol. Rev. *58*, 837-862.

Tonelli, A., D'Angelo, M.G., Salati, R., Villa, L., Germinasi, C., Frattini, T., Meola, G., Turconi, A.C., Bresolin, N., and Bassi, M.T. (2006). Early onset, non fluctuating spinocerebellar ataxia and a novel missense mutation in *CACNA1A* gene. J. Neurol. Sci. *241*, 13-17.

Tottene, A., Volsen, S., and Pietrobon, D. (2000). α_{1E} subunits form the pore of three cerebellar R-type calcium channels with different pharmacological and permeation properties. J. Neurosci. *1*, 171-178.

Tottene, A., Fellin, T., Pagnutti, S., Luvisetto, S., Striessnig, J., Fletcher, C., and Pietrobon, D. (2002). Familial hemiplegic migraine mutations increase Ca^{2+} influx through single human $Ca_V2.1$ channels and decrease maximal $Ca_V2.1$ current density in neurons. Proc. Natl. Acad. Sci. USA *99*, 13284-13289.

Tottene, A., Pivotto, F., Fellin, T., Cesetti, T., van den Maagdenberg, A.M., and Pietrobon, D. (2005). Specific kinetic alterations of human $Ca_V2.1$ calcium channels produced by mutation S218L causing familial hemiplegic migraine and delayed cerebral edema and coma after minor head trauma. J. Biol. Chem. *280*, 17678-17686.

Tottene, A., Conti, R., Fabbro, A., Vecchia, D., Shapovalova, M., Santello, M., van den Maagdenberg, A.M, Ferrari, M.D, and Pietrobon, D. (2009). Enhanced excitatory transmission at cortical synapses as the basis for facilitated spreading depression in $Ca_V2.1$ knockin migraine mice. Neuron *61*, 762-773.

Ulrich, D., and Bettler, B. (2007). $GABA_B$ receptors: synaptic functions and mechanisms of diversity. Curr. Opin. Neurobiol. *17*, 298-303.

van den Maagdenberg, A.M., Pietrobon, D., Pizzorusso, T., Kaja, S., Broos, L.A., Cesetti, T., van de Ven, R.C., Tottene, A., van der Kaa, J., Plomp, J.J., et al. (2004). A *Cacna1a* knockin migraine mouse model with increased susceptibility to cortical spreading depression. Neuron *41*, 701-710.

van den Maagdenberg, A.M, Pizzorusso, T., Kaja, S., Terpolilli, N., Shapovalova, M., Hoebeek, F.E., Barrett, C.F., Gherardini, L., van de Ven, R.C, Todorov, B., Broos, L.A, Tottene, A., Gao, Z., Fodor, M., De Zeeuw, C.I., Frants, R.R., Plesnila, N., Plomp, J.J., Pietrobon, D., and Ferrari, M.D. (2010). High CSD susceptibility and migraine-associated symptoms in $Ca_V2.1$ S218L mice. Ann. Neurol. *in press*.

Wan, J., Carr, J.R., Baloh, R.W., and Jen, J.C. (2005). Nonconsensus intronic mutations cause episodic ataxia. Ann. Neurol. *57*, 131-135.

Watase, K., Barrett, C.F., Miyazaki, T., Ishiguro, T., Ishikawa, K., Hu, Y., Unno, T., Sun, Y., Kasai, S., Watanabe, M., et al. (2008). Spinocerebellar ataxia type 6 knockin mice develop a progressive neuronal dysfunction with age-dependent accumulation of mutant $Ca_V2.1$ channels. Proc. Natl. Acad. Sci. U S A *105*, 11987-11992.

Weiss, N., Arnoult, C., Feltz, A., and De Waard, M. (2006). Contribution of the kinetics of G protein dissociation to the characteristic modifications of N-type calcium channel activity. Neurosci. Res. *56*, 332-343.

Weiss, N., Tadmouri, A., Mikati, M., Ronjat, M., and De Waard, M. (2007). Importance of voltage-dependent inactivation in N-type calcium channel regulation by G-proteins. Pflugers Arch. *454*, 115-129.

Weiss, N., Sandoval, A., Felix, R., van den Maagdenberg, A.M., and De Waard, M. (2008). The S218L familial hemiplegic migraine mutation promotes deinhibition of $Ca_V2.1$ calcium channels during direct G-protein regulation. Pflugers Arch. *457*, 315-326.

Westenbroek, R.E., Sakurai, T., Elliott, E.M., Hell, J.W., Starr, T.V., Snutch, T.P., and Catterall, W.A. (1995). Immunochemical identification and subcellular distribution of the alpha1A subunits of brain calcium channels. J. Neurosci. *15,* 6403-6418.

Wu, L.G., Westenbroek, R.E., Borst, J.G., Catterall, W.A., and Sakmann, B. (1999). Calcium channel types with distinct presynaptic localization couple differentially to transmitter release in single calyx-type synapses. J. Neurosci. *19*, 726-736.

Zaitsev, A.V., Povysheva, N.V., Lewis, D.A., and Krimer, L.S. (2007). P/Q-type, but not N-type, calcium channels mediate GABA release from fast-spiking interneurons to pyramidal cells. J. Neurophysiol. *97*, 3567-3573.

Zhang, X., Levy, D., Kainz, V., Jakubowski, M., and Burstein, R. (2009). Activation of meningeal nociceptor by cortical spreading depression. 39th Annual Meeting, Chicago, USA. Soc. Neurosci. *Abstract 339.5*.

Zhuchenko, O., Bailey, J., Bonnen, P., Ashizawa, T., Stockton, D.W., Amos, C., Dobyns, W.B., Subramony, S.H., Zoghbi, H.Y., and Lee, C.C. (1997). Autosomal dominant cerebellar ataxia (SCA6) associated with small polyglutamine expansions in the alpha 1A-voltage-dependent calcium channel. Nat. Genet. *15*, 62-69.